

Global Optimisation Applied To Molecular Architecture

by

Wayne John Pullan

A thesis submitted toward the degree of

Doctor of Philosophy

Central Queensland University

Department of Mathematics and Computing

Faculty of Applied Science

November, 1996

Abstract

This thesis addresses the problem of identifying configurations of molecular structures which correspond to the globally minimum potential energy for that structure. Molecular structures arise as a result of non-bonded and bonded atomic interactions and experimental evidence shows that, in the great majority of cases, the potential energy global minimum corresponds to the most stable configuration of the molecular structure. This configuration is of particular importance as it dictates most of the physical properties of the molecular structure.

The potential energy of a molecular structure may be calculated, as a function of the atomic positions, using appropriate molecular models. However, as these give rise to potential energy functions that are typically non-convex with many local minima, finding the global minima is an extremely difficult problem. For many years this problem has been investigated by chemists and physicists however, in more recent years, researchers from optimisation and computer science have also become involved and, in fact, the minimisation of non-convex potential energy functions arising from molecular conformation or protein folding problems has become one of the most important interdisciplinary problems [43].

This thesis develops and analyses a molecular structure global optimisation method using both deterministic local and stochastic global optimisation techniques within a genetic algorithm based environment. By incorporating different genetic operators, the one basic method was able to globally optimise a number of different types of molecular structures.

From an experimental point of view, the method was particularly successful and found

- all currently accepted global minima for scaled Lennard-Jones atomic

clusters of 2 to 80 atoms.

- two new global minima for 77 and 78 atom scaled Lennard-Jones atomic clusters.
- all currently accepted and some improved global minima for mixed argon-xenon atomic clusters of 7, 13 and 19 atoms. In addition, minima were determined for all remaining clusters in the 2, ..., 20 atom range.
- all currently accepted global minima for clusters of benzene molecules of 2 to 6 molecules and new minima for clusters of 8 to 12 molecules.
- all currently accepted global minima for a two-dimensional model molecular structure where the number of atoms ranged from 3 to 42.
- currently accepted global minima for a number of small molecules.

Of particular importance is that, in determining these global minima, the method always started from randomly generated initial configurations and at no stage used any heuristic information to accelerate the search.

From a theoretical point of view, this thesis presents an analytical comparison of the phenotype crossover operators used in the method with the more standard (genotype) crossover operators normally used in genetic algorithms. This analysis is confirmed with experimental results. In addition, a proof of convergence for the stochastic global optimisation technique used within the genetic algorithm environment and analytical evaluation of all potential energy gradients required by the deterministic local optimiser are presented.

Chapter 1 of this thesis describes the molecular architecture problem and presents a review of local and global optimisation techniques. Chapter

2 describes the development of APSE, the stochastic global optimisation technique used in this study while the results obtained by applying APSE to the pure atomic cluster problem are presented in Chapter 3.

Chapter 4 describes the development of GEM*, the major computational method used in this study. GEM* implements a combination of local optimisation and APSE probabilistic searches within a genetic algorithm based environment. The results obtained by applying GEM* to the pure atomic cluster problem and a theoretical comparison of phenotype genetic crossover operators with more standard genetic crossover operators are presented in Chapter 5.

The results obtained by applying GEM* to mixed argon-xenon atomic cluster problems are described in Chapter 6 while the optimisation of clusters of benzene and water molecules by GEM* is discussed in Chapter 7. Chapter 8 describes the GEM* optimisation results obtained for a model molecular structure and Chapter 9 presents the GEM* optimisation results for a number of small molecules.

A summary and future research directions are presented in Chapter 10 while the appendices contain the analytical derivation of the potential energy gradients required for the implementation of the BFGS local optimiser and tables describing the structures obtained for mixed atomic clusters.

Within this thesis

- Chapter 2 and Sections 3.3.1 and 3.4.1 appeared in the Australian Computer Journal, Vol. 28, No. 4, November 1996.
- Chapter 6 has been accepted for publication by the Journal of Computational Chemistry.
- Sections 4.2, 5.2, 5.3 and 5.4 have been submitted to the Journal of

Global Optimization.

- Section 3.3.2 appeared as Technical Report 95 – 010, Department of Mathematics and Computing, Central Queensland University.
- Chapter 7 appeared as Technical Report 96 – 005, Department of Mathematics and Computing, Central Queensland University.
- Chapters 8 and 9 appeared as Technical Report 96 – 006, Department of Mathematics and Computing, Central Queensland University.

Contents

| | | |
|----------|------------------------------------|-----------|
| 1 | Introduction | 1 |
| 1.1 | Overview | 1 |
| 1.2 | Molecular Architecture | 2 |
| 1.2.1 | Atomic Clusters | 6 |
| 1.2.2 | Molecular Clusters | 7 |
| 1.2.3 | Molecules | 9 |
| 1.3 | Local Optimisation | 12 |
| 1.4 | Global Optimisation | 13 |
| 1.4.1 | Random Search | 14 |
| 1.4.2 | Simulated Annealing | 14 |
| 1.4.3 | Genetic Algorithms | 15 |
| 1.5 | Outline of Thesis | 20 |
| 2 | APSE Computational Method | 24 |
| 2.1 | Introduction | 24 |
| 2.2 | APS and APSE Algorithms | 25 |
| 2.3 | Convergence of APSE | 29 |
| 2.4 | Test Functions | 32 |
| 2.4.1 | Beale Function | 32 |
| 2.4.2 | Goldstein-Price Function | 34 |
| 2.4.3 | Rastrigin Function | 35 |

| | | |
|----------|--|-----------|
| 2.4.4 | Griewank-2 Function | 37 |
| 2.4.5 | Variable Dimension Test Function | 38 |
| 2.5 | Discussion | 40 |
| 3 | APSE Optimisation of Pure Atomic Clusters | 42 |
| 3.1 | Introduction | 42 |
| 3.2 | Pure Atomic Clusters | 43 |
| 3.3 | Computational Methods | 51 |
| 3.3.1 | APSE and Atomic Build-up | 53 |
| 3.3.2 | APSE and PES Smoothing | 54 |
| 3.4 | Results | 65 |
| 3.4.1 | APSE and Atomic Build-up | 65 |
| 3.4.2 | APSE and PES Smoothing | 65 |
| 3.5 | Discussion | 67 |
| 4 | GEM* Computational Method | 70 |
| 4.1 | Introduction | 70 |
| 4.2 | GEM* Algorithm | 72 |
| 4.3 | GEM* Software | 77 |
| 4.4 | Discussion | 78 |
| 5 | GEM* Optimisation of Pure Atomic Clusters | 80 |
| 5.1 | Introduction | 80 |
| 5.2 | GEM* Computational Method | 80 |
| 5.3 | Results | 84 |
| 5.4 | GEM* Crossover Analysis | 94 |
| 5.4.1 | χ_1 Crossover | 98 |
| 5.4.2 | χ_2 Crossover | 100 |
| 5.4.3 | Theoretical - Numerical Comparison | 102 |

| | | |
|----------|---|------------|
| 5.5 | Discussion | 104 |
| 6 | GEM* Optimisation of Mixed Atomic Clusters | 105 |
| 6.1 | Introduction | 105 |
| 6.2 | Mixed Atomic Clusters | 106 |
| 6.3 | GEM* Computational Method | 109 |
| 6.4 | Results | 110 |
| 6.5 | Discussion | 110 |
| 7 | GEM* Optimisation of Molecular Clusters | 121 |
| 7.1 | Introduction | 121 |
| 7.2 | Molecular Clusters | 122 |
| 7.2.1 | Benzene Clusters | 123 |
| 7.2.2 | Water Clusters | 125 |
| 7.3 | GEM* Computational Method | 129 |
| 7.3.1 | Genetic Encoding | 129 |
| 7.3.2 | Genetic Mutation | 131 |
| 7.4 | Results | 131 |
| 7.4.1 | Benzene Clusters | 131 |
| 7.4.2 | Water Clusters | 133 |
| 7.5 | Discussion | 136 |
| 8 | GEM* Optimisation of a Model Molecular Structure | 137 |
| 8.1 | Introduction | 137 |
| 8.2 | Model Molecular Structure | 138 |
| 8.3 | GEM* Computational Method | 141 |
| 8.3.1 | Genetic Encoding | 141 |
| 8.3.2 | Genetic Crossover | 142 |
| 8.3.3 | Genetic Mutation | 143 |

| | | |
|-----------|---------------------------------------|------------|
| 8.4 | Results | 143 |
| 8.5 | Discussion | 143 |
| 9 | GEM* Optimisation of Molecules | 147 |
| 9.1 | Introduction | 147 |
| 9.2 | Molecules | 148 |
| 9.2.1 | United Atom Butane | 150 |
| 9.2.2 | Pseudoethane | 150 |
| 9.2.3 | Acetyl Chloride | 152 |
| 9.3 | GEM* Computational Method | 154 |
| 9.3.1 | Genetic Encoding | 154 |
| 9.3.2 | Genetic Mutation | 154 |
| 9.4 | Results | 155 |
| 9.4.1 | United Atom Butane | 155 |
| 9.4.2 | Pseudoethane | 155 |
| 9.4.3 | Acetyl Chloride | 155 |
| 9.5 | Discussion | 155 |
| 10 | Conclusion | 156 |
| 10.1 | Thesis Summary | 156 |
| 10.1.1 | APSE | 157 |
| 10.1.2 | GEM* | 158 |
| 10.1.3 | Pure Atomic Clusters | 161 |
| 10.1.4 | Mixed Atomic Clusters | 161 |
| 10.1.5 | Benzene Clusters | 162 |
| 10.1.6 | Water Clusters | 162 |
| 10.1.7 | Model Molecular Structure | 163 |
| 10.1.8 | Molecules | 163 |

| | |
|---|-----|
| 10.2 Further Work | 163 |
| BIBLIOGRAPHY | |
| | 165 |
| APPENDICES | |
| | 174 |
| A Analytical Energy Gradients | 174 |
| A.1 Pure Atomic Clusters | 174 |
| A.2 Mixed Atomic Clusters | 175 |
| A.3 Benzene Clusters | 175 |
| A.4 Water Clusters | 178 |
| A.5 Model Molecular Structure | 186 |
| B Argon-Xenon Clusters | 189 |

List of Figures

| | | |
|------|--|----|
| 1.1 | Optimal structure - 55 atom Lennard-Jones cluster. | 8 |
| 1.2 | Optimal structure - benzene tetramer. | 10 |
| 1.3 | Octane molecule. | 11 |
| 1.4 | GA parameter mappings to objective function | 19 |
| 2.1 | Beale function - effect of λ and β . | 33 |
| 2.2 | Beale function - comparison of APS and APSE. | 33 |
| 2.3 | Goldstein-Price function - effect of λ and β . | 34 |
| 2.4 | Goldstein-Price function - comparison of APS and APSE. | 35 |
| 2.5 | Rastrigin function - effect of λ and β . | 36 |
| 2.6 | Rastrigin function - comparison of APS and APSE. | 36 |
| 2.7 | Griewank-2 function - effect of λ and β . | 37 |
| 2.8 | Griewank-2 function - comparison of APS and APSE. | 38 |
| 2.9 | Number of minima for $F(x)$. | 39 |
| 2.10 | Comparison of APS and APSE for $F(x)$. | 40 |
| 3.1 | Scaled Lennard-Jones pair potential. | 43 |
| 3.2 | Optimal structures - $N = 8, \dots, 13$ atomic clusters. | 45 |
| 3.3 | Lennard-Jones and Morse pair potentials. | 54 |
| 3.4 | Three atom cluster configuration. | 56 |
| 3.5 | Cross-section of PES for $N = 3$. | 56 |
| 3.6 | Pair potentials for $v_1(\alpha, r)$. | 58 |

| | | |
|------|--|-----|
| 3.7 | Pair potentials for $v_2(\alpha, r)$ | 59 |
| 3.8 | Pair potentials for $v_3(\alpha, r)$ | 59 |
| 3.9 | PES around global minimum, $N = 6$, $v_3(\alpha, r)$ | 60 |
| 3.10 | PES around global minimum, $N = 18$, $v_3(\alpha, r)$ | 61 |
| 3.11 | PES around global minimum, $N = 29$, $v_3(\alpha, r)$ | 61 |
| 3.12 | Minimal energy structures - $N = 29, \dots, 31$ atomic clusters | 69 |
| 4.1 | GEM* processing context | 77 |
| 5.1 | GEM* optimised structure - $N = 77$ atomic cluster | 84 |
| 5.2 | GEM* optimised structure - $N = 78$ atomic cluster | 85 |
| 5.3 | Minimum, maximum and average population energies, $N = 72$ | 85 |
| 5.4 | Generations required to optimise atomic clusters, $N = 2, \dots, 80$ | 86 |
| 5.5 | Multiprocessor scalability of GEM* | 87 |
| 5.6 | Structures found - GEM* optimisation of an $N = 18$ cluster | 89 |
| 5.7 | Structures found - GEM* optimisation of an $N = 18$ cluster | 90 |
| 5.8 | Structures found - GEM* optimisation of an $N = 56$ cluster | 91 |
| 5.9 | Structures found - GEM* optimisation of an $N = 56$ cluster | 92 |
| 5.10 | Structures found - GEM* optimisation of $N = 37, 38$ clusters | 93 |
| 5.11 | Initial and final energies for χ_1 crossover | 95 |
| 5.12 | Initial and final energies for χ_2 crossover | 95 |
| 5.13 | Energy trajectories for χ_1 crossover | 96 |
| 5.14 | Energy trajectories for χ_2 crossover | 96 |
| 5.15 | Effect of close atoms on the BFGS optimised energy | 97 |
| 5.16 | Expected number of close atoms from a χ_1 crossover | 99 |
| 5.17 | Expected number of close atoms from a χ_2 crossover | 102 |
| 5.18 | Expected and average number of close atoms for χ_1 | 103 |
| 5.19 | Expected and average number of close atoms for χ_2 | 103 |

| | | |
|------|---|-----|
| 6.1 | Lennard-Jones pair potentials for Ar , Xe | 107 |
| 6.2 | Minimum population energies for $Ar_{10}Xe_{10}$ | 111 |
| 6.3 | Optimised structure for Ar_5Xe_2 | 113 |
| 6.4 | ΔE for $Ar_{7-n}Xe_n$, $Ar_{13-n}Xe_n$ and $Ar_{19-n}Xe_n$ | 114 |
| 6.5 | ΔE for $Ar_{10-n}Xe_n$ | 114 |
| 6.6 | GEM* optimised structures - $Ar_5Xe_5, \dots, Ar_2Xe_8$ | 116 |
| 6.7 | ΔE for $Ar_{12-n}Xe_n$ | 117 |
| 6.8 | GEM* optimised structures - Ar_1Xe_{11}, Ar_0Xe_{12} | 117 |
| 6.9 | ΔE for $Ar_{17-n}Xe_n$ | 118 |
| 6.10 | GEM* optimised structures - $Ar_6Xe_{11}, \dots, Ar_3Xe_{14}$ | 119 |
| 7.1 | Intermolecular pair potentials for benzene molecules. | 124 |
| 7.2 | Intramolecular pair potentials for water molecules. | 128 |
| 7.3 | Intermolecular pair potentials for water molecules. | 128 |
| 7.4 | Coulombic potentials for water molecules. | 129 |
| 7.5 | GEM* optimised structures - benzene dimer...pentamer. . . . | 134 |
| 7.6 | GEM* optimised structures - benzene hexamer...nonamer. . . | 135 |
| 7.7 | GEM* optimised structures - water dimer and hexamer. . . . | 136 |
| 8.1 | Globally optimal $N = 61$ model molecular structure. | 139 |
| 8.2 | Globally optimal energies - model molecular structure. | 139 |
| 8.3 | Changes in optimal energy - model molecular structure. . . . | 140 |
| 8.4 | Genetic encoding for the model molecular structure. | 142 |
| 8.5 | GEM* optimised structures - model molecular structure. . . . | 145 |
| 8.6 | GEM* optimised structures - model molecular structure. . . . | 146 |
| 9.1 | Structure of the united atom butane molecule. | 151 |
| 9.2 | Structure of the pseudoethane molecule. | 151 |
| 9.3 | Structure of the acetyl chloride molecule. | 153 |

List of Tables

| | | |
|-----|---|-----|
| 2.1 | Summary test results for APS and APSE. | 40 |
| 3.1 | Minimum energies - atomic clusters, $N = 2, \dots, 105$ | 46 |
| 3.2 | Counts of Lennard-Jones and Morse local minima. | 55 |
| 3.3 | APSE function evaluations required for $N = 3, \dots, 20$ | 65 |
| 3.4 | Energy trajectories for APSE with PES smoothing. | 66 |
| 3.5 | Total energy trajectories for APSE with PES smoothing. . . . | 66 |
| 6.1 | Lennard-Jones parameters for Ar and Xe pair potentials. . . | 106 |
| 7.1 | Structural parameters for benzene. | 123 |
| 7.2 | Potential energy parameters for benzene. | 124 |
| 7.3 | RWK2 potential parameters. | 127 |
| 7.4 | Optimised potential energy values for benzene clusters. . . . | 133 |
| 7.5 | Optimised potential energy values for water clusters. . . . | 133 |
| 8.1 | Performance of search methods - model molecular structure. . | 141 |
| 8.2 | Packed hexagonal energies for the model molecular structure. | 144 |
| 9.1 | Lennard-Jones parameters - pseudoethane. | 152 |
| 9.2 | Local minima for pseudoethane. | 152 |
| 9.3 | Van der Waals parameters for acetyl chloride. | 153 |
| 9.4 | Acetyl chloride Cartesian coordinates | 153 |

Acknowledgments

I first commenced doctoral studies in optimal control theory and, while investigating optimisation theory in that context, had the good fortune to meet my current supervisor, Professor Graham Wood. I certainly must thank him for introducing me to the fascinating field of molecular optimisation. Over the last few years Graham has been very supportive and encouraging. In particular, his high academic standards and professionalism set a standard which I hope that I have gone some way towards achieving. In addition, I must thank him for the provision of Newton, an IBM RS6000 workstation, without which none of this work would have been possible.

During the course of these studies I had the opportunity to be present at a considerable number of seminars/discussion groups on various aspects of global optimisation. I certainly benefited from these occasions and would like to thank Graham, Dr. Victor Korotkikh, Professor Zelda Zabinsky (University of Washington) and Dr. Bill Baritompa (University of Canterbury) for sharing their knowledge.

I also owe a considerable debt to the late Professor John Smith who provided me with the opportunity to come to Central Queensland University and commence these studies. Finally, I would like to acknowledge the support I received from Central Queensland University, in particular the Department of Mathematics and Computing and the Faculty of Applied Science, in providing the resources and time away that were so necessary for this work.

Declaration

All computer software used to produce the results contained in this thesis is, with the exception of the BFGS local optimiser, the Powell Direction Set local optimiser and the XMOL software, the work of the candidate.

Except for that attributed to other authors and included for the purpose of setting the appropriate context, all material in this thesis is the work and writing of the candidate. Of the material due to the candidate, only the following has appeared, or is expected to appear, elsewhere:

- Chapter 2 and Sections 3.3.1 and 3.4.1 appeared in the Australian Computer Journal, Vol. 28, No. 4, November 1996.
- Chapter 6 has been accepted for publication by the Journal of Computational Chemistry.
- Sections 4.2, 5.2, 5.3 and 5.4 have been submitted to the Journal of Global Optimization.
- Section 3.3.2 appeared as Technical Report 95 – 010, Department of Mathematics and Computing, Central Queensland University.
- Chapter 7 appeared as Technical Report 96 – 005, Department of Mathematics and Computing, Central Queensland University.
- Chapters 8 and 9 appeared as Technical Report 96 – 006, Department of Mathematics and Computing, Central Queensland University.



Wayne Pullan (C9302023X)

Chapter 1

Introduction

1.1 Overview

This thesis addresses the problem of identifying those configurations of molecular structures which correspond to the globally minimum potential energy for that structure. In general terms, this global optimisation problem can be stated as:

$$\min_{x \in S} f(x)$$

where $S \subset R^n$ and $f : R^n \rightarrow R$ is a function, usually referred to as the objective function, which may be both non-continuous and non-convex. There appears to be no single algorithm which effectively solves all global optimisation problems. Deterministic optimisation methods such as branch and bound are practical for low dimension problems, while stochastic methods such as simulated annealing and genetic algorithms theoretically converge to the global optimum, but in practice are slow, requiring large numbers of function evaluations.

Molecular architecture is concerned with structures which arise as a result of non-bonded and bonded interactions between atoms. The potential energy of these structures can be calculated using appropriate force field models and, as shown by experimental evidence [30], in the great majority

of cases, the global minimum of the potential energy corresponds to the most stable configuration of the molecular structure. As this configuration dictates most of the properties of the molecular structure, it is of particular importance. However, as the potential energy function is non-convex and typically has many local minima, global minimisation of potential energy functions is an extremely difficult problem which, for many years, has been investigated by chemists and physicists. In more recent years however, researchers from optimisation and computer science have also investigated this problem and, in fact, the minimisation of non-convex potential energy functions arising from molecular conformation or protein folding problems has become one of the most important interdisciplinary problems [43, 38].

Within this chapter, Section 1.2 presents an overview of molecular structures and their associated potential energy functions. Section 1.3 provides a brief review of local optimisation techniques while Section 1.4 contains an overview of the major global optimisation methods. The layout of the remaining chapters of this thesis is described in Section 1.5.

1.2 Molecular Architecture

According to the theory of quantum mechanics [2], the energy and many properties of a stationary state of a molecular structure can be obtained by solution of Schrödinger's partial differential equation

$$\hat{H}\Psi = E\Psi$$

where

- \hat{H} is the Hamiltonian, a differential operator representing the total energy.
- E is the energy of the state.

- Ψ is the wave function which depends on the Cartesian coordinates of all particles (which may take on any value from $-\infty$ to $+\infty$) and also on the spin coordinates (which may take only a finite number of values corresponding to spin angular momentum components in a particular direction). The square of the wave function, $|\Psi|^2$, is interpreted as a measure of the probability distribution of the particles within the molecule.

In principle, solution of Schrödinger's equation could lead to a direct quantitative prediction (ignoring relativistic effects) of most, if not all, chemical phenomena using only the values of a small number of physical constants (Planck's constant, the velocity of light, and the masses and charges of electrons and nuclei). Such a procedure constitutes an ab initio approach to chemistry, independent of any experiment other than determination of these constants. However, as has been recognised since shortly after Schrödinger's equation was discovered, solution of Schrödinger's equation is a formidable, if not completely impossible, mathematical problem for all but the very simplest of systems.

The underlying physical laws necessary for the mathematical theory of a large part of physics and the whole of chemistry are thus completely known, and the difficulty is only that the exact application of these laws leads to equations much too complicated to be soluble [P.A.M. Dirac, Proc. Roy. Soc. (London), 123, 714 (1929)]

In practice, Schrödinger's equation is replaced by approximate mathematical models for which the possibility of solution exists. Two models in common use are:

- Ab Initio Methods [2], which generally model the true waveform in terms of a linear combination of atomic orbitals. Schrödinger's equation has been solved exactly for the hydrogen atom but never for any more complicated structure. Ab Initio methods introduce an approximation for the wave functions by using a sum of atomic orbitals. The larger the expansion of the wave function in terms of the atomic orbitals, the more accurate the approximation becomes. However, as commonly used atomic orbitals involve the calculation of large number of integrals, the computational requirements rapidly become excessive. For this reason, rather short expansions must be used for large molecules, so the resulting energy may be far from the global minimum.

Ab Initio methods are not considered in this thesis.

- Molecular Mechanics [4], which uses the concept of a classical force field to describe the restoring forces that occur in a molecule when the geometry of minimal potential energy is disturbed. Force fields describe forces with respect to a so-called “strain-free” molecular geometry or, more generally, with respect to a molecular “reference geometry”.

Molecular Mechanics is a widely used calculation method which determines reasonably accurate structures and energies for molecules. The method is a natural outcome of older ideas of bonds between atoms in molecules and van der Waals forces between non-bonded atoms. It employs the fundamental formulations of vibrational spectroscopy, in that bonds have “natural” lengths and angles, and molecules will tend to adjust their geometries so as to take up these values.

The Born-Oppenheimer approximation, which is commonly used in molecular and quantum mechanics, states that Schrödinger's equation for a molecule can be separated into a part describing the motions of the electrons and a part describing the motions of the nuclei, and that these two sets of motions can be studied independently. For studies involving molecules near their (nuclear) local or global minimum structures in the electronic ground state, it is a reasonable approximation. Molecular mechanics uses this approximation in that the motions of the nuclei are studied and the electrons are not explicitly examined at all (they are simply assumed to find an optimal distribution about the nuclei) so the energy of the molecule in the ground electronic state becomes solely a function of the nuclear positions. The Born-Oppenheimer surface is the multi-dimensional “surface” that describes the energy of the molecule in terms of the nuclear positions and is usually referred to as the Potential Energy Surface (PES).

Molecular mechanics calculations employ an empirically derived set of equations for the Born-Oppenheimer surface whose mathematical form is familiar from classical mechanics. This set of potential functions, conventionally (and incorrectly) referred to as the “force field”, contains adjustable parameters that are optimised to obtain the best fit of calculated and experimental properties of molecules (such as geometry, conformational energy and heat of formation). The assumption is always made in molecular mechanics that these adjustable parameters and force constants may be transferred from one molecule to another. In other words, these parameters are evaluated for a set of simple molecules, and thereafter the values are fixed and can be used for other similar molecules.

The molecular structures studied in this thesis are now described in more detail.

1.2.1 Atomic Clusters

Atomic clusters are currently an active field of theoretical and experimental research. Atomic clusters are aggregates of atoms¹, sufficiently small so that a significant proportion of the atoms are present on the surface of the cluster. Theoretical investigations of atomic clusters address the following optimisation problem

*Given N particles, interacting with two-body central forces,
find the configuration in three-dimensional Euclidean space for
which the total potential energy attains its global minimum.*

Simplifications normally used are:

- Many-body and angle dependent interactions are ignored.
- Quantum effects are not taken into account.
- All particles are assumed to be spherical and of equal size.

Using these simplifications, the potential energy (V) of an N atom cluster can be written as:

$$V = \sum_{i=1}^{N-1} \sum_{j=i+1}^N v(r_{ij})$$

where r_{ij} is the Euclidean distance between atoms i and j and $v(r_{ij})$ is the pair potential acting between atoms i and j . A number of different forms of $v(r)$ have been used in physical models, of which the following three are of particular interest to this study

$$\begin{aligned}v_{lj}(r) &= r^{-12} - 2r^{-6} \\v_m(r) &= (1 - \exp(3(1 - r)))^2 - 1 \\v_b(r) &= A \exp(Br) + Cr^{-6}\end{aligned}$$

¹Within this thesis, the symbol N is reserved for the number of atoms or molecules in a molecular structure.

where v_{lj} is the scaled Lennard-Jones pair potential, v_m the Morse pair potential and v_b the Buckingham pair potential. The repulsive components of these pair potentials are due to coulombic nuclear-nuclear and electron-electron interactions, while the attractive components are due to electron-nuclear interactions. For the Lennard-Jones pair potential, the attractive term $-2r^{-6}$ is rigorously derived for a pair of identical, spherically symmetrical and chemically saturated atoms while the r^{-12} term is an approximation for the repulsive component for which no rigorously derived expression exists [30].

Even with the simplifying assumptions specified above, global minimisation of the potential energy of an atomic cluster is very difficult as it is a non-convex optimisation problem involving numerous local minima. In fact, Hendrickson [17] has shown that, in theory, even simple versions of the problem are NP -complete.

As an example of the structure of these atomic clusters, Figure 1.1 shows the optimal structure for the 55 atom scaled Lennard-Jones cluster obtained by the optimisation method presented in Chapter 5. In this structure, one atom is positioned at the centre, 12 are positioned on the vertices of an icosahedral lattice which is centred on the first atom and the remaining 42 are positioned at the vertices of a second enclosing icosahedral lattice which is also centred on the first atom.

1.2.2 Molecular Clusters

For a considerable period of time, the structure and energy levels of small molecular clusters, generated by free jet expansion, have been extensively studied by optical spectroscopy, mass spectrometry and electron diffraction. These studies are of considerable importance for the understanding of molecular interactions as they relate to a phase of matter between the gaseous

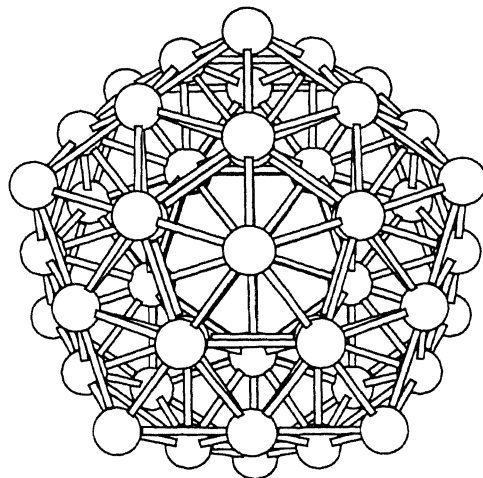


Figure 1.1: Optimal structure for the 55 atom scaled Lennard-Jones cluster. While this is a non-bonded structure, bonds have been included in the figure to highlight the basic icosahedral lattice structure of the optimal cluster.

and condensed phase. The most direct information about cluster structure is obtained by electron diffraction methods. However, for smaller clusters, structural models are required to calculate the intensity functions. Using a crystalline model is probably inappropriate in this size domain so other models incorporating the equilibrium geometry are required. Using appropriate force field models, global optimisation methods allow these minimum energy structures to be determined.

Whenever molecules are in close proximity to each other, the following three types of interactions occur

- a long-range coulombic interaction arising from the molecular electric potential, usually viewed as originating from net charges on the atoms, and which may be either an attractive or repulsive interaction.
- an intermediate-range dispersion interaction which is always attractive.

- a short-range exchange repulsion interaction which increases rapidly at close range and is responsible for the “size” of each atom within the molecule.

This combination of short, intermediate and long-range interactions leads to a complicated intermolecular potential energy surface which includes many local minima as well as the global minimum.

Optimisation of molecular clusters is inherently more difficult than that of atomic clusters for two reasons. Firstly, three extra parameters (normally the Euler angles) are required for each molecule so that its orientation may be specified and secondly, the molecule may not be a rigid body so that additional parameters are required to specify the shape of the molecule.

Figure 1.2 shows the optimal configuration for a cluster of four rigid benzene molecules, obtained by the optimisation method presented in Chapter 7, where the molecular force field was modelled using both the Buckingham pair potential and a coulombic interaction. This optimal configuration has a basic tetrahedral structure with an edge-to-plane orientation of molecules.

1.2.3 Molecules

As distinct from clusters, molecules are created when a group of atoms are joined via electronic bonds. These bonds may involve a sharing of electrons to form a covalent bond, or a transfer of electrons to form an ionic bond. As well as these relatively high energy bonds, atoms within a molecule interact via pairwise van der Waals potentials and also possibly through a coulombic effect. In the molecular mechanics model of a molecule, the concept of a force field is used to describe the restoring forces that occur in a molecule when the geometry of minimal potential energy is disturbed.

Simple molecular mechanics force fields include bond stretching (E_S),

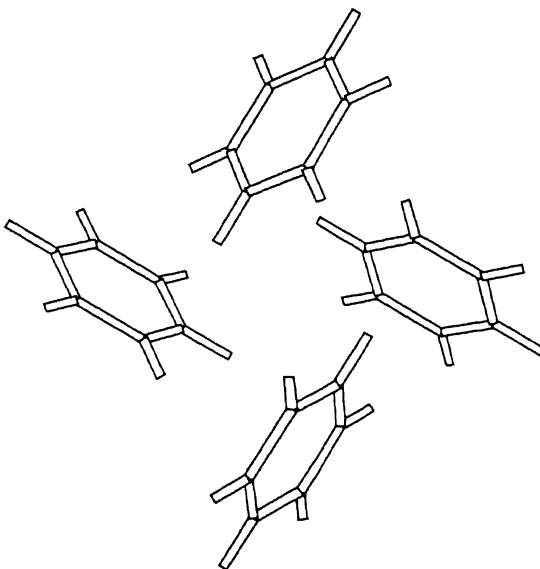


Figure 1.2: Optimal structure for the benzene tetramer. This is a tetrahedral configuration with a basic edge-to-plane orientation of molecules.

bond angle bending (E_θ), torsion (or dihedral) angle (E_ω) and van der Waals (E_v) interactions in their make-up. The sum of all these terms is the potential energy E of the molecule

$$E = \sum E_s + \sum E_\theta + \sum E_\omega + \sum E_v$$

where the sums extend over all bonds, bond angles, torsion angles, and non-bonded interactions between all atoms not bound to each other or to a common atom, respectively.

The structure of the octane molecule is shown in Figure 1.3. With reference to this figure, atoms 1 through 8 form the carbon atom backbone of the octane molecule while atoms 9 through 26 are bonded hydrogen atoms. The structure of this molecule can be specified using 8 torsion angles (for example, the torsion angle between the plane defined by atoms 9, 1 and 2 and the plane defined by atoms 1, 2 and 12), all possible bond angles (for example, the bond angle defined by atoms 11, 1 and 2) and all bond lengths.

As the energy associated with changing bond angles and lengths is relatively high, to a first approximation, the molecule may be modelled using a force field which assumes that bond angles and lengths remain constant and only torsion angles vary.

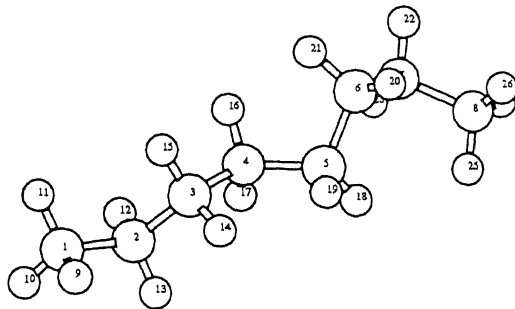


Figure 1.3: Molecular structure of the octane molecule.

With more complicated molecules there will, in general, be a large number of energy minima of different depths. To a first approximation, the molecule is described by the structure corresponding to the global energy minimum. To the next approximation, it is described by an equilibrium mixture of molecules at all minima in a Boltzmann distribution. A still more refined approximation allows for the fact that the molecules do not remain motionless at points at the bottom of these energy wells, but rather are vibrating over a portion of the surface around the energy minima. Finally, thermal motions carry some of the molecules across saddle points from one minimum to another, at a rate corresponding to the Gibbs free energy of activation.

1.3 Local Optimisation

The fundamental structure of all deterministic local optimisation techniques for finding an optimal value for an objective function f is

Local Optimisation Algorithm

Initial Step:

Set $k = 0$.

Supply an initial guess, \mathbf{x}_k , within any specified constraints.

Iterative Step:

- a) Calculate a search direction \mathbf{p}_k .
- b) Determine an appropriate step length λ_k .
- c) Set \mathbf{x}_{k+1} to $\mathbf{x}_k + \lambda_k \mathbf{p}_k$.

Stopping Criteria:

If convergence criterion reached

Optimum vector is \mathbf{x}_{k+1} .

stop.

else

Set $k = k + 1$.

Repeat Iterative Step.

Local optimisation algorithms may be classified into non-derivative, gradient and second derivative (Newton) categories depending on the techniques used to determine the search direction \mathbf{p}_k . The convergence criterion normally involves the following gradient condition

$$\|\mathbf{g}_k\| \leq \epsilon_g(1 + |f(\mathbf{x}_k)|), \text{ for all } k$$

where \mathbf{g}_k is the gradient at the k th iteration and ϵ_g is a small positive number (such as the square root of the computer's floating point precision).

The two local optimisation techniques used as components within the global optimisation method developed in this thesis are Powell's Direction Set method (a non-derivative method) and the Broyden, Fletcher, Goldfarb and Shanno (BFGS) gradient method. A theoretical description of these methods may be found in [42].

Clearly the major disadvantage of deterministic local optimisers is that, when a function has multiple minima, the minimum found is totally dependent on the starting point, x_0 , and may not in fact be the global minimum. However, in the global optimisation context, these techniques are useful as they enable the search to proceed directly to the local minimum of a “catchment basin”.

1.4 Global Optimisation

Global optimisation is concerned with the identification of global minima or maxima of non-linear functions. These functions may have several local minima with very different function values. The problem of designing algorithms to obtain global solutions is very difficult since, in general, there is no local criterion for deciding whether a local solution is, in fact, the global solution. From the complexity point of view, global optimisation belongs to the class of *NP*-hard problems. That is, the computational time to solve a problem increases exponentially as a function of the problem size.

A large number of publications have appeared during the past three decades on the subject of global optimisation or related problems. These papers discuss a variety of deterministic and stochastic methods for finding global solutions to non-linear optimisation problems. Deterministic methods, which may be effective for low-dimensional problems, include enumerative techniques, cutting planes, branch and bound, decomposition based approaches, bilinear programming, interval analysis, homotopy methods, interior point methods, and approximate algorithms for large-scale problems. Stochastic methods include random search and clustering techniques, simulated annealing and genetic algorithms.

As the optimisation problems to be addressed in this thesis are

high-dimensional, deterministic methods are not suitable and the focus is on the development of stochastic methods. A summary of the more important existing stochastic methods is now presented.

1.4.1 Random Search

In its purest form, random search ([44], [49], [51]) simply consists of evaluating the objective function at a number of points selected from the domain using a uniform distribution. In spite of its evident simplicity, random search offers an asymptotic guarantee of convergence [45]. However, because of the computational overhead, pure random search is seldom an efficient global optimisation method. Most practical implementations of random search have incorporated two phases. A global phase, where the function is sampled randomly at a number of points, and a local phase where, starting from the randomly sampled points local optimisations are performed, are used to find candidate global minimum (the Multistart technique [45]).

1.4.2 Simulated Annealing

Simulated Annealing (SA) ([25], [26]) is a general purpose optimisation technique which is an extension of a Monte Carlo method developed by Metropolis et al. [33] to determine the equilibrium states of a collection of atoms at any given temperature, T . SA exploits an analogy between the way in which a metal cools and freezes into a minimum energy crystalline structure (the annealing process) and the search for a minimum in a more general system. As described in [25], the SA algorithm employs a random search which not only accepts changes that decrease the objective function f , but also some changes that increase it. Within the SA algorithm, whenever a new point is evaluated, it will be accepted as the current point with probability

$$\exp(-\delta f/kT)$$

where δf is the difference in objective function values between the current point and the new point, k is Boltzmann's constant and T is known as the system "temperature", irrespective of the objective function involved. As the SA algorithm progresses, T is slowly reduced according to an annealing schedule. This determines the degree of uphill movement permitted during the search and is critical to the algorithm's performance. The principle underlying the choice of a suitable annealing schedule is easily stated – the initial temperature should be high enough to "melt" the system completely and should be reduced towards its "freezing point" as the search progresses. However there is no known analytical procedure for choosing the rate at which the temperature decreases in the annealing schedules and choices vary from a simple exponential cooling schedule such as

$$T_{k+1} = \alpha T_k$$

(where α is less than but close to 1) to more elaborate adaptive cooling schedules using statistical measures of the algorithm's current performance to modify its control parameters.

In summary, SA's major advantage over random search is that it allows movement to higher energy states, with decreasing probability, which increases the probability of transitions out of the catchment basins of local minima. As is the case for random search, SA offers an asymptotic guarantee of convergence [1].

1.4.3 Genetic Algorithms

Genetic Algorithms (GAs) are based on the process of natural selection [22] where the proportion of "fitter" individuals in a population tends to increase at each generation. Standard GAs operate on a binary encoded version of the parameters of a problem and use genetic operators such as selection

based on a fitness factor, random mutation and crossover to generate a new population from an existing population of individuals. As the genetic algorithm is the basis for the main computational method developed within this thesis, their theoretical basis is now described in detail.

The concept of building blocks within individuals is a central part of GAs and the proliferation of “good” building blocks is the fundamental mechanism by which GAs assemble good solutions to problems. These building blocks, usually referred to as schemata (singular schema), can be thought of as pattern matching templates. Schemata multiply under the influence of genetic operators as the GA proceeds at a rate predicted by the Schema Theorem [13]. An account of this theorem is now presented.

At the end of each generation of a GA, individuals are selected for inclusion in the next generation on the basis of their fitness, f_i . If there are n individuals in the population at generation t , then, using a fitness based probabilistic selection method, the expected number of copies of individual i in generation $t + 1$ ($m_i(t + 1)$) is

$$m_i(t + 1) = f_i/\bar{f}$$

where

$$\bar{f} = \sum_i f_i/n$$

If a schema H was only present in individual i , this equation tells us how many copies of the schema should occur in the new population. However, as one schema may be contained in several different individuals, each with its own fitness, the expected number of copies of the schema H in the $(t + 1)$ th generation becomes

$$m(H, t + 1) = m(H, t)f(H)/\bar{f} \quad (1.1)$$

in which $f(H)$ is the average fitness of all individuals containing the schema

H . The rate at which a schema proliferates in the population therefore depends upon the ratio of the average fitness of the individuals which contain the schema to the average fitness of the population as a whole. Thus a schema which confers a large fitness benefit upon any individual that contains it will multiple rapidly in the population and, conversely, a low fitness schema will be rapidly discarded.

If a schema H is always fitter than the average fitness by a fixed proportion β then

$$\begin{aligned} m(H, t+1) &= m(H, t)(\bar{f} + \beta\bar{f})/\bar{f} \\ &= (1 + \beta)m(H, t) \end{aligned}$$

Starting at $t = 0$, the number of examples of the schema in the population grows according to the equation

$$m(H, t) = m(H, 0)(1 + \beta)^t$$

That is, the number of copies of a consistently above average schema increases geometrically in a population, while the number of copies of below average schema ($\beta < 0$) will diminish geometrically. This growth in numbers of high quality schema takes place for all schemata simultaneously. In fact, it can be shown [13] that the number of schemata processed usefully at each generation is of the order of n^3 for a population of n individuals. This simultaneous processing of many schemata is known as “implicit parallelism” and is a crucial reason why GAs can successfully search even massive surfaces.

However, this growth of schemata is also affected by the action of any genetic operators. The probability p that a schema will not be cut by a genetic crossover operator is at least

$$1 - p_c\delta(H)/(l - 1)$$

where p_c is the probability of crossover, $\delta(H)$ is the total length of the schema and l is the length of the individual. Combining this with Equation 1.1, the expression for the rate at which reproduction causes schema to proliferate, we have

$$m(H, t + 1) \geq m(H, t)f(H)[1 - p_c\delta(H)/(l - 1)]/\bar{f} \quad (1.2)$$

This equation shows that schema of low defining length contained in individuals of high fitness are those that multiply most rapidly.

If $o(H)$ represents the order of the schema H (the number of fixed positions) then the probability that a schema will not be affected by a random genetic mutation operator is $(1 - p_m)^{o(H)}$ where p_m is the probability of mutation. For small values of p_m , this may be approximated by $1 - o(H)p_m$. Combining this with Equation 1.2 we get the result known as the schema theorem or the fundamental theorem of genetic algorithms

$$m(H, t + 1) \geq m(H, t)f(H)[1 - p_c\delta(H)/(l - 1) - o(H)p_m]/\bar{f} \quad (1.3)$$

From this result it can be concluded that standard (binary-coded) GAs are efficient when applied to problems whose parameters can be encoded as short, low-order schema which are relevant to the underlying problem and relatively unrelated to schema over other fixed positions.

To improve the convergence of genetic algorithms, a number of techniques may be utilised. For example, the “elitist” approach, where the fittest individual found so far is always maintained as a pool member, invariably enhances convergence to the global minimum. In fact, as shown in [46], a simple standard genetic algorithm using the elitist approach will always converge to the global minimum. Alternatively, a hybrid genetic algorithm incorporating other optimisation methods within the genetic algorithm environment may be used to improve convergence. For example, a

standard (binary-coded) GA with coarse parameter resolution may be used in conjunction with a local optimiser. The GA would produce near optimal solutions while the local optimiser would perform a fine-tuning operation. The major problem inherent in this method is that the discretisation of the parameters may be such that the difference between two adjacent parameter values covers a number of minima (i.e. spans a number of catchment basins as shown in Figure 1.4(a)). As the local optimiser is a deterministic

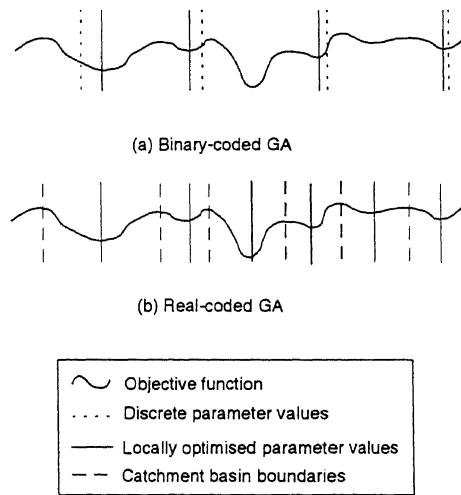


Figure 1.4: GA parameter mappings to objective function - (a) Binary-coded parameter values and corresponding locally optimised values and (b) Real-coded parameters (mapping to the complete surface) and locally optimised values.

method, unless a random start is used within the range of the discretisation, the same minimum will always be found. As this local minimum could be relatively large, a solution may tend to be discarded rather than retained, even though it might be the closest possible to the global minimum.

An alternative approach is to use a real-coded GA in conjunction with a local optimiser. While the real-coded GA is able to map to all points on

the surface, the local optimiser will subsequently translate each point to the local minimum of the catchment basin within which the point lies. Because of this mapping of all points within a catchment basin to a single point, this real-coded GA/local optimiser hybrid is, in effect, a variable interval, discretised GA where the interval of discretisation at any point is related to the “size” of the catchment basin within which the point lies (Figure 1.4(b)). For both these hybrid methods, as the basic “building blocks” required by the Schema Theorem (1.3) exist, it is reasonable to expect that this theorem (or a variant) is still applicable and the search will benefit from implicit parallelism. However, the real-coded GA with local optimisation is preferable to the binary-coded GA with local optimisation as it adapts to the “surface” being searched and does not have the potential to hide minima.

1.5 Outline of Thesis

Chapter 2 of this thesis describes the work which lead to the development of APSE, a stochastic direct search method, while Chapter 3 describes the results obtained by applying APSE, in conjunction with a build-up approach, local optimisation and PES smoothing, to the pure atomic cluster problem. This technique was relatively successful and found all currently accepted global minimum energy values for clusters in the range $N = 2, \dots, 30$. However, as discussed in Section 3.5, whenever there is a major “structural discontinuity” in the cluster size range, the use of a build-up approach actually inhibits rather than enhances the optimisation method. From the analysis presented in Section 4.1, it became apparent that the best approach for designing a global optimisation method for the molecular architecture problem was to implement an algorithm which used a combination of APSE global optimisation and local optimisation within a genetic algorithm environment.

Chapter 4 describes the development of such an algorithm, GEM^{*2}, the major computational method used in this study. Using suitable tailoring of algorithms within GEM*, global optimisation software targeted at particular classes of molecular structures may be generated.

Chapter 5 describes the results obtained by applying GEM* to the pure atomic cluster problem and presents a theoretical comparison of the phenotype genetic crossover operators implemented in GEM* with more standard genetic crossover operators. GEM* was particularly successful in optimising pure atomic clusters and, from random initial configurations, found all currently accepted global minima for clusters containing between 2 and 80 atoms. In addition, new lower minima were found for the 77 and 78 atom clusters.

The results obtained by applying GEM* to mixed argon–xenon atomic cluster problems are described in Chapter 6. Optimisation of these mixed clusters is complicated by the presence of two additional forms of pair potential. Prior to this work, a lattice-based search had found minima energy structures for 7, 13 and 19 mixed atom structures. GEM*, using random initial configurations, found global minima for all mixed clusters in the range 2, . . . , 20 atoms and was also able to improve some of the previous results.

Optimisation of clusters of benzene and water molecules by GEM* is discussed in Chapter 7. As these molecules cannot be regarded as simple points, extra parameters are required to specify their orientation and, in the case of water, the shape of the molecule. In addition, the presence of different types of atoms within the molecules gives rise to a number of different pair potentials which further complicates the optimisation problem. Previous attempts at optimising benzene clusters used lattice-based techniques

²GEM* → a schema for “Global Energy Minimiser for pure and mixed atomic clusters, molecular clusters and molecules”.

and optimised some clusters containing between 2 and 13 molecules. The only attempt using random initial configurations was successful for clusters containing between 2 and 4 molecules. GEM* obtained all global minima for benzene clusters of 2 to 6 molecules and very good values for all clusters containing between 7 and 12 molecules. For clusters of water molecules, GEM* was less successful, mainly because of the limited computational resources which were available. The calculation of the potential energy for a water cluster is computationally intensive and the time required on the available computers became excessive. However, GEM* did obtain results suggesting that, given more powerful computing facilities, it would be successful on these problems.

Chapter 8 describes the optimisation results obtained by GEM* for a two-dimensional model molecule consisting of N atoms connected by rigid bonds of unit length where the potential energy is given by the pairwise addition of scaled Lennard-Jones potentials. While this model problem is a very simple representation of a molecule, it is useful for developing molecular structure optimisation methods, as the dimension of the problem is easily adjusted and the global minimum energy can be easily determined for any dimension (all optimal configurations are approximately located on a hexagonal grid with unit spacing [23]). Of particular interest are 19, 37 and 61 atom structures whose optimal configurations form maximally compact hexagonal structures of radii 2, 3 and 4. Prior to this study, only the 19 atom structure had been successfully optimised, whereas GEM* was successful for both the 19 and 37 atom structures. In addition, GEM* successfully optimised all other structures in the range $N = 3, \dots, 42$ as well as those for $N = 44, 45, 46, 49, 50$ and 53 atoms.

Chapter 9 presents the optimisation results obtained by GEM* for the

united atom butane, pseudoethane and acetyl chloride molecules. All these molecules were successfully optimised by GEM* and while all are relatively simple in structure, they did require that all features necessary for optimisation of larger molecules be implemented and used within GEM*.

A summary of this thesis and future research directions are presented in Chapter 10 while the appendices contain the analytical derivation of the potential energy gradients required for the implementation of the BFGS local optimiser and tables describing the structures obtained for mixed atomic clusters.

Chapter 2

APSE Computational Method

2.1 Introduction

The development of an existing Adaptive Probabilistic Search (APS) algorithm [3] to produce APSE (Adaptive Probabilistic Search Extended) is described in this chapter. APS is a direct search method for locating the global minimum of a multimodal function and requires no prior assumptions about the search domain, nor about the continuity, differentiability or modality of the function. In [3], Benke and Skinner used a number of benchmark problems and some practical applications to compare the performance of APS with other global optimisation algorithms including random search, various adaptive and guided random search methods, and stochastic automata. They found that, compared to these methods, APS required fewer function evaluations and obtained more accurate results.

APSE implements the basic APS algorithm but also adaptively focuses on those subsets of the search domain which have a greater probability of producing an improving objective function value. In addition, APSE is also able to perform searches where the parameters are constrained to specified ranges. This allows operations such as a “global” search within a particular

subset of the search domain to be performed. For global optimisation of molecular architectures, this is a particularly useful operation as it allows an intensive search to be performed within a structurally “close” region of a particular configuration.

Within this chapter, Section 2.2 describes the APS algorithm and extensions implemented in APSE. A proof of convergence for APSE is presented in Section 2.3 while Section 2.4 evaluates both APS and APSE using standard test functions and also investigates the relationship between problem dimensionality and the number of function evaluations required by APSE to find a global minimum. These tests clearly demonstrate the improvements in efficiency that the extensions to the base APS algorithm produced.

2.2 APS and APSE Algorithms

Informally, to minimise a function $f < 0$, APS implements an adaptive probabilistic search algorithm by iteratively performing the following sequence:

Given a current point in the search domain of x_1 with objective value f_1 , randomly generate a new trial point x_2 resulting in objective value f_2 . A third trial point, x_3 (objective value f_3) is then generated according to

$$x_3 = \frac{f_1 x_1 + f_2 x_2}{f_1 + f_2}$$

The next iteration of this sequence uses $\arg \min(f_1, f_2, f_3)$ as the initial point x_1 . The assumption underlying APS is that, as the search progresses, improving points will tend to be found in the vicinity of the current best point x_1 . So, for every random point x_2 selected, another point x_3 is proportionally selected on a line between x_2 and the current best point x_1 . Clearly the x_2 point gives APS its global search of the domain while the x_3 point, as

the search progresses, provides a more local search around the current best point x_1 .

In more detail, the basic algorithm for APS, to minimise a function $f < 0$ is as follows:

APS Algorithm

Initial Step:

Set $k = 0$

Generate random vector x_1^k within specified constraints.

Set $f_1^k = f(x_1^k)$

Iterative Step:

a) Generate random vector x_2^k within specified constraints.

Set $f_2^k = f(x_2^k)$

b) Set $x_3^k = \frac{f_1^k x_1^k + f_2^k x_2^k}{f_1^k + f_2^k}$

Set $f_3^k = f(x_3^k)$

c) Set $x_1^k = \arg \min(f_1^k, f_2^k, f_3^k)$

Set $f_1^k = f(x_1^k)$

Stopping Criteria:

If termination criterion reached

Optimum vector is x_1^k

Optimum function value is f_1^k

stop.

else

Set $x_1^{k+1} = x_1^k$

Set $f_1^{k+1} = f_1^k$

Set $k = k + 1$

Repeat Iterative Step.

As suggested in [3], a possible mechanism for accelerating the rate at which APS converges to a minimum function value is to systematically contract the search domain during the course of the optimisation. That is if, after some number of iterations x_1 remains unchanged, then the domain over which x_2 is generated is progressively contracted in size. After the first contraction step, the centre of the contracted search domain is taken as the current x_1 and, whenever x_1 is changed, the contracted search do-

main is recentred at x_1 . Obviously the danger inherent in contracting the search domain is that the chance of finding a local minima rather than the global minimum is increased. To reduce this possibility, the extension was implemented in APSE as follows:

- if APSE remains at x_1 for a number of function evaluations then the search domain is contracted.
- this contraction occurs repeatedly for a specified number of iterations, then the process reverses and the search domain is expanded in steps until the original search domain is reached.
- this cycle of contraction/expansion is repeated a number of times and has the effect of biasing the search around x_1 but does not ignore more distant regions of the search domain.

Within APSE, all contractions/expansions of the search domain are by a factor of two with the parameters that control the contraction/expansion cycles being:

- the number of x_1 repeats required before a contraction/expansion of the search domain is performed, λ .
- the number of contractions performed before the expansion phase is entered, β .

Clearly the best values to be used for λ and β depend on the nature of the function being optimised.

Given λ and β , as defined above, plus the following definitions

- c_1 , the number of current x_1 repeats.
- c_2 , the net count of the number of contraction/expansion operations performed on the search domain S .

- Contracting, a boolean flag which is True when the search is in the phase of contracting the search domain.
- $\text{contract}(S)$, a function which contracts the search domain by one half in all dimensions.
- $\text{expand}(S)$, a function which doubles the search domain in all dimensions.
- $\text{recentre}(S, x)$, a function which recentres the search domain around x .

the APSE algorithm, to minimise a function $f < 0$ is as follows:

APSE Algorithm

Initial Step:

Set $k = 0$

Generate random vector x_1^k within specified constraints.

Set $f_1^k = f(x_1^k)$

Set Contracting = True; Set $c_1 = 0$; Set $c_2 = 0$

Iterative Step:

a) Generate random vector x_2^k within specified constraints.

Set $f_2^k = f(x_2^k)$

b) Set $x_3^k = \frac{f_1^k x_1^k + f_2^k x_2^k}{f_1^k + f_2^k}$

Set $f_3^k = f(x_3^k)$

c) If $f_1^k = \min(f_1^k, f_2^k, f_3^k)$ and $c_1 = \lambda$

$c_1 = 0$

If Contracting

If $c_2 < \beta$

$S = \text{contract}(S); c_2 = c_2 + 1$

else

Contracting = False; $S = \text{expand}(S); c_2 = c_2 - 1$

else

If $c_2 > 0$

$S = \text{expand}(S); c_2 = c_2 - 1$

else

Contracting = True; $S = \text{contract}(S); c_2 = c_2 + 1$

else

If $f_1^k = \min(f_1^k, f_2^k, f_3^k)$

$c_1 = c_1 + 1$

```

        else
             $c_1 = 0$ 
d) Set  $x_1^k = \arg \min(f_1^k, f_2^k, f_3^k)$ 
    Set  $f_1^k = f(x_1^k)$ ; recentre( $S, x_1$ )
Stopping Criteria:
If termination criterion reached
    Optimum vector is  $x_1^k$ ; Optimum function value is  $f_1^k$ ; stop.
else
    Set  $x_1^{k+1} = x_1^k$ ; Set  $f_1^{k+1} = f_1^k$ ; Set  $k = k + 1$ 
    Repeat Iterative Step.

```

Intuitively, the contraction/expansion of the current search domain assists convergence of the search because:

- when f_1 is considerably greater than the global minimum, there is a low probability that c_1 will reach the value required for a contraction in the search domain. Therefore the rate at which contraction/expansion cycles take place will be relatively slow. That is, the search will, on average, have a more “global” scope.
- when f_1 is close to the global minimum, there is a higher probability that c_1 will reach the value required for a contraction in the search domain. Therefore the rate at which contraction/expansion cycles take place will be relatively fast. That is, the search will, on average, be more localised around the current x_1 .

2.3 Convergence of APSE

A desirable feature of any search method is a theoretical proof that the method will converge to the global minimum. We present this now for APSE by first reducing APSE to the following conceptual algorithm:

APSE Conceptual Algorithm

| | |
|--|-------------------------------------|
| Step 1: | (APSE, Initialise Step) |
| Set $k = 0$. | |
| Find x_1^0 in S . | |
| Step 2: | (APSE, Iteration Step, Part a) |
| Generate x_2^k on R^n via μ_k . | |
| Step 3: | (APSE, Iteration Step, Part b) |
| Compute $x_3^k = G(x_1^k, x_2^k)$. | |
| Step 4: | (APSE, Iteration Step, Parts c & d) |
| Set $x_1^{k+1} = D(x_1^k, x_2^k, x_3^k)$. | |
| Step 5: | (APSE, Stopping Criteria) |
| Choose μ_{k+1} , set $k = k + 1$. | |
| Return to Step 2. | |

where:

- the map G has domain a subset of $S \times S$ and range S .
- the map D has domain a subset of $S \times S \times S$ and range S .
- the μ_k are probability measures corresponding to distribution functions defined on R^n .

Given the following definition and conditions:

Definition 1 If the global minimum value of f is denoted by y_* , then the ϵ -optimal region for f , with $\epsilon > 0$, is defined by $R_\epsilon = \{x \in S \mid f(x) < y_* + \epsilon\}$

Condition 1 The map D satisfies $f(D(x_1, x_2, x_3)) \leq f(x_1)$ and if $x_2 \in S, f(D(x_1, x_2, x_3)) \leq f(x_2)$ and if $x_3 \in S, f(D(x_1, x_2, x_3)) \leq f(x_3)$

Condition 2 For any subset A of S with n -dimensional volume greater than zero, we have that $\prod_{k=0}^{\infty} [1 - \mu_k(A)] = 0$ where $\mu_k(A)$ is the probability that x_2^k or x_3^k are in A .

Condition 2 ensures that, given any subset A of S with positive “volume”, the probability of repeatedly missing the set A , when generating x_2^k and x_3^k , must be zero. Clearly this condition is satisfied by APSE because the cyclic nature of the contraction/expansion cycle ensures that no portion of the search region is ever discarded.

As APSE satisfies conditions 1 and 2, the proof of convergence for APSE is identical to that in [49] for global search. We present this now:

Theorem 1 *Let S be a measurable subset of \mathbb{R}^n , f be a measurable function and assume that Conditions 1 and 2 above are satisfied. Let R_ϵ denote the ϵ -optimal region for f and $\{x_1^k\}_{k=0}^\infty$ be a sequence generated by APSE. Then $\lim_{k \rightarrow \infty} P[x_1^k \in R_\epsilon] = 1$ where $P[x_1^k \in R_\epsilon]$ is the probability that at step k , the point x_1^k generated by APSE is in R_ϵ .*

Proof: From Condition 1, it follows that x_1^k or x_2^k or x_3^k in R_ϵ implies that $x_1^k \in R_\epsilon$ for all $k \geq k + 1$. Thus

$$\begin{aligned} P[x_1^k \in S \setminus R_\epsilon] &= \prod_{l=0}^k (1 - \mu_l(R_\epsilon)) \\ &= (1 - \mu_k(R_\epsilon)) \prod_{l=0}^{k-1} (1 - \mu_l(R_\epsilon)) \\ &\leq \prod_{l=0}^{k-1} (1 - \mu_l(R_\epsilon)) \end{aligned}$$

Therefore

$$\begin{aligned} P[x_1^k \in R_\epsilon] &= 1 - P[x_1^k \in S \setminus R_\epsilon] \\ &\geq 1 - \prod_{l=0}^{k-1} (1 - \mu_l(R_\epsilon)) \end{aligned}$$

and hence

$$1 \geq \lim_{k \rightarrow \infty} P[x_1^k \in R_\epsilon] \geq 1 - \lim_{k \rightarrow \infty} \prod_{l=0}^{k-1} (1 - \mu_l(R_\epsilon)) = 1$$

where the last equality follows from Condition 2.

2.4 Test Functions

Tests to determine the effectiveness of the extension to APS were made using a number of standard test functions. For each test function, the basic test procedure was:

- perform a series of APSE runs, using different values of λ and β , to determine the optimal values for a particular test function.
- run 100 trials for each test function using APS and then repeat these 100 trials using APSE with the optimum values for λ and β determined above. Each trial used a random starting point and terminated when a function value within 0.0001 of the global minimum was obtained.

As the molecular structure problem has high dimensionality (for example, the atomic cluster problem has dimension $3N - 6$, where N is the number of atoms), an additional test was also performed to evaluate the effect of problem dimensionality on APSE.

The results obtained by APS and APSE for these test cases are now presented.

2.4.1 Beale Function

Minimise

$$\sum_{i=1}^3 U_i^2, \text{ where } U_i = a_i - x_1(1 - x_2^i)$$

with $a_1 = 1.5$, $a_2 = 2.25$, $a_3 = 2.625$, $-10 \leq x_i \leq 10$, using a random starting point [41]. This function has a narrow curving valley which approaches the line $x_2 = 1$ and a minimum at $(3, 0.5)$. While this function has only one minimum, it does test the ability of APS and APSE to “track” along a narrow valley. Figure 2.1 shows the result of varying λ and β on the

number of function evaluations required by APSE to find the minimum. By inspection, it can be seen that $\lambda = 6$ and $\beta = 3$ result in the lowest number of function evaluations for APSE. Figure 2.2 shows the results of 100 trials for both APS and APSE (using $\lambda = 6$ and $\beta = 3$).

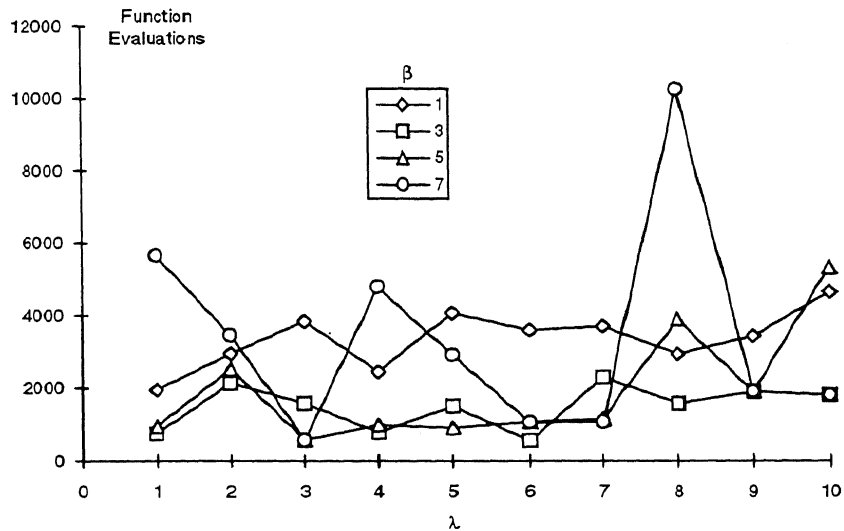


Figure 2.1: Number of function evaluations required by APSE to find the global minimum of the Beale test function for different λ and β values. Each data point is the result of a single trial.

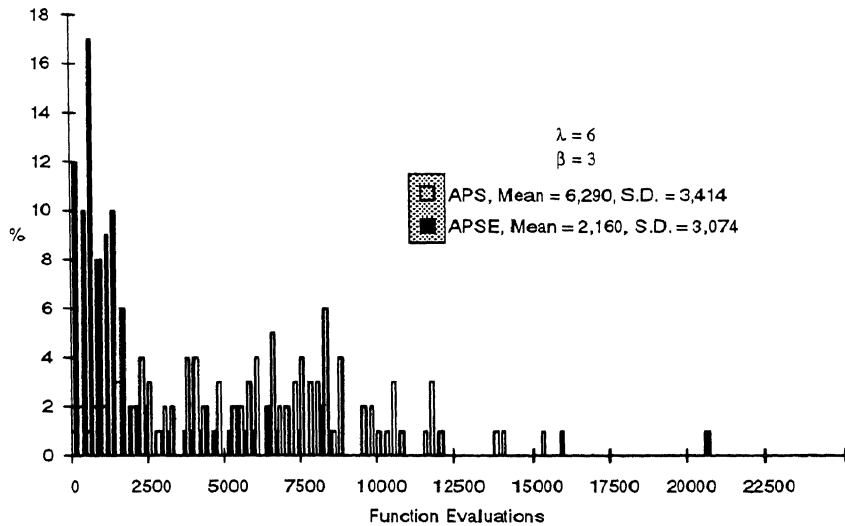


Figure 2.2: Distribution of function evaluations required (using 100 trials) to find the global minimum of the Beale test function for APS and APSE.

2.4.2 Goldstein-Price Function

Minimise

$$[1 + (x_1 + x_2 + 1)^2(19 - 14x_1 + 3x_1^2 - 14x_2 + 6x_1x_2 + 3x_2^2)] \times \\ [30 + (2x_1 - 3x_2)^2(18 - 32x_1 + 12x_1^2 + 48x_2 - 36x_1x_2 + 27x_2^2)]$$

where $-2 \leq x_i \leq 2$, $i = 1, 2$, using a random starting point [51]. This function has a global minimum of 3 when $x = (0, -1)$ and four local minima within the region of interest. Figure 2.3 shows the result of varying λ and β on the number of function evaluations required by APSE to find the minimum. By inspection, it can be seen that $\lambda = 2$ and $\beta = 2$ result in the lowest number of function evaluations for APSE. Figure 2.4 shows the results of 100 trials for both APS and APSE (using $\lambda = 2$ and $\beta = 2$).

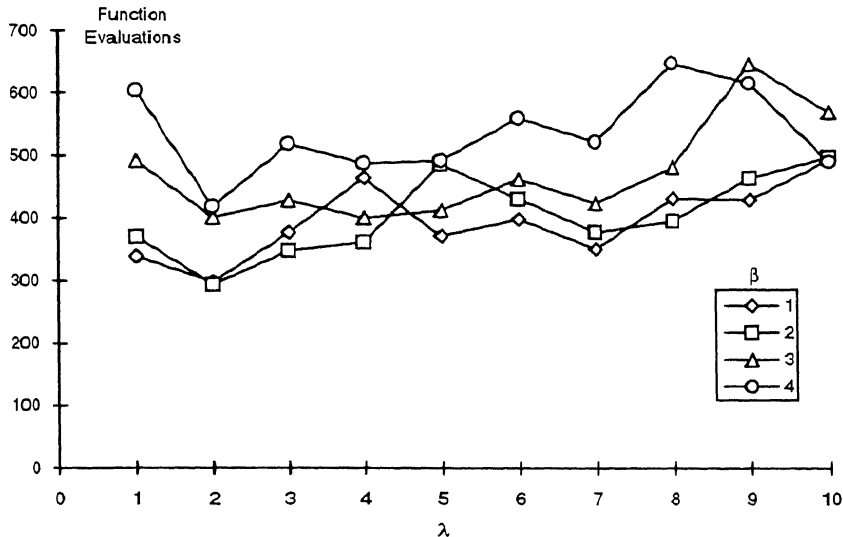


Figure 2.3: Number of function evaluations required by APSE to find the global minimum of the Goldstein-Price test function for different λ and β values. Each data point is the result of a single trial.

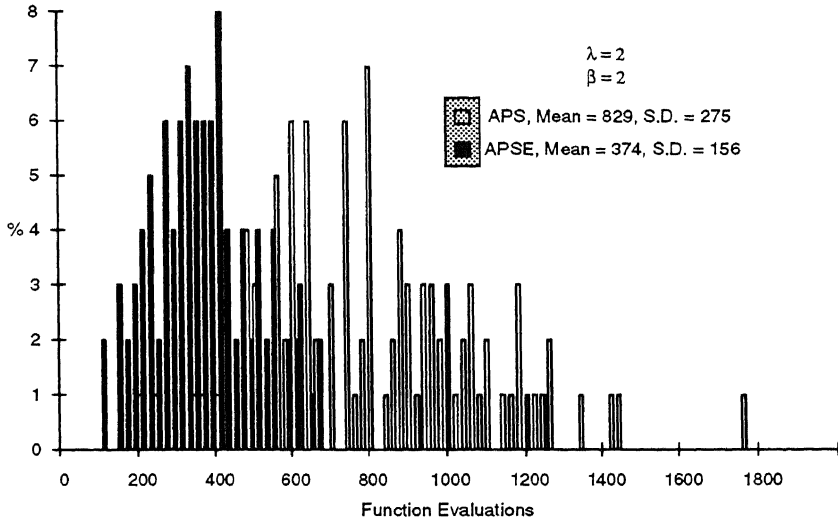


Figure 2.4: Distribution of function evaluations required (using 100 trials) to find the global minimum of the Goldstein-Price test function for APS and APSE.

2.4.3 Rastrigin Function

Minimise

$$x_1^2 + x_2^2 - \cos 18x_1 - \cos 18x_2$$

where $-1 \leq x_i \leq 1$, using a random starting point [51]. This function has a global minimum of -2 when $x = (0, 0)$ and some 50 local minima arranged in a lattice configuration within the region of interest. Figure 2.5 shows the result of varying λ and β on the number of function evaluations required by APSE to find the minimum. By inspection, it can be seen that $\lambda = 5$ and $\beta = 9$ result in the lowest number of function evaluations for APSE. Figure 2.6 shows the results of 100 trials for both APS and APSE (using $\lambda = 5$ and $\beta = 9$).

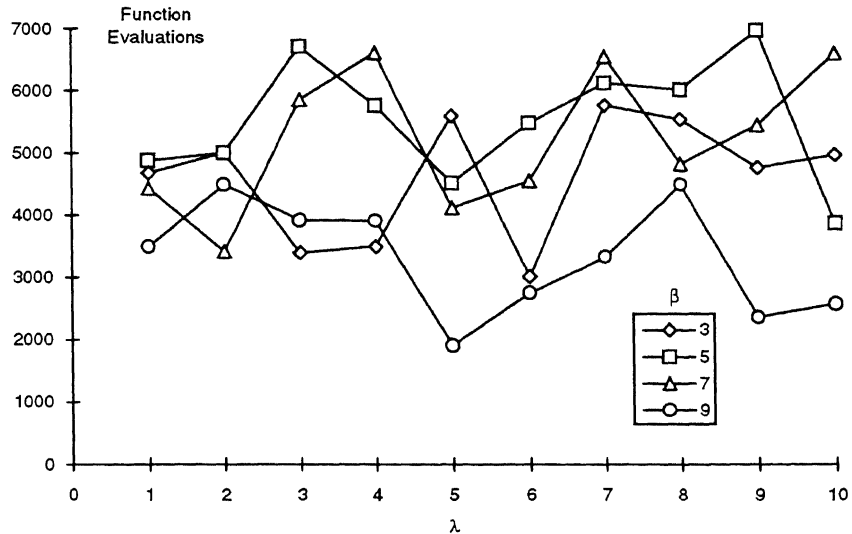
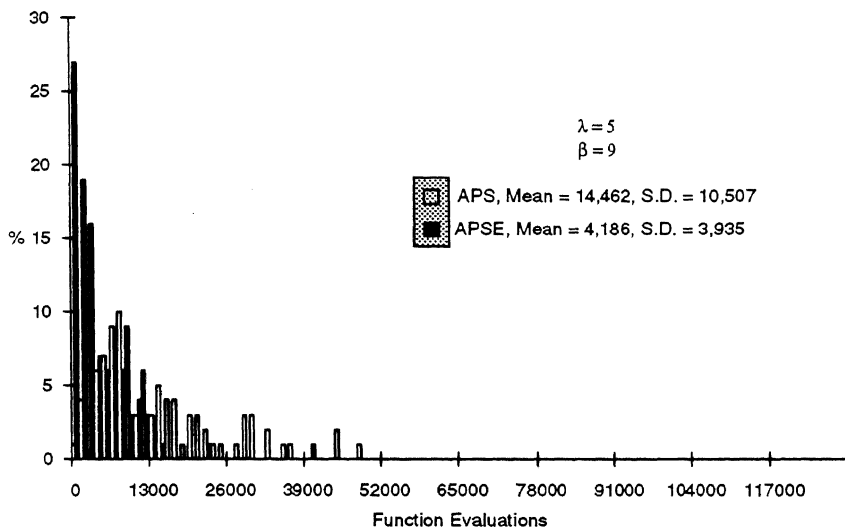


Figure 2.5: Number of function evaluations required by APSE to find the global minimum of the Rastrigin test function for different λ and β values. Each data point is the result of a single trial.



2.4.4 Griewank-2 Function

Minimise

$$\sum_{i=1}^n \frac{x_i^2}{d} - \prod_{i=1}^n \cos(x_i/i^{0.5}) + 1$$

where $n = 2$, $d = 200$ and $-100 \leq x_i \leq 100$, using a random starting point [51]. This function has a global minimum of 0 when $x = 0$ and some 500 local minima in the region of interest.

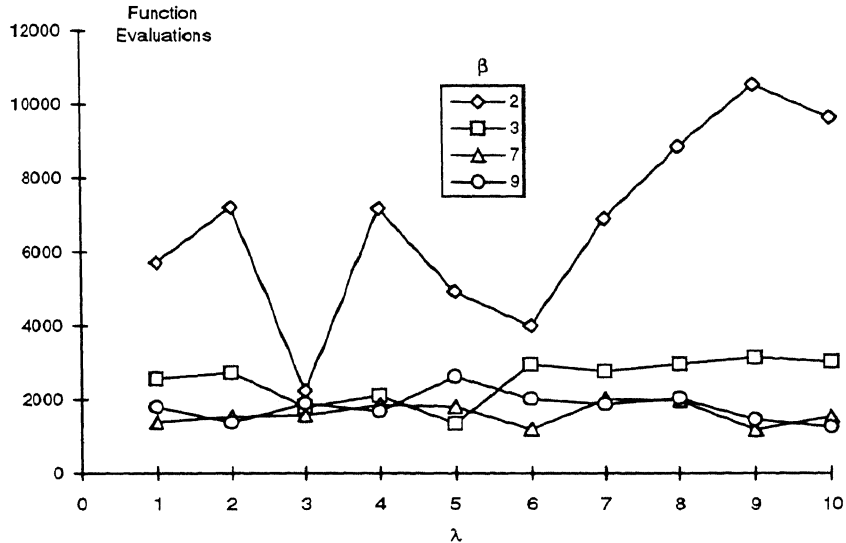


Figure 2.7: Number of function evaluations required by APSE to find the global minimum of the Griewank-2 test function for different λ and β values. Each data point is the result of a single trial.

Figure 2.7 shows the result of varying λ and β on the number of function evaluations required by APSE to find the minimum. By inspection, it can be seen that $\lambda = 6$ and $\beta = 7$ result in the lowest number of function evaluations for APSE. Figure 2.8 shows the results of 100 trials for both APS and APSE (using $\lambda = 6$ and $\beta = 7$).

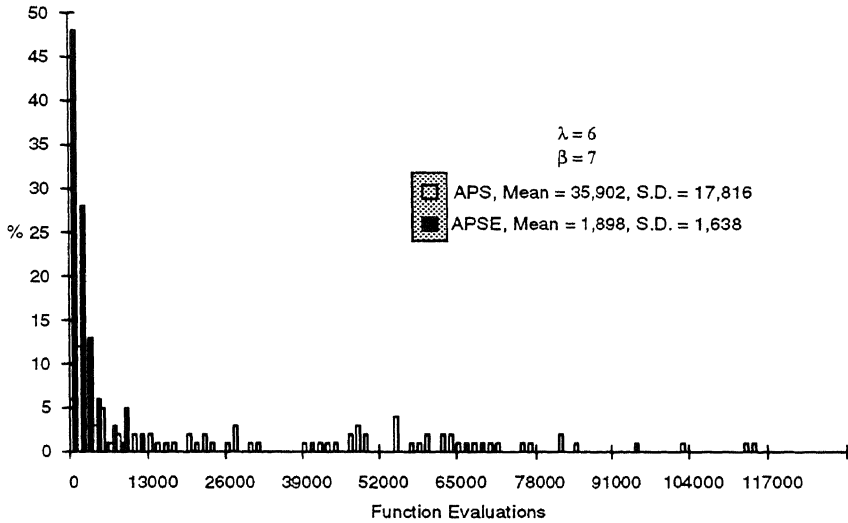


Figure 2.8: Distribution of function evaluations required (using 100 trials) to find the global minimum of the Griewank-2 test function for APS and APSE.

2.4.5 Variable Dimension Test Function

The variable dimension test function used was

$$F(x) = -5 \prod_{k=1}^n \sin(x_k) - \prod_{k=1}^n \sin(5x_k)$$

which has a global minimum value of -6.0 at $x_k = \pi/2, k = 1, \dots, n$. The test problem is to minimise $F(x)$ where $0 \leq x_k \leq \pi, k = 1, \dots, n$. The number of local minima for F is given by [66]

$$\sum_{i=0}^{n/2} \frac{n!}{(n-2i)!(2i)!} 3^{n-2i} 2^{2i}$$

and is plotted, as a function of n , in Figure 2.9.

Inspection of Figures 2.1, 2.3, 2.5 and 2.7 show that parameter settings of $\lambda = 6$ and $\beta = 3$ for APSE would obtain near optimal results for all the previous test functions. Accordingly these values were used for the APSE optimisation of F .

The average number of function evaluations taken by APS and APSE ($\lambda = 6, \beta = 3$), as a function of dimension, is shown in Figure 2.10. Each

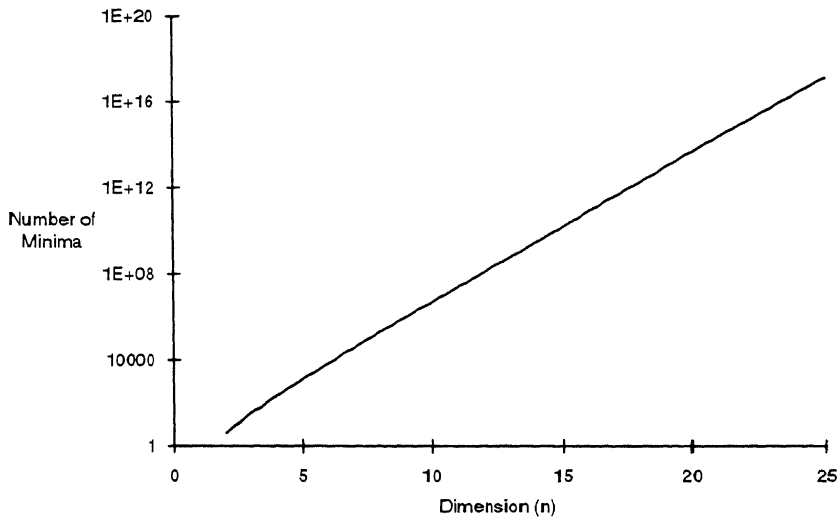


Figure 2.9: Number of minima for $F(x)$ as a function of dimension.

sample point is the average of five separate runs with the starting point for each run randomly chosen. Runs are terminated when the objective function is within 0.001 of the known global minimum.

As can be seen from Figure 2.10, at least up to 25 dimensions, and as a function of dimension, APSE performed better than APS for this particular function and the improvement increased with increasing dimension. In fact, as a function of dimension d , the number of function evaluations required for APS is approximately given by

$$f_{APS}(d) = 1000(6.9681d^6 - 9.0982d^5 + 3.7782d^4 - 0.6708d^3 + 0.0577d^2 - 0.0024d)$$

whereas, for APSE the corresponding function is

$$f_{APSE}(d) = 1000(1.1308d^2 - 0.2978d + 0.0212)$$

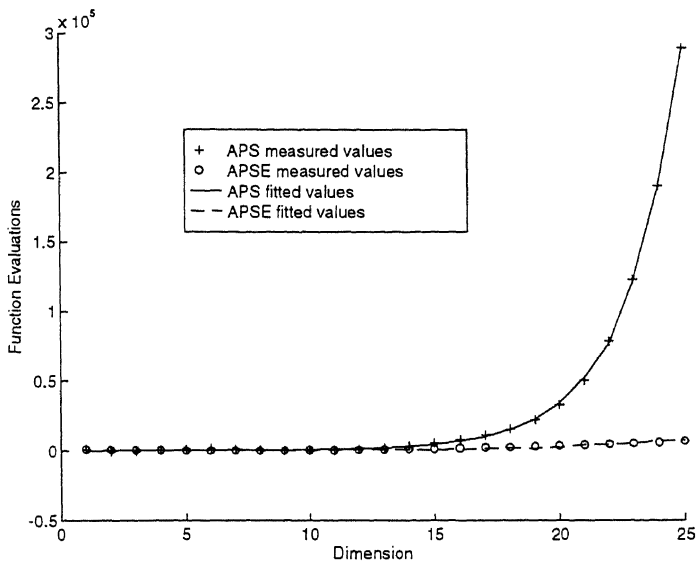


Figure 2.10: Comparison of function evaluations required by APS and APSE for F as a function of dimension. Each data point is the average of five trials with random starting points. Also shown is the fit of the polynomials f_{APS} and f_{APSE} to the experimental measurements for APS and APSE.

2.5 Discussion

Clearly APSE is an improvement over APS in that consistently fewer function evaluations were required to find the global minimum for all test functions. Importantly, for a given test function using different starting points, there was also less variability for APSE in the number of function evaluations required to find the global minimum.

| Function | Mean No. of Function Evaluations | | Mean Standard Deviation | |
|-----------------|----------------------------------|-------|-------------------------|-------|
| | APS | APSE | APS | APSE |
| Beale | 6,290 | 2,160 | 3,414 | 3,074 |
| Goldstein-Price | 829 | 374 | 275 | 156 |
| Rastrigin | 14,462 | 4,186 | 10,507 | 3,935 |
| Griewank-2 | 35,902 | 1,898 | 17,816 | 1,638 |

Table 2.1: Summary test results for APS and APSE. Each value is the average of 100 trials.

From Table 2.1, on average APSE required only 28% of the number of function evaluations needed by APS to globally optimise the test functions. In addition, the average standard deviation for the number of function evaluations required for APSE was 48% of that for APS. Given that APSE was always used in full “global” mode for these tests, these results clearly demonstrate the benefits of the adaptive focusing enhancement implemented in APSE. While these results were obtained using problem specific optimal values for the APSE λ and β parameters, inspection of Figures 2.1, 2.3, 2.5 and 2.7 show that similar results could be obtained by using APSE with a constant value of $\lambda = 6$ and $\beta = 3$ for all test functions. Accordingly, for all the subsequent studies in this thesis, APSE was used with these parameter settings.

For the particular multi-dimension test function used, APSE ($\lambda = 6, \beta = 3$) clearly out-performed APS. As molecular architecture problems are highly dimensional, this apparent low scalability of APSE with respect to dimension is an important attribute.

Chapter 3

APSE Optimisation of Pure Atomic Clusters

3.1 Introduction

The application of APSE to the problem of finding minimum energy configurations of pure Lennard-Jones atomic clusters is presented in this chapter. Section 3.2 describes the Lennard-Jones cluster optimisation problem and presents a review of previous optimisation methods applied to this problem. As described in Section 3.3, in conjunction with a build-up technique, APSE was able to find minimum energy structures for all Lennard-Jones clusters of two to twenty atoms. A build-up technique is commonly used in molecular structure problems and, in the case of atomic clusters, involves using the globally minimum configuration for an N atom cluster, in conjunction with a strategically placed new atom, as the initial configuration for the optimisation of an $N + 1$ atom cluster. By incorporating local optimisation and a technique of initially smoothing the PES, using APSE to find minima on this smoothed PES and then tracking these minima as the degree of smoothing is slowly reduced, global minima were found for all Lennard-Jones clusters of two to thirty atoms. These results are described in detail in Section 3.4 while Section 3.5 contains a review, a summary of future directions and

conclusion.

3.2 Pure Atomic Clusters

An extensive review of the theory and structure of atomic clusters is presented in [20] where the question of the number and types of local minima possible in an atomic cluster is addressed. In terms of the energy function, the only quantitative statement that can be made is that, for an N atom cluster, using the scaled Lennard-Jones pair potential, $v(r) = r^{-12} - 2r^{-6}$ (Figure 3.1), there exists a weak lower bound on the potential energy given by

$$-N(N-1)/2$$

That is, a simplex in $N-1$ dimensions in which all atoms are nearest neighbours (distance 1 apart), gives the lowest energy possible. The equality holds in the case where $N=2$ (a pair), $N=3$ (an equilateral triangle), and $N=4$ (a regular tetrahedron).

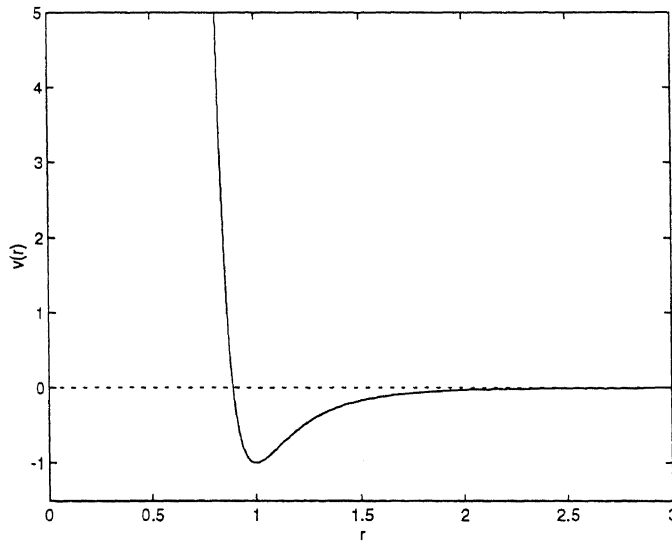


Figure 3.1: Scaled Lennard-Jones pair potential.

For smaller Lennard-Jones clusters, the globally minimum configurations are:

- Five atoms - a triagonal bipyramid, slightly contracted along the symmetry axis and distended in the symmetry plane.
- Six atoms - the regular octahedron with slightly contracted sides.
- Seven atoms - a partial icosahedron with slightly distended edges and contracted axial distances.

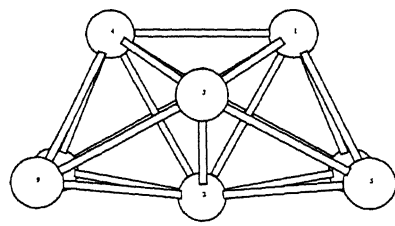
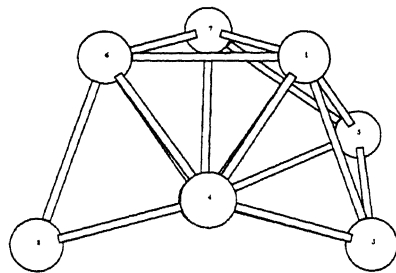
For more than seven atoms, minimum energy structures are based on icosahedral lattice structures as shown in Figure 3.2.

Determining the number of distinct local minima (which includes the global minimum) is not straightforward due to the symmetries involved. Minima associated with structures which differ only in labelling of atoms must first be eliminated. In addition, minima which are associated with structures which are equivalent under proper symmetry operations in three dimensions must also be eliminated. Finally, there are some pairs of structures which must be eliminated as they share the same potential energy and the same distances between atoms (to within atom numbering) but are not superimposable under normal symmetry operations. From [20], the total number of distinct local minima for $N = 2, \dots, 13$ atom clusters, using a scaled Lennard-Jones pair potential, is 1, 1, 1, 1, 2, 4, 8, 18, 57, 145, 366, and 988. As stated in [20], this data is approximated by the equation

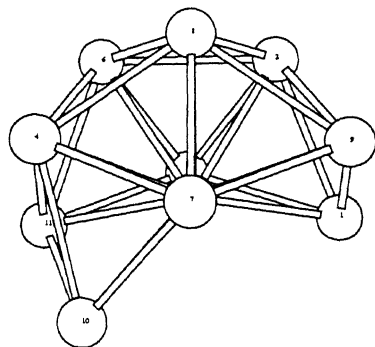
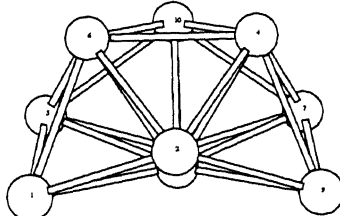
$$m(N) = \exp(-2.5176 + 0.3572N + 0.0286N^2)$$

which, if correct, predicts that the potential energy surface for a 100 atom cluster has of the order of 10^{140} local minima!

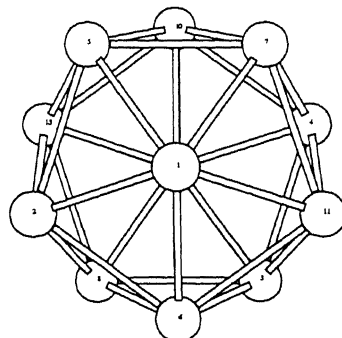
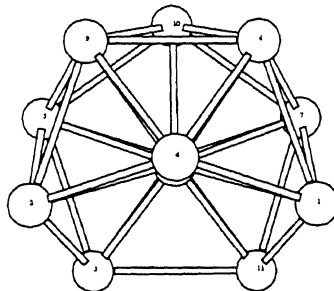
Liao [28] has shown that, for an N atom cluster using a scaled Lennard-Jones potential function, a global minimum exists and the corresponding



(a) $N = 8$, energy = -19.822 . (b) $N = 9$, energy = -24.113 .



(c) $N = 10$, energy = -28.423 . (d) $N = 11$, energy = -32.766 .



(e) $N = 12$, energy = -37.968 . (f) $N = 13$, energy = -44.327 .

Figure 3.2: Globally optimal structures for $N = 8, \dots, 13$ atom scaled Lennard-Jones clusters.

configuration is contained within a sphere, centred at the origin, and of radius

$$(N - 1)\sqrt{N - 1}$$

All currently accepted globally minimum potential energies for scaled Lennard-Jones atomic clusters containing between 2 and 105 atoms are shown in Table 3.1. These values were obtained by Deaven et al. [11], Northby [37], Xue [64], Sloane et al. [48] and this study.

| N | Energy | N | Energy | N | Energy | N | Energy |
|-----|----------|-----|----------|-----|----------|-----|----------|
| 2 | -1.0 | 28 | -117.822 | 54 | -272.209 | 80 | -428.084 |
| 3 | -3.0 | 29 | -123.587 | 55 | -279.248 | 81 | -434.344 |
| 4 | -6.0 | 30 | -128.287 | 56 | -283.643 | 82 | -440.550 |
| 5 | -9.104 | 31 | -133.586 | 57 | -288.343 | 83 | -446.924 |
| 6 | -12.712 | 32 | -139.636 | 58 | -294.378 | 84 | -452.657 |
| 7 | -16.505 | 33 | -144.843 | 59 | -299.738 | 85 | -459.056 |
| 8 | -19.822 | 34 | -150.045 | 60 | -305.876 | 86 | -465.385 |
| 9 | -24.113 | 35 | -155.757 | 61 | -312.009 | 87 | -472.098 |
| 10 | -28.423 | 36 | -161.825 | 62 | -317.354 | 88 | -479.033 |
| 11 | -32.766 | 37 | -167.034 | 63 | -323.490 | 89 | -486.054 |
| 12 | -37.968 | 38 | -173.929 | 64 | -329.620 | 90 | -492.434 |
| 13 | -44.327 | 39 | -180.033 | 65 | -334.971 | 91 | -498.811 |
| 14 | -47.845 | 40 | -185.250 | 66 | -341.111 | 92 | -505.185 |
| 15 | -52.323 | 41 | -190.536 | 67 | -347.252 | 93 | -510.878 |
| 16 | -56.816 | 42 | -196.278 | 68 | -353.395 | 94 | -517.264 |
| 17 | -61.318 | 43 | -202.365 | 69 | -359.845 | 95 | -523.640 |
| 18 | -66.531 | 44 | -207.689 | 70 | -366.892 | 96 | -529.879 |
| 19 | -72.660 | 45 | -213.785 | 71 | -373.350 | 97 | -536.681 |
| 20 | -77.177 | 46 | -220.680 | 72 | -378.638 | 98 | -543.643 |
| 21 | -81.685 | 47 | -226.012 | 73 | -384.789 | 99 | -550.667 |
| 22 | -86.810 | 48 | -232.200 | 74 | -390.909 | 100 | -557.040 |
| 23 | -92.844 | 49 | -239.092 | 75 | -396.283 | 101 | -563.411 |
| 24 | -97.349 | 50 | -244.550 | 76 | -402.386 | 102 | -569.278 |
| 25 | -102.373 | 51 | -251.254 | 77 | -408.520 | 103 | -575.659 |
| 26 | -108.316 | 52 | -258.230 | 78 | -414.795 | 104 | -582.038 |
| 27 | -112.874 | 53 | -265.203 | 79 | -421.811 | 105 | -588.267 |

Table 3.1: Currently accepted global minimum energies for scaled Lennard-Jones atomic clusters, $N = 2, \dots, 105$.

Given the rapid growth in local minima, the problem of finding the global minimum of the energy function for any but the smallest of atomic clusters is probably not practical unless some means of tailoring the global optimisation algorithm towards this specific problem is employed. For the atomic cluster problem, algorithms have been developed which incorporate, to a greater or lesser degree, heuristic information obtained from the physical observation of the nature of the system in its stable states.

Prior to 1987, the most extensive study of atomic clusters was the work of Hoare et al. ([18], [19], [20], [21]). They developed a general growth algorithm and used it to generate large numbers of stable structures, mainly for $N \leq 55$. These were compared to find the lowest energy structures which, in turn, became candidates for the absolute minimal structures. Hoare and Pal [18] observed that, while what they termed as the “icosahedral growth sequence” did not, in general, produce minimal structures, icosahedral sub-units did appear regularly in relaxed configurations generated by other sequences. The icosahedral lattice can be described as 20 slightly flattened tetrahedrally shaped face-centred-cubic units with 12 vertices on a sphere centred at the origin. For the icosahedral lattice, the total number of lattice points on each layer is 1, 12, 42, 92,.... Therefore the number of lattice points in the sequence of closed shell icosahedral lattices is 1, 13, 55, 147,.... Using these results from Hoare and Pal, Northby [37] produced an algorithm for minimising Lennard-Jones clusters which obtained putative global minima for all clusters in the range $N = 13, \dots, 147$. At a high level of abstraction, Northby’s algorithm proceeds as follows:

- For N atoms, define the set S of all possible icosahedral shell lattices (with inner shells densely packed).

- Define a potential function for optimising this discrete problem (that is, optimising where each atom must remain on a lattice vertex). Northby primarily used a “square well” potential of the form

$$v(r) = \begin{cases} 0 & 0 \leq r \leq 0.8 \\ -1 & 0.8 < r < 1.2 \\ 0 & 1.2 \leq r < \infty \end{cases}$$

- Perform a lattice-based search optimisation across each lattice in the set S to identify minimum energy lattice-based configurations.
- Using the Lennard-Jones potential function and a gradient search method, optimise all geometrically distinct minimum energy structures found in the previous step.

Clearly the critical assumption in Northby’s algorithm is that a well-defined set of lattice structures contains at least one initial cluster configuration which relaxes to the ground state.

Xue ([64], [65]) implemented a two-level parallel version of simulated annealing for use with an icosahedral lattice-based search technique which had increased computational efficiency over that used by Northby [37]. Xue’s two-level simulated annealing algorithm uses a local optimiser to determine the local minimum for the catchment basin within which each generated point lies. New points are moved to by comparing the function values of these local minima rather than the function values associated with the generated points¹. When the temperature gets low, two-level simulated annealing still accepts moves which lead to worse function values, but these moves all lead to better (or equal) local minima. That is, the two-level simulated annealing algorithm can easily climb up a hill at any temperature, but is very careful in moving into the catchment basin of a worse local minima

¹ As the random probes and the decision to move to a new point are made at different levels, the method is referred to as two-level simulated annealing.

when the temperature is low. Using this technique, Xue found lower energy structures for clusters with 65, 66, 75, 76 and 77 atoms and also obtained satisfactory results for clusters as large as 100,000 atoms.

Wille [57] applied simulated annealing to Lennard-Jones clusters for $4 \leq N \leq 25$. For small cluster sizes ($4 \leq N \leq 13$), one of the atoms was kept in a fixed central position to eliminate translational degrees of freedom. For larger clusters ($14 \leq N \leq 25$), 13 atoms were kept in a central icosahedral environment during annealing. However, in common with all other applications of simulated annealing, the difficult part proved to be the determination of a suitable cooling schedule. A cooling rate that is too slow is time consuming, while a fast cooling rate will lead to minima other than the global minimum. In order to analyse the influence of the cooling schedule on the final state, Wille performed a number of simulations on 13 atom clusters making the number of attempted steps per atom at each temperature equal to $K(1 - \log T)$, where $K = 200$ or 2500 with the temperature reduction factor being 0.9. In the first case, 3 out of 30 runs produced the icosahedral structure, whereas in the second case 4 out of 5 runs gave this result. This indicates how the likelihood of detecting the global minimum increases with decreasing cooling rate.

Hartke [16] used a genetic algorithm to find global minimum energy structures for four atoms. An encoding method, using just four parameters to specify the four atom configuration, allowed a standard GA to find the global minimum energy. Mestres and Scuseria [32] also used a GA to find global minimum energy configurations for Lennard-Jones atomic clusters of up to 13 atoms and Gregurick et al. [15] employed a modified deterministic/stochastic genetic algorithm to find all currently accepted global minima for Lennard-Jones atomic clusters in the range $2, \dots, 29$. However their

technique did require a seed growth method for generating initial structures for all clusters containing more than 20 atoms. More recently, Deaven et al. [11], using a real-coded GA with innovative phenotype genetic crossover operators, were able to find all global minimum energies for Lennard-Jones clusters in the range $2, \dots, 100$ including new minima for 38, 65, 69, 76, 88 and 98 atom clusters.

A number of optimisation methods ([7], [8], [9], [27], [61]) that have been applied to the atomic cluster problem used a spatial averaging approach, where the objective function is averaged over a large region of space so that an approximate location for the global minimum can be determined. The size of the space over which the objective function is averaged is then slowly reduced while sequential minimisations are performed. If the global minimum varies in a continuous manner, then it is possible to start from the approximate global minimum and track to the final global minimum using local optimisation techniques only. However, if the global minimum varies in a discontinuous manner then, as long as there is only a bounded number of discontinuities and the configuration differences are small, it is normally possible to track from the approximate global minimum to the actual global minimum using a combination of local and restricted global optimisation methods.

These methods have achieved varying success, depending on the smoothing function used, and have generally been limited to atomic clusters in the $N = 2, \dots, 30$ range.

Maranas and Floudas [29] developed a global optimisation method which involved the transformation of the initial non-convex total potential energy function to the difference of two convex functions (DC transformation) and the application of a primal-relaxed dual global optimisation approach, guar-

anteed to converge to the global optimum in a finite number of iterations. For $N \leq 7$ the total potential energy corresponding to the global minimum potential energy configuration of the atomic clusters were obtained. For $8 \leq N \leq 24$ the method yielded upper and lower bounds on the global minimum potential energy.

Byrd et al. [5] applied a stochastic perturbation global optimisation algorithm to the atomic cluster problem. The method consists of an initial phase that locates some reasonably low local minima followed by the main phase which progresses from the best current local minima to even lower local minima. The method combines portions that work on small subsets of the parameters, including small-scale global optimisations using stochastic methods, with local minimisations involving all the parameters. Initially [5] this method was able to successfully solve all Lennard-Jones problems with up to 30 atoms. In recent years, the method has been extended and, using more computational resources, has been successful for all clusters in the $N = 2, \dots, 76$ range [47].

3.3 Computational Methods

During the development of the global optimisation methods described in the following subsections, a number of alternative techniques were implemented, tested and ultimately discarded. Two such techniques were

- A parallel build-up approach where the base $N - 1$ atom optimal cluster was treated as a rigid structure and constrained such that, while three rotational degrees of freedom were allowed, the centre of mass remained fixed. The new N th atom was originally placed some distance from the $N - 1$ cluster and incrementally moved, in a straight line directly towards the centre of mass of the $N - 1$ cluster. At each

step, constrained APSE and local optimisations were performed using only the three rotational degrees of freedom of the $N - 1$ cluster. When the N th atom was “close” to the $N - 1$ cluster, all atoms were allowed to move and a final local optimisation performed. The expectation was that the global minimum for the constrained system would be “tracked” by the constrained local optimisations and that eventually this minimum would lie within the catchment basin of the global minimum for the unconstrained N atom cluster.

The basic mechanism of this technique is easily demonstrated by considering an atom approaching two optimally configured atoms. As the third atom approaches the closest of the first two, it will tend to “push” against it. As the centre of mass of the first two atoms is constrained to remain fixed, the pair will rotate about this centre of mass until equilibrium is achieved. The next movement of the third atom will cause more rotation until, finally, the third atom is equidistant from the first two atoms. This places the third atom on the optimal “trajectory” for docking in the globally optimal position, the apex of an equilateral triangle with the first two atoms forming the base. This technique can be parallelised by, for each processor, starting the new N th atom from a different position relative to the base $N - 1$ cluster.

While this technique was successful for small clusters ($N < 10$), it was unable to locate global minima for larger clusters probably due to the large number of possible trajectories, of which only a few actually lead to the optimal configuration.

- In $N - 1$ dimensions, the globally optimal configuration for an N atom cluster, is an $N - 1$ dimensional simplex where each atom is distance 1 unit from all other atoms. This optimisation method started with

a globally optimal configuration in $N - 1$ dimensions, and by slowly constraining to zero each higher dimension in turn while performing constrained APSE and local optimisations, tracked the globally optimal configuration from the $N - 1$ dimensional simplex to the globally optimal configuration in three dimensions.

While this method was effective for low-dimensional problems ($N < 10$), the computational requirements rapidly became excessive with increasing dimension. As there is no apparent method of parallelising the technique, these computational requirements rendered the method ineffective.

3.3.1 APSE and Atomic Build-up

Because of the complexity ($O(\exp(N^2))$) of the atomic cluster problem, APSE was used in association with a build-up technique. Each run of APSE started from a two atom cluster (which has the obvious solution of two atoms separated by a distance of 1 unit) and constructed larger clusters by adding single atoms to the globally optimal configuration found for the $N - 1$ atom cluster, to produce an N atom cluster. As each new atom was added, APSE and BFGS optimisations were performed. The calculations of the analytical energy gradients $V_{x_i}, V_{y_i}, V_{z_i}$, where $1 \leq i \leq N$, required for local optimisation of pure atomic clusters are shown in Appendix A.1.

The best method for initially placing the N th atom appeared to be in the vicinity of the $(N - 1)$ th atom. During APSE optimisations, atoms which were part of the initial $N - 1$ cluster were relatively (externally) constrained while the N th atom was totally unconstrained (this tended to preserve the initial structure). Results obtained by this method are presented in Section 3.4.1.

3.3.2 APSE and PES Smoothing

The following subsection describes the use of heuristic knowledge of the atomic cluster problem to smooth the potential energy surface and, using a build-up approach in addition to global (APSE) and local optimisation, implement an effective optimisation method. All results obtained by this method are presented in Section 3.4.2.

Optimisation Method

As noted in [20], at least for smaller atomic clusters, there is a dramatic reduction in the number of distinct PES local minima for atomic clusters formed using a Morse potential ($v_m(r) = (1 - \exp(3(1 - r)))^2 - 1$, Figure 3.3) compared with those formed using a Lennard-Jones potential. In [20] the local minima counts shown in Table 3.2 were obtained.

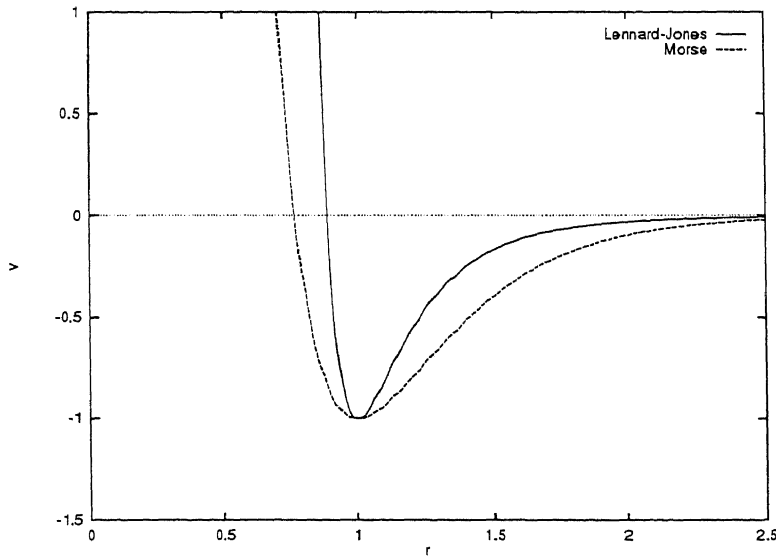


Figure 3.3: Lennard-Jones and Morse pair potentials. As a consequence of the smoother curve for the Morse pair potential, the PES for Morse atomic clusters has considerably fewer minima than that for Lennard-Jones atomic clusters.

| N | v_{lj} | v_m | N | v_{lj} | v_m |
|-----|----------|-------|-----|----------|-------|
| 6 | 2 | 1 | 10 | 57 | 16 |
| 7 | 4 | 3 | 11 | 145 | 24 |
| 8 | 8 | 5 | 12 | 366 | 22 |
| 9 | 18 | 8 | 13 | 988 | 36 |

Table 3.2: Counts of Lennard-Jones and Morse local minima.

As can be seen from Figure 3.3, the Morse potential is a “smoother” function than the Lennard-Jones potential so it is not unreasonable to expect the PES for Morse atomic clusters to be smoother, resulting in fewer minima and correspondingly larger catchment basins. The surface smoothing effect of the Morse potential can easily be demonstrated using three atoms where the first atom is fixed at $(0, 0, 0)$, the second atom fixed at $(1, 0, 0)$ and the third atom moves, in a straight line, from $(-2, 0.866, 0)$ to $(3, 0.866, 0)$ passing through the optimal point at $(0.5, 0.866, 0)$ (Figure 3.4). The variation in potential energy for this atomic cluster as a function of the position of the third atom is plotted in Figure 3.5 for both Lennard-Jones and Morse potentials. As can be seen, the location of the global minima is identical for both potentials. However, for the Morse potential, the energy curve has only one minimum compared to three minima for the Lennard-Jones potential. Clearly, finding the global minimum for this atomic configuration is trivial when a Morse potential is used, and in fact, also gives the global minimum for the relatively more complex Lennard-Jones cluster.

The main question addressed in this subsection is, given a family (indexed by α) of pair potentials of the form

$$v(\alpha, r)$$

where:

$$\alpha_{\min} \leq \alpha \leq \alpha_{\max}$$

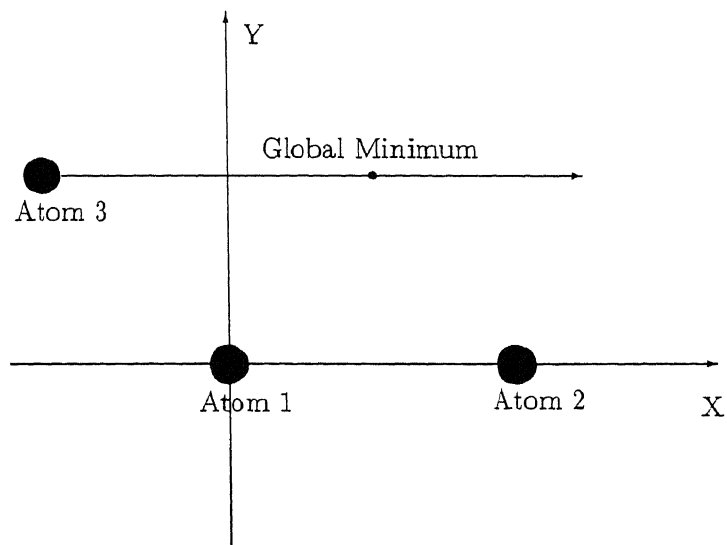


Figure 3.4: Three atom cluster configuration used to generate Figure 3.5. Atom 3 follows the trajectory shown which passes through the global minimum position.

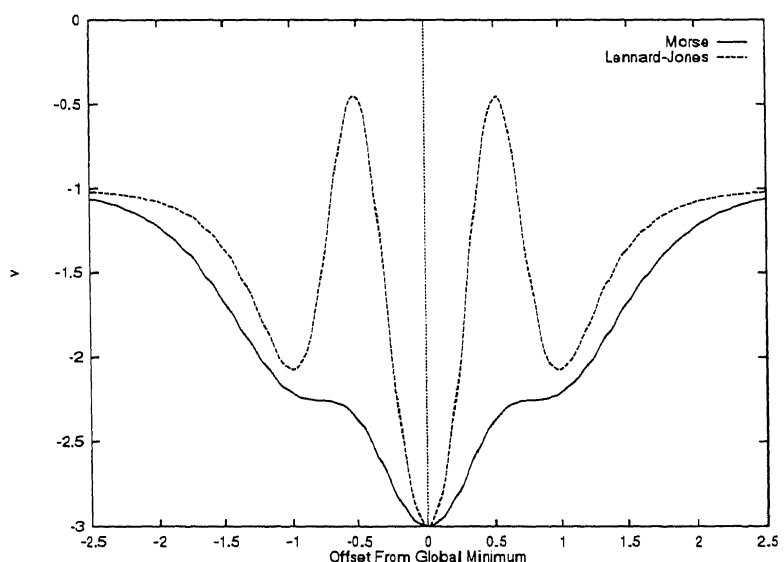


Figure 3.5: Cross-sections through the PES of $N = 3$ Lennard-Jones and Morse atomic clusters along a trajectory through the global minimum position and parallel to a line joining atoms 1 and 2 (as shown in Figure 3.4).

$$\begin{aligned}
\alpha_1 < \alpha_2 &\implies v(\alpha_1, r) \leq v(\alpha_2, r), \text{ for all } r \geq 0 \\
v(\alpha_{\max}, r) &= v_{lj}(r), \text{ for all } r \geq 0 \\
v(\alpha, r) &\rightarrow 0 - \text{ as } r \rightarrow \infty \\
v'(\alpha, r_0) &= 0 \text{ for a unique } r_0 \\
v''(\alpha, r_0) &> 0 \\
v(\alpha, r_0) &< 0,
\end{aligned}$$

is it possible to identify PES minima for a $v(\alpha_{\min}, r)$ atomic cluster and, while slowly increasing α to α_{\max} , track these minima and arrive at the global minimum for the $v(\alpha_{\max}, r)$ atomic cluster? As with the direct surface smoothing techniques([7], [8], [9], [27], [61]), if the global minimum varies in a continuous manner as α increases then, using appropriate increments for α , it should be possible to start from the global minimum for the $v(\alpha_{\min}, r)$ pair potential and move to the global minimum for $v(\alpha_{\max}, r)$ using local optimisation techniques only. However, if the global minimum varies in a discontinuous manner then, as long as there is only a finite number of discontinuities in the position of the global minimum and the configuration differences are small, it should be possible to track from the $v(\alpha_{\min}, r)$ global minimum to the $v(\alpha_{\max}, r)$ global minimum using a combination of local and constrained global optimisation methods.

A number of potential candidate functions exist for $v(\alpha, r)$. For example, in [47], the following family of smoothing functions was proposed

$$\tilde{p}(r, P, \gamma) = \left(\frac{1 + \gamma}{r^P + \gamma} \right)^2 - 2 \left(\frac{1 + \gamma}{r^P + \gamma} \right)$$

In this study however, the following three are considered

$$v_1(\alpha, r) = v_m(r)(1 - \alpha) + v_{lj}(r)\alpha, \quad \alpha_{\min} = 0, \alpha_{\max} = 1$$

$$v_2(\alpha, r) = r^{-2\alpha} - 2r^{-\alpha}, \quad \alpha_{\min} = 1, \alpha_{\max} = 6$$

$$v_3(\alpha, r) = \begin{cases} (1 - \exp(\alpha(1 - r)))^2 - 1, & \alpha < 5 \\ r^{-12} - 2r^{-6}, & \alpha = 5 \end{cases} \quad \alpha_{\min} = 0.5, \alpha_{\max} = 5$$

These functions were chosen as they generate families of curves which have progressively “smoother” curves for $v(\alpha_{\min}, r)$. That is, for all $r \geq 0$, $v_1(\alpha_{\min}, r) \geq v_2(\alpha_{\min}, r) \geq v_3(\alpha_{\min}, r)$. Examples of the families of curves that can be generated from $v_1(\alpha, r)$, $v_2(\alpha, r)$ and $v_3(\alpha, r)$ are shown in Figures 3.6, 3.7 and 3.8 respectively.

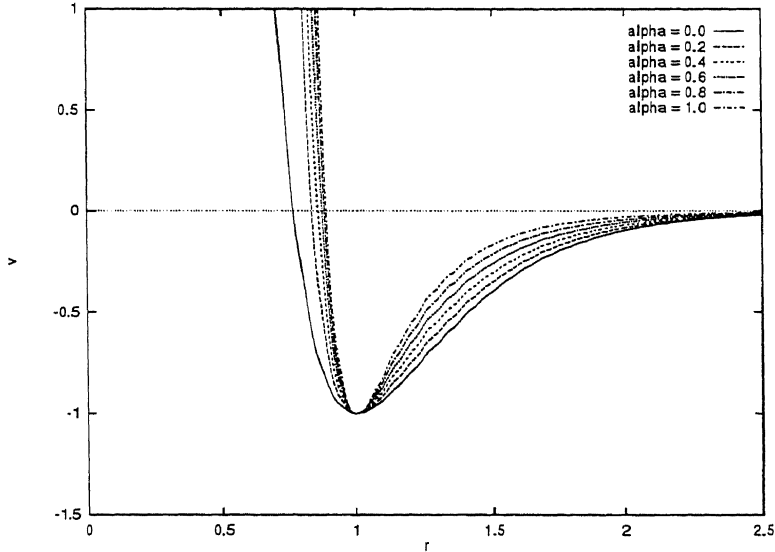


Figure 3.6: Pair potentials for $v_1(\alpha, r)$ as α varies.

For optimisation purposes, we are particularly interested in changes in the PES around the global minimum and these are shown, using the $v_3(\alpha, r)$ pair potential, in Figures 3.9 through 3.11, for various sized atomic clusters. The smoothing effect as α is decreased is clear, as is the narrowness of the catchment basin for the $v_3(\alpha_{\max}, r)$ global minimum and how this increases

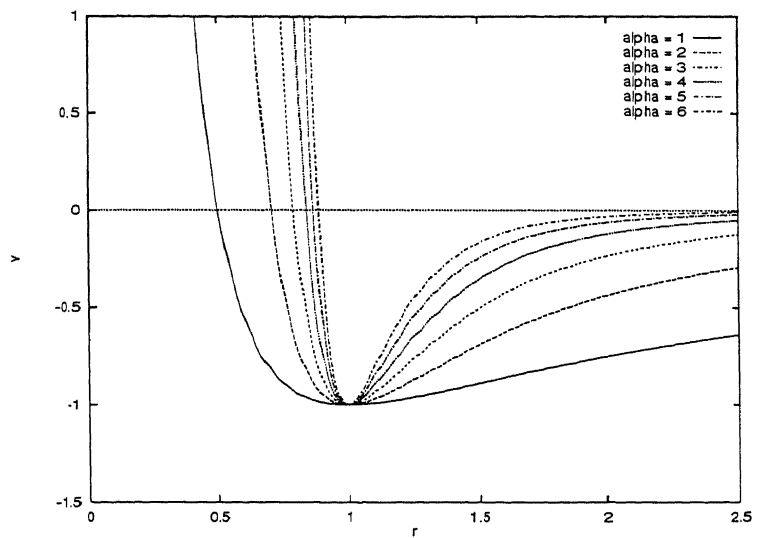


Figure 3.7: Pair potentials for $v_2(\alpha, r)$ as α varies.

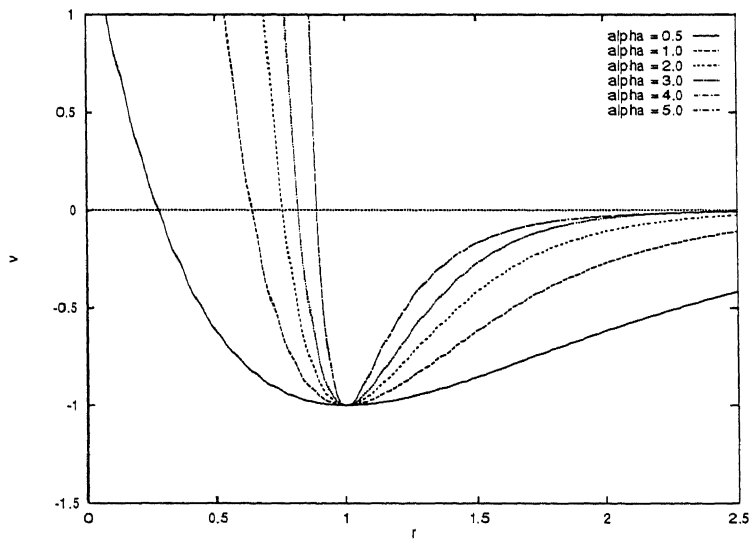


Figure 3.8: Pair potentials for $v_3(\alpha, r)$ as α varies.

in size as α decreases. Also of interest is the disappearance of local minima as α decreases and the results for the 6 and 18 atom clusters, both of which have narrow catchment basins around the global minima, where the same configuration produces the global minimum for all values of α . Because of the disappearance of local minima, finding the global minimum is relatively straightforward for the smoother Morse potentials and in some cases it may be possible to track to the Lennard-Jones global minimum using local optimisation only.

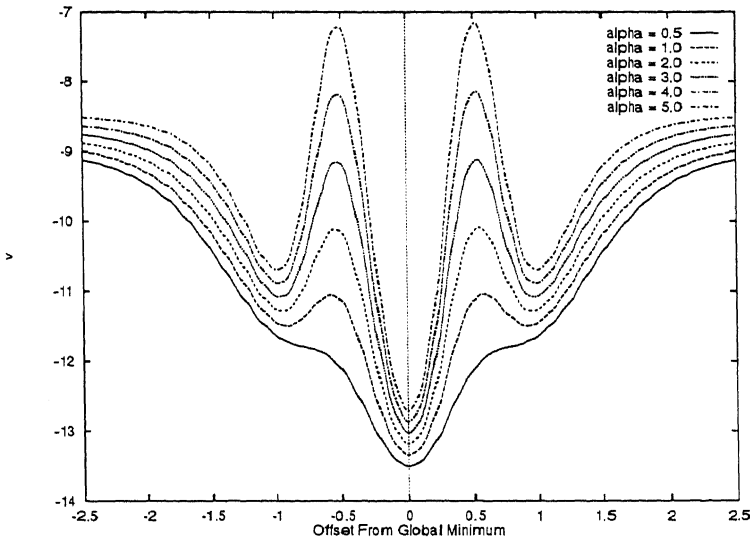


Figure 3.9: Cross-section of the PES along a trajectory through the global minimum for an $N = 6$ atomic cluster using different forms of the $v_3(\alpha, r)$ pair potential.

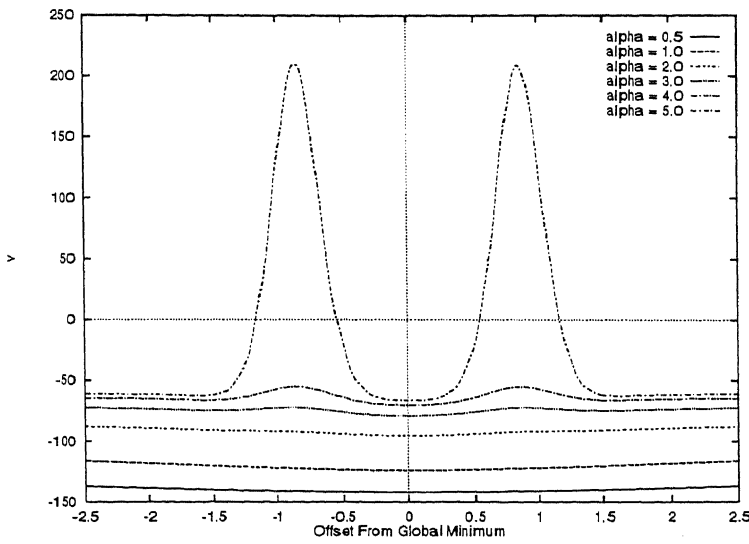


Figure 3.10: Cross-section of the PES along a trajectory through the global minimum for an $N = 18$ atomic cluster using different forms of the $v_3(\alpha, r)$ pair potential.

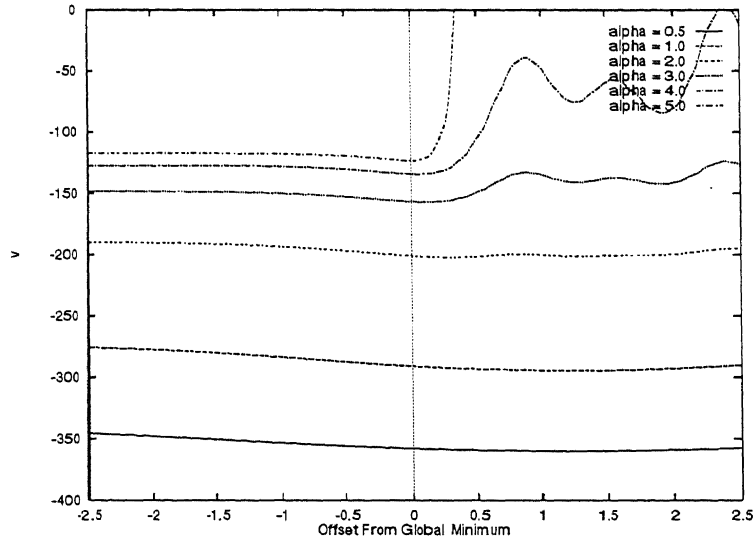


Figure 3.11: Cross-section of the PES along a trajectory through the global minimum for an $N = 29$ atomic cluster using different forms of the $v_3(\alpha, r)$ pair potential. For this cluster, the location of the global minimum varies as α changes. In addition, bifurcations are present and prevent “tracking” of the global minimum using only a local optimiser.

Given the reduction in local minima for smoother pair potentials and the existence of local and global optimisation methods, an effective optimisation algorithm for determining the global minimum of a Lennard-Jones cluster can be implemented by repeatedly applying the following steps:

1. Generate a starting configuration.
2. Using one of v_1, v_2, v_3 as the pair potential, slowly vary α from α_{min} to α_{max} performing global/local optimisations at each change in α .
3. If the final energy found when $\alpha = \alpha_{max}$ is not less than or equal to the currently accepted global minimum then repeat this sequence.

For a more complete description of the algorithm we need the following definitions:

- i , a counter which is incremented each time a new starting configuration is generated.
- k , a counter which is reset to one each time a new starting configuration is generated and incremented by one each time α changes.
- f_i^k , the energy value at the k th step of the i th iteration. For a given value of i , the sequence of f_i^k as k varies gives a sequence of energy values (or energy trajectory).

Using these definitions, the optimisation algorithm implemented is

APSE with PES Smoothing Algorithm

```
Step 0: Set  $i = 0$ 
Step 1: Set  $k = 1$ 
        Set  $i = i + 1$ 
        Set  $\alpha = \alpha_{\min}$ 
        <generate initial configuration  $x$ >
Step 2: Set  $x_k = APSE(x, v(\alpha, r))$ 
        Set  $f_i^k = V(x_k, v(\alpha, r))$ 
        if  $k > 2$  and <same energy trajectory>
            Go To Step 1.
Step 3: If <terminate>
        Optimum vector is  $x_k$ 
        Optimum function value is  $f_i^k$ 
        stop.
    else if  $\alpha < \alpha_{\max}$ 
        <increment  $\alpha$ >
        Set  $x = x_k$ 
        Set  $k = k + 1$ 
        Go To Step 2.
    else
        Go To Step 1.
```

where:

- <generate initial configuration x > generates the initial configuration using either a completely random start or a build-up technique. A completely random start generates atomic positions randomly within a cube of side eight units. As the currently accepted globally optimal structures for all atomic clusters investigated in this study may be contained within a sphere of approximately two units radius, the choice of this size cube for generating initial configurations does not add any bias to the optimisation method and also keeps atoms close enough to each other so that they are able to interact via the pair potential. The build-up technique, for an N atom cluster, uses the optimal configuration for the $N - 1$ atom cluster with the N th atom

randomly placed one unit from the $(N - 1)$ th atom and not within one unit of any other atom.

- <same energy trajectory> determines if the sequence f_i^{k-1} and f_i^k has occurred in any previous iteration. If this is the case then the search is abandoned and a new search started. This reduces the chances of retracing an energy trajectory that has already been traversed and which did not terminate at the global minimum for the Lennard-Jones cluster.
- $APSE(x, v(\alpha, r))$ performs a restricted global minimisation in the sense that the search space is constrained to be close to x . Global minimisation is performed using the APSE search technique described in Section 2.2. Following the global minimisation a local minimisation is performed.
- $V(x_k, v(\alpha, r)) = \sum_{i=1}^{N-1} \sum_{j=i+1}^N v(\alpha, r_{ij})$, where r_{ij} is the Euclidean distance between atoms i and j .
- <terminate> terminates the algorithm if $\alpha = \alpha_{max}$ and f_i^k is within 0.001 of the currently best known result.
- <increment α > increments the current value of α as follows:
 - if $v(\alpha, r) = v_1(\alpha, r)$, $\alpha = 0.0, 0.2, 0.4, 0.6, 0.8$ and 1.0 .
 - if $v(\alpha, r) = v_2(\alpha, r)$, $\alpha = 1, 2, 3, 4, 5$ and 6 .
 - if $v(\alpha, r) = v_3(\alpha, r)$, $\alpha = 0.5, 1.0, 2.0, 3.0, 4.0$ and 5.0 .

3.4 Results

3.4.1 APSE and Atomic Build-up

Table 3.3 shows the number of function evaluations required by a single run of APSE to find potential energy values which agree, to two decimal places, with currently accepted values (Table 3.1) for clusters in the range $N = 3, \dots, 20$. The number of function evaluations, when compared with those needed for the test function in Section 2.4.5 (Figure 2.10), clearly demonstrates the complexity of the potential energy surface for atomic clusters.

| N | Function Evaluations | N | Function Evaluations |
|-----|----------------------|-----|----------------------|
| 3 | 909 | 12 | 76515 |
| 4 | 4361 | 13 | 122150 |
| 5 | 5665 | 14 | 55860 |
| 6 | 103334 | 15 | 9943 |
| 7 | 12166 | 16 | 252949 |
| 8 | 20046 | 17 | 106052 |
| 9 | 11462 | 18 | 71467 |
| 10 | 11476 | 19 | 236523 |
| 11 | 6891 | 20 | 114344 |

Table 3.3: Function evaluations required by APSE to find the global minimum energies for Lennard-Jones atomic clusters, $N = 3, \dots, 20$.

3.4.2 APSE and PES Smoothing

The optimisation algorithm described in Subsection 3.3.2 was implemented on an IBM RS6000 and tests performed using pair potentials v_{lj} , $v_1(\alpha, r)$, $v_2(\alpha, r)$ and $v_3(\alpha, r)$ for atomic clusters in the range $N = 2, \dots, 30$ atoms. While the pair potential v_{lj} has no dependence on α , it is included as a basis for comparison (the algorithm used the same number of steps within each iteration for v_{lj} as that used for the other pair potentials). Table 3.4 shows the number of distinct energy trajectories required to obtain the currently

accepted result for each atomic cluster (X denotes that the global minimum was not found) while Table 3.5 presents a summary of these results.

| N | v_{lj} | v_1 | v_2 | v_3 | N | v_{lj} | v_1 | v_2 | v_3 |
|-----|----------|-------|-------|-------|-----|----------|-------|-------|-------|
| 3 | 1 | 1 | 1 | 1 | 17 | X | 4 | X | 23 |
| 4 | 2 | 1 | 1 | 1 | 18 | X | 2 | 1 | 7 |
| 5 | 3 | 1 | 1 | 1 | 19 | 40 | 2 | 2 | 2 |
| 6 | 33 | 1 | 1 | 1 | 20 | 4 | 3 | 3 | 2 |
| 7 | 13 | 2 | 1 | 1 | 21 | 8 | 1 | 3 | 9 |
| 8 | 1 | 4 | X | X | 22 | 2 | 4 | 1 | 2 |
| 9 | 1 | 2 | 2 | 3 | 23 | 1 | 4 | 2 | 1 |
| 10 | 1 | 5 | 2 | 1 | 24 | 8 | 5 | 1 | 2 |
| 11 | 17 | 2 | 1 | 1 | 25 | 17 | 8 | 2 | X |
| 12 | 3 | 1 | 1 | 1 | 26 | 38 | 5 | 1 | 1 |
| 13 | 2 | 1 | 1 | 1 | 27 | X | 4 | X | X |
| 14 | 1 | 1 | 2 | 1 | 28 | 21 | 1 | 20 | 6 |
| 15 | 44 | 1 | 13 | 30 | 29 | 86 | 6 | 9 | 2 |
| 16 | 1 | 2 | 19 | 43 | 30 | X | 7 | X | X |

Table 3.4: Number of energy trajectories required for APSE with build-up, local optimisation and PES smoothing to find global minimum energies for Lennard-Jones atomic clusters, $N = 3, \dots, 30$. X signifies that the global minimum was not found after 50 trajectories had been performed.

| $v(\alpha, r)$ | Total Energy Trajectories | Failed to find Global Minimum |
|----------------|---------------------------|-------------------------------|
| v_{lj} | 348 | 4 |
| v_1 | 81 | 0 |
| v_2 | 91 | 4 |
| v_3 | 143 | 4 |

Table 3.5: Total number of energy trajectories required for APSE with build-up, local optimisation and PES smoothing to find global minimum energies for Lennard-Jones atomic clusters, $N = 3, \dots, 30$.

From Table 3.5 it is clear that the $v_1(\alpha, r)$ family of pair potentials modified the PES such that a sufficient proportion of local minima were eliminated but the global minimum remained accessible. Pair potentials $v_2(\alpha, r)$ and $v_3(\alpha, r)$ tended to produce PESs which were too smooth in the initial stages and were unable to “direct” the search in the appropriate

direction. The “optimal” family of smoothing pair potentials would appear to lie between the $v_1(\alpha, r)$ and $v_2(\alpha, r)$ families.

3.5 Discussion

Molecular structure problems, particularly for larger atomic clusters, are set in a large number of dimensions and involve a complicated potential energy surface. APSE, in conjunction with local optimisation and a build-up approach, was successful for pure atomic clusters in the range $N = 2, \dots, 20$. The use of a pair potential smoothing technique in conjunction with APSE, a build-up approach and local optimisation was also investigated. In this method, minima were first found for atomic clusters interacting via potential functions that are “smoother” than the Lennard-Jones potential and these minima tracked, using a combination of APSE and local optimisers, while the potential function was incrementally transformed into the Lennard-Jones potential function. This method, using the v_1 family of pair potentials, found all global minima for clusters in the range $N = 2, \dots, 30$ and demonstrated that the global minimum for a Lennard-Jones cluster can be more efficiently determined by starting with a pair potential which is “smoother” than the Lennard-Jones pair potential but which is not radically different.

Extensions that could be made to this smoothing technique include:

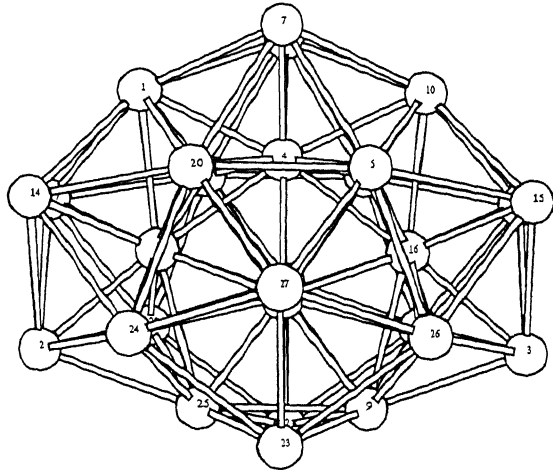
- As shown in Figure 3.11, bifurcations may occur in an energy trajectory. Currently these would not be detected and explored because the same trajectory checking mechanism prevents repeated traversals of energy trajectories that have already been traversed. A more effective technique would be to enforce branching into an unexplored region when the same energy trajectory is detected. The determination of when to branch and how many branches to allow at each step are

aspects that need to be evaluated.

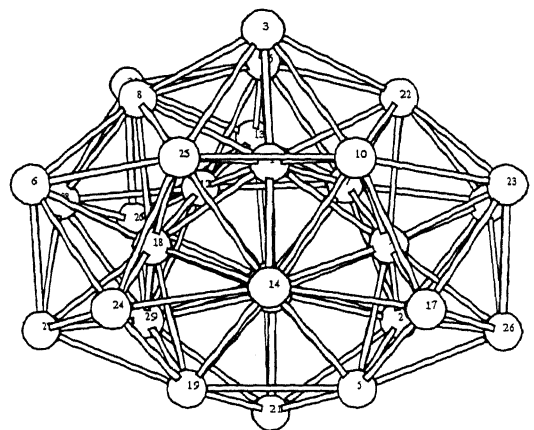
- A number of options exist for parallelising the method. For example, a processor pipeline could be implemented, with each processor handling a particular value of α . Alternatively, a master processor could determine trajectory starting points and pass these to slave processors for traversal.

In summary, in comparison with other methods, APSE performed well for the pure atomic cluster problem when used in conjunction with a build-up technique, local optimisation and PES smoothing. However, the use of the build-up technique brings an inherent bias into the search which prevented APSE from globally optimising the 31 atom cluster. As shown by Northby [37], there is considerable rearrangement of all 17 atoms in the outer icosahedral shell when transitioning from the globally optimal 30 atom cluster to that of the 31 atom cluster. The qualitative argument put forward by Northby is that, initially the atoms in the outer shell are more tightly bound to the core but, as the shell fills, intrashell interactions become more important. Figures 3.12(a), (b) and (c) show the sequence of structures obtained by APSE (in conjunction with the build-up technique, local optimisation and PES smoothing) for $N = 29, 30$ and 31 . Figure 3.12(d) is the currently accepted globally minimum structure for $N = 31$ atoms.

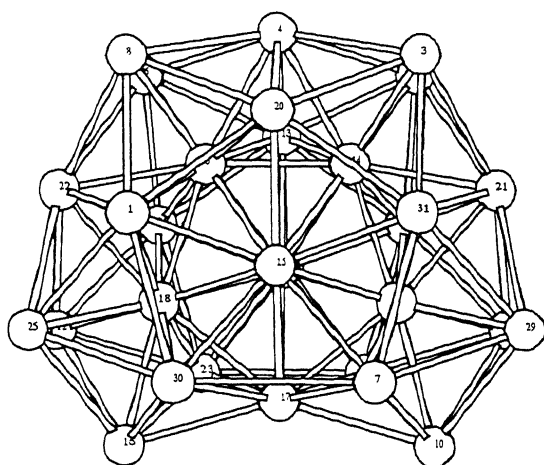
These structural discontinuities also occur at other points within the sequence of atomic cluster sizes [11] and, while techniques which incorporate build-up will typically find very good local minima and most global minima for a range of atomic clusters, they are generally unable to transition correctly through a structural discontinuity. This tends to result in all subsequent structures being sub-optimal.



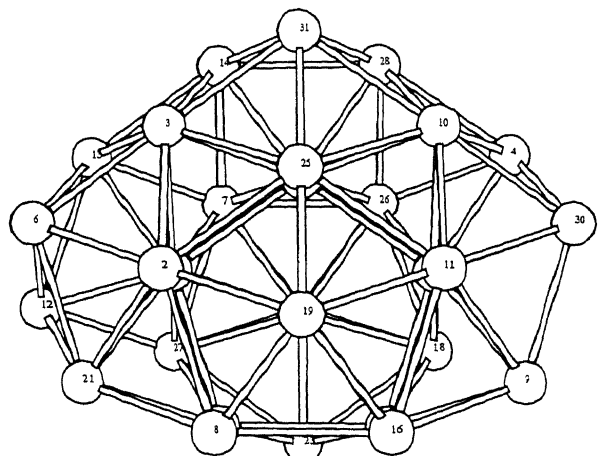
(a) $N = 29$, energy = -123.587 .



(b) $N = 30$, energy = -128.287 .



(c) $N = 31$, energy = -133.294 .



(d) $N = 31$, energy = -133.586 .

Figure 3.12: Structures (a), (b) and (d) are the respective minimum energy structures for the $N = 29, 30$ and 31 atomic clusters. Structure (b) is correctly found by APSE (with build-up, local optimisation and PES smoothing) using Structure (a) as the base structure for the build-up generation of initial structures. Structure (c) is that obtained by APSE using Structure (b) as the base structure for the build-up generation of initial structures. Structure (d) is the currently accepted globally minimum structure and was not found by APSE.

Chapter 4

GEM* Computational Method

4.1 Introduction

GEM*, the main computational method developed within this thesis, is now presented. As described in the previous chapter, the APSE search method, in conjunction with a build-up approach, local optimisation and PES smoothing was able to find all currently accepted global minimum configurations for scaled Lennard-Jones atomic clusters in the range $N = 2, \dots, 30$. However this method was unable to successfully optimise the $N = 31$ atomic cluster and, for the reasons pointed out in Section 3.5, it is unlikely that any build-up based global optimisation method could be developed that would, for example, successfully optimise all Lennard-Jones clusters in the range $N = 2, \dots, k$ where $30 < k < 100$. Consequently, a global optimisation method not based on a build-up technique would appear to be a basic requirement for successfully optimising a range of pure atomic clusters. In addition, other important requirements for a successful pure atomic cluster optimisation method are

1. The ability to go directly to the minimum of a catchment basin from any point within the catchment basin. This simplifies the global op-

timisation problem in that the global optimisation method need only find a point within that catchment basin for which the local minimum is also the global minimum rather than directly locate the global minimum.

2. The ability to intensively search a subset of the domain. In some situations, the global minimum is closely surrounded by a number of local minima and there is a need for the search method to be able to traverse from a catchment basin into adjacent catchment basins.
3. Maximise the use of computational resources. For example, a method that can be efficiently parallelised is to be preferred to a sequential method and facilities such as restarting optimisation runs should be able to be implemented.
4. When dealing with partially separable problems, such as the optimisation of molecular architectures, the ability to automatically recognise subsets of configurations which are inherently “good” and incorporate these subsets in new configurations. Preferably, this process should not rely on the use of heuristic information.

Clearly local optimisation techniques and APSE (in constrained mode) can be used to implement requirements 1 and 2 listed above. However, these methods need to be used in conjunction with a technique which satisfies requirements 3 and 4. Of the global optimisation methods described in Section 1.4, the genetic algorithm would appear to be the most appropriate candidate. Random Search (Section 1.4.1) is effectively implemented within APSE while Simulated Annealing (Section 1.4.2) clearly fails to implement requirements 3 or 4. However GAs, as described in Section 1.4.3, have an inherent parallelism which can be efficiently overlaid with a parallel

implementation at the processor level so they clearly satisfy requirement 3. The Schema Theorem [13] proves the ability of the GA to recognise “good” subsets within a solution and thus satisfy requirement 4.

As a result of these considerations, a new optimisation method, GEM*, was developed which incorporates APSE, in conjunction with local optimisation, into a genetic algorithm based environment. To maximise the amount of computational power available for the algorithm, the method was extended by developing a version which effectively uses any number of processors operating in parallel.

Within this chapter, Section 4.2 describes the basic GEM* algorithm, Section 4.3 overviews the GEM* software implementation and operational environment while Section 4.4 presents a discussion and summary.

4.2 GEM* Algorithm

GEM* implements a parallel hybrid real-coded genetic algorithm incorporating local and global optimisers and genetic operators which function in both the problem (phenotype) and genotype domains. Using the following definitions

| | | |
|--------------------|---|---|
| g | = | Generation number |
| P_g | = | Current population for generation g |
| $\mathcal{P}(P_g)$ | = | Set of all possible pairings which may be generated from P_g |
| T_g | = | Temporary population generated from P_g |

the basic GEM* algorithm is

| GEM* Algorithm | |
|------------------------------------|------------------------------------|
| Master Processor | Slave Processors |
| $g = 0$ | |
| Initialise | Initialise |
| <i>Next Generation:</i> | |
| $g = g + 1$ | |
| Select | |
| StartAll | Wait |
| For a subset of $\mathcal{P}(P_g)$ | For a subset of $\mathcal{P}(P_g)$ |
| Crossover | Crossover |
| Mutate | Mutate |
| if finished | |
| stop all processes | |
| else | |
| go to <i>Next Generation</i> | Go to <i>Next Generation</i> |

The elements of this algorithm, with respect to the optimisation of pure atomic clusters, are

1. **Initialise** creates a population T_g of N atom clusters by randomly placing each atom within a cube, where the size of the cube is dependent on N . These clusters are then locally optimised.
2. **Select** chooses clusters from T_{g-1} for inclusion in P_g . Selection is based on cluster energy where, to maintain diversity in the pool, only one cluster is chosen with a given energy (plus or minus a small delta). At the completion of **Select**, T_g is cleared.
3. **StartAll** sends a message from the master processor to all slave processors to start processing their subset of $\mathcal{P}(P_g)$. To evenly balance the workload, each processor, including the master processor, is allocated the same number of pairs of structures to crossover and mutate.

4. **Wait** is used by the slave processors to wait for the start message from the master processor.
5. **Crossover** applies crossover genetic operators, using all pairings in $\mathcal{P}(P_g)$, to generate new clusters for input to the subsequent **Mutate** operator. A number of crossover operators, some tailored to specific molecular structures, were implemented and are described in detail in subsequent chapters.
6. **Mutate** accepts new clusters generated by **Crossover** and, with a specified probability, performs one of a number of possible mutations. The basic components of **Mutate** are APSE and a local optimiser, used either separately or in conjunction, to perform the following mutations
 - μ_1 , no modification other than full local optimisation and was applied to all child clusters. This mutation produces a structure corresponding to a local minimum.
 - μ_2 , a repeating sequence of restricted APSE optimisations and full local optimisations. The APSE optimisation is restricted in that the search domain is constrained to be close to the starting configuration. This mutation operation is designed for situations where there are a number of close local minima of which one may be the global minimum.
 - μ_3 , a general APSE optimisation followed by local optimisation is performed. This performs a global search and tends to maintain a flow of diverse structures into the population.
 - μ_4 , one randomly chosen element of the structure is perturbed by a relatively small amount and a partial local optimisation per-

formed allowing only this element to vary. This, and the following mutation, are designed for situations where there are just a few problem areas within an otherwise good solution.

- μ_5 , one randomly chosen element of the structure is perturbed by a relatively large amount and a partial local optimisation performed allowing only this element to be modified.

Mutations μ_2, μ_3, μ_4 and μ_5 were applied repetitively to each structure and the number of repetitions increased at each generation. At the completion of the **Mutate** operator, all new clusters are added to the T_g pool.

The population size used for GEM* was normally in the range 6, . . . , 12. This appeared to balance the need for diversity in the pool against the computational requirements of local optimisation. The mutation probability was low (≈ 0.01) and all possible crossovers were performed.

The use of GAs has not been particularly successful in the past for globally optimising molecular structures because, as described in Section 1.4.3, standard (binary-coded) GAs are efficient when applied to problems whose parameters can be encoded as short, low-order schema which are relevant to the underlying problem and relatively unrelated to schema over other fixed positions. For molecular structures however,

- the GA parameters are the atomic positions which are real-valued.

Using a binary-coded GA requires that these positions be discretised so they can be coded as binary integers. To obtain an accuracy of 3 digits after the decimal place; for a 30 atom cluster, a binary solution vector of length 1260 bits is required. This in turn generates a search space of approximately 10^{420} elements over which a binary-coded GA

can be expected to perform poorly.

- when evaluating the potential energy (and hence the fitness factor) of a cluster, the position of each atom is only meaningful in the context of the positions of all other atoms. That is, schema over different positions are not unrelated, so standard GAs can be expected to perform poorly when applied to the cluster problem.

The first problem is addressed in GEM* by the use of a hybrid real-coded GA. As described in Section 1.4.3, real-coded GAs incorporating local optimisation are, in effect, a variable metric discretised GA and alleviate the first problem listed above by limiting the search space to the local minima.

The second problem is addressed in GEM* by

- using phenotype genetic operators which are able to produce “building blocks” in the problem space and then incorporate these in new solutions.
- local optimisation of all new solutions before the selection process.

In the situation where a solution is basically “good” but has a small number of atoms which are close together resulting in a high potential energy, local optimisation will generally result in a significant reduction of this potential energy and increase the probability that the solution will remain in the genetic pool.

From the parallel processing point of view, GEM* implements a synchronous concurrent genetic algorithm where there is a single pool of solutions, and at the start of each generation, each processor (including the master processor) is allocated a subset of possible pairings from this pool. To maximise processor efficiency, these subsets are constructed so that they are all the same size with, if necessary, repeated occurrences of pairings.

Each processor performs **Crossover** and **Mutate** operations using only its subset of pairings and generates a new list of possible solutions to be aggregated into the temporary pool T_g . When all processors have completed the generation, the master processor creates a new pool of solutions P_{g+1} from the temporary pool T_g and the next generation is started.

4.3 GEM* Software

GEM* is implemented in the C++ programming language and executable code may be conditionally generated for a number of target computers including the parallel IBM SP2 computer (using any number of processors) and a range of non-parallel computers (to date, GEM* has been implemented on IBM RS6000, Digital Alpha and Sun workstations).

The processing context diagram for GEM* is shown in Figure 4.1. With

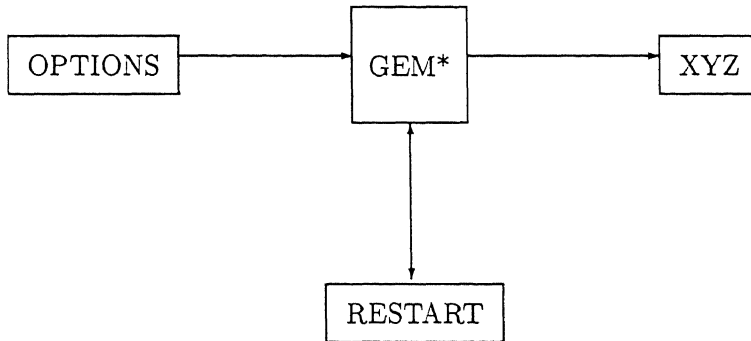


Figure 4.1: GEM* processing context. The OPTIONS file defines the molecular structure to be optimised and also specifies options for the genetic algorithm. RESTART is updated at the end of each generation and allows optimisation runs to be restarted at the last completed generation. The output XYZ files contain Cartesian coordinates for the atomic positions of all solutions in the genetic pool.

reference to this diagram, the OPTIONS input defines the scope and type of optimisation to be performed by GEM* and includes the following data

- **Structural Options**, which define the type and size of molecular structure to be optimised. For example, for pure atomic clusters, the number of atoms in the cluster may be specified.
- **GA Options**, which define the maximum number of generations, the population size, the mutation rate and the number of processors to be utilised.
- **Restart Options**, which optionally allow a restart to be performed from a RESTART file created by a previous optimisation.

The RESTART file, which contains the genetic pool of solutions and other restart options, is generated at the completion of each generation. Using the data from this file, a previously terminated run of GEM* can be restarted at the last completed generation.

The output XYZ data files contain Cartesian coordinates for the atomic positions for all structures in the genetic pool. In conjunction with the XMOL [63] software, this allows molecular structure diagrams such as that shown in Figure 1.1 to be generated.

4.4 Discussion

This chapter described the rationale for GEM*, the main computational method used in this study. GEM* provides a software system which is easily modified and may be applied to a number of different molecular architecture problems. The features provided by the base GEM* software include

- both Powell Direction Set and BFGS local optimisers.
- the APSE global optimisation method.
- a parallel hybrid genetic algorithm.

- an operational environment appropriate for complex global optimisation processing.
- an interface which is straightforward to modify for different molecular structures.

Components of the GEM* software which must be tailored for specific molecular architecture problems include phenotype genetic crossover operators, genetic mutation operators and the genetic encoding method. In addition, functions for potential energy and potential energy gradient calculations are generally problem specific and must be added.

The remainder of this thesis describes the GEM* optimisation of specific molecular architecture problems, including the problem specific modifications required to GEM*, and the results obtained.

Chapter 5

GEM* Optimisation of Pure Atomic Clusters

5.1 Introduction

Compared to the other optimisation methods described in Section 3.2, GEM* was particularly successful in optimising pure Lennard-Jones atomic clusters and found all currently accepted global minima for scaled Lennard-Jones atomic clusters of 2 to 80 atoms. In addition, new lower minima for 77 and 78 atom clusters were found.

Section 5.2 of this chapter describes the extensions required to the base GEM* software for the atomic cluster problem while the results obtained for this problem are described in Section 5.3. An analytical and experimental comparison of the efficiency of two types of genetic crossover operators used in GEM* is presented in Section 5.4. Finally, Section 5.5 contains a review and conclusion.

5.2 GEM* Computational Method

The following genetic crossover operators were added to the base GEM* algorithm described in Section 4.2

- χ_1 which randomly selects a crossover point in the vector of atomic positions. This is the basic GA crossover technique and generates new clusters by interchanging a random number of randomly selected atoms between the parent clusters.
- χ_2 which randomly rotates the coordinate system around each axis and, with equal probability, uses atoms within a hemisphere, a quadrant or an octant of the parent clusters to construct new clusters by simply exchanging corresponding volume elements between parents. If the resulting number of atoms in the child cluster is incorrect, it is discarded and another crossover performed. Stepwise optimisations were performed on all new clusters by initially physically separating the two volume elements used to construct the cluster and incrementally moving them towards each other, calculating the potential energy of the cluster at each step. Using that configuration where the potential energy was a minimum, a local optimisation was then performed.
- χ_3 which randomly selects an atom as the crossover point in each parent cluster and swaps these atoms, along with a randomly chosen number of nearest neighbours. This has the effect of interchanging an arbitrarily shaped volume from each parent while still maintaining relative atomic positions within this volume. The two crossover atoms are directly interchanged and neighbouring atoms interchanged such that they maintain their original positions relative to their respective crossover atom and the centre of mass of the cluster.
- χ_4 selects the atoms with the highest and lowest binding energies as the crossover point in each parent. The lowest binding energy atom and all neighbours whose binding energies are less than the average

binding energy for the cluster are replaced with the highest binding energy atom and its nearest neighbours from the other parent. This has the effect of replacing an arbitrarily shaped volume, which has a low contribution to the energy of the cluster, with another portion which contributes more energy. As for χ_3 , the two crossover atoms are directly interchanged and the neighbour atoms interchanged such that they maintain their original position relative to their respective crossover atom.

Of these crossover operators, χ_2 was that primarily used to obtain the results of this chapter.

Clearly the genetic algorithm environment within GEM* is similar to that of Deaven et al. ([10], [11]) in that small genetic populations are used, all possible crossovers are performed and phenotype crossover operators are employed. However there are essential differences and these are now summarised

- Deaven et al. used a single “cut and paste” genetic operator, where the cluster was cut along a plane through the centre of mass and hemispheres from each parent cluster combined to produce a new child cluster. If this resulted in the incorrect number of atoms in the child cluster, the cutting plane was translated in opposing directions in each parent cluster until the correct number of atoms was obtained in the child clusters. In contrast, GEM* uses a number of operators to interchange different sized volumes between clusters. If the resulting number of atoms in the child cluster is incorrect, it is discarded and another crossover performed. The rationale for using different size volumes (hemisphere, quadrant, octant and arbitrary shaped volumes around a particular atom) is that, as the GA progresses, structures

in the genetic pool become “closer” to that of the globally optimal configuration and require smaller and smaller adjustments. The use of a range of volume sizes provides a mechanism whereby GEM* is able to perform a range of adjustments during genetic crossover.

- Deaven et al. physically separated atoms in new clusters that were “close” to each other. As most local minima occur at high energies [36], this physical translation of atoms reduces the complexity of the optimisation problem by effectively eliminating these local minima. In fact, Neumaier [36] estimates that removing these high energy local minima reduces the number of local minima on the PES from $O(\exp(N^2))$ to $O(\exp(N))$. While this physical separation of close atoms would appear to be a reasonable operation to perform, given the form of the Lennard-Jones pair potential, it does incorporate heuristic information into the Deaven et al. optimisation technique and, for example, would not be as effective in situations involving more than a single type of pair potential (for example, the mixed atom clusters discussed in Chapter 6). In contrast, GEM* incorporates no heuristic information at any point in the optimisation process and is, in effect, solving a more difficult problem than that attempted by Deaven et al.
 - to move to adjacent catchment basins, Deaven et al. used an algorithm which took a random number of steps and, at each step, changed direction so as to maintain travel along a direction slightly uphill to an equipotential line. GEM* used the less complicated restricted APSE search to locate catchment basins adjacent to the current point.

The results obtained by GEM* for pure atomic clusters are now presented.

5.3 Results

GEM* successfully located all currently accepted global minima presented in Table 3.1 for Lennard-Jones clusters in the range $N = 2, \dots, 80$. In addition, new lower energy clusters were found for 77 (Figure 5.1) and 78 (Figure 5.2) atom clusters with energies of -408.520 (previously -408.463) and -414.795 (previously -414.681) respectively.

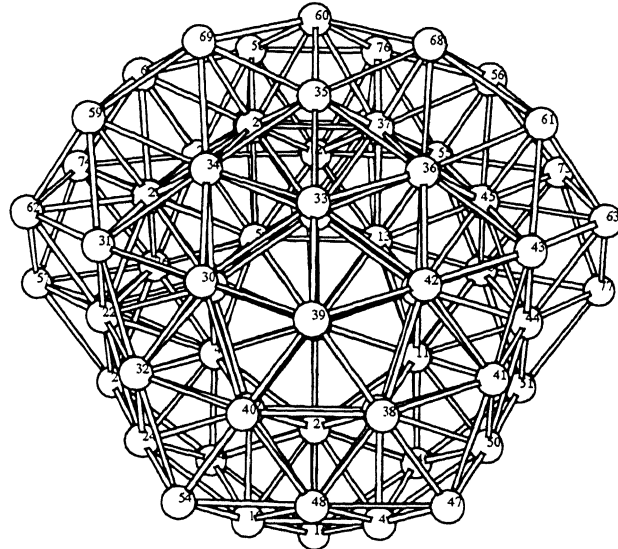


Figure 5.1: GEM* optimised structure for the $N = 77$ atomic cluster with an energy of -408.520 .

Figure 5.3 shows how the minimum, maximum and average energies for the clusters in the population changed, as a function of generation, for a 72 atom cluster. This pattern, with an initial sharp decrease in energy followed by a slow approach to the global minimum, was observed for all clusters.

The number of generations required to find the global minimum as a function of the number of atoms in the cluster is shown in Figure 5.4. A

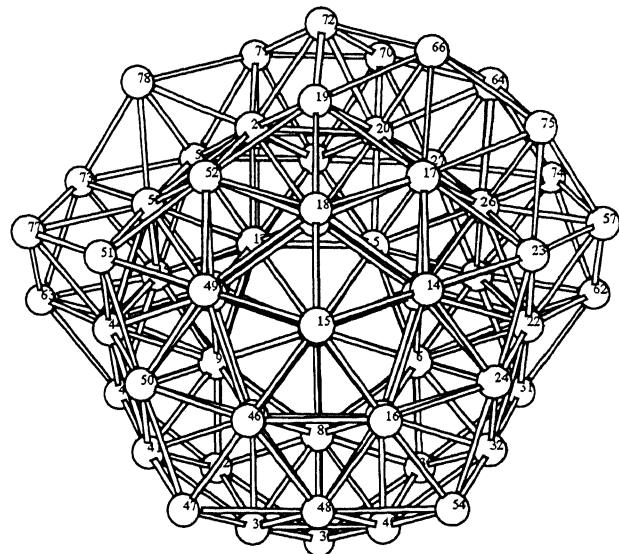


Figure 5.2: GEM* optimised structure for the $N = 78$ atomic cluster with an energy of -414.795 .

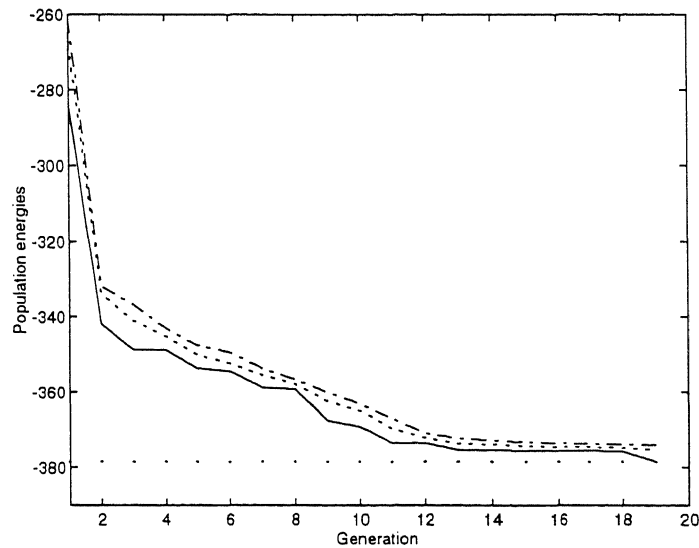


Figure 5.3: Minimum, maximum and average population energies at the completion of each generation for the GEM* optimisation of an $N = 72$ scaled Lennard-Jones atomic cluster.

least-squares fit of the data gives

$$G = 0.0065N^2 - 0.0970N + 4.028$$

where G is the number of generations required. However, as each data point is the result of a single optimisation run for a cluster, and as there appears to be a new trend developing for $N \geq 74$, this fit may be inappropriate for larger values of N .

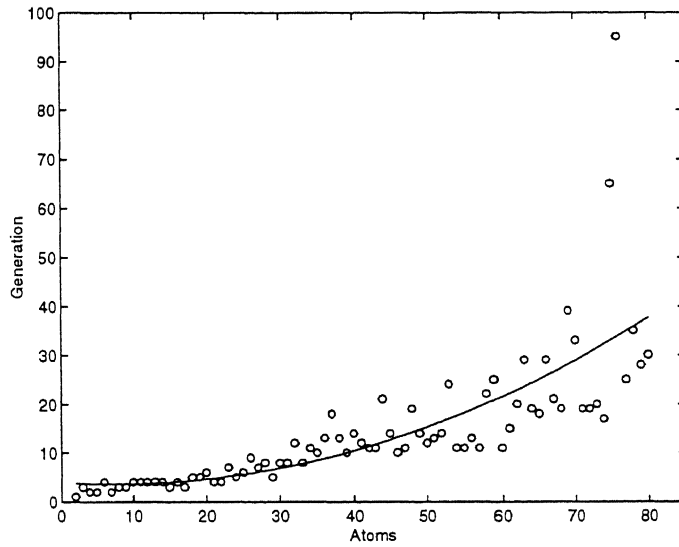


Figure 5.4: Generations required for GEM* to optimise atomic clusters in the range $N = 2, \dots, 80$. Each data point is the result of a single trial.

The multiprocessor scalability of GEM* is shown in Figure 5.5 for a 40 atom cluster using 1 to 10 processors (taking the elapsed time for the single processor case as unity). A least-squares fit of this data gives

$$E = 0.0105P^2 - 0.2022P + 1.113$$

where P is the number of processors and E is the ratio of the elapsed time for P processors to the elapsed time for a single processor. Inefficiencies

arise in the multiprocessor implementation from normal message handling and also when there is a mismatch between the population size and the number of processors. That is, the required crossover/mutation operations cannot be equally spread across the available processors.

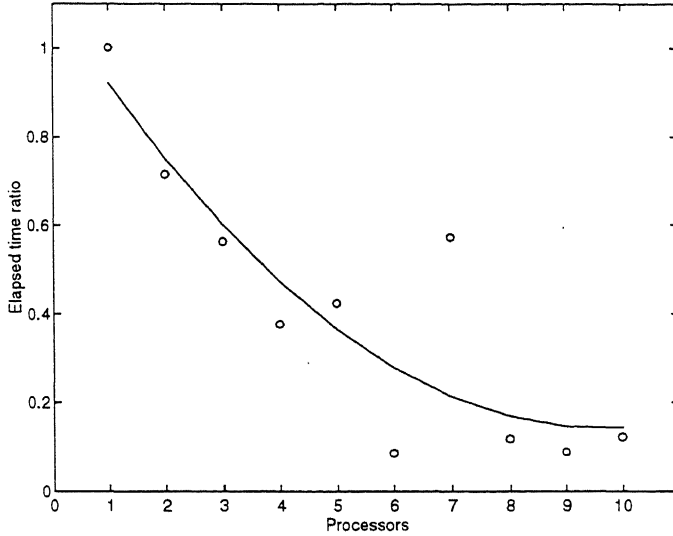


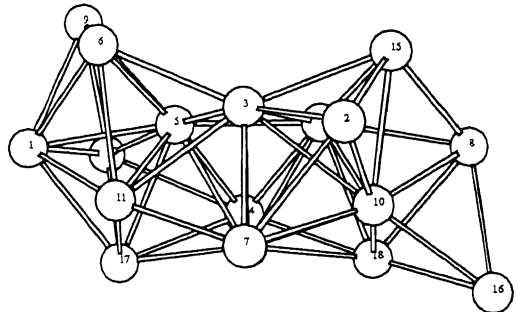
Figure 5.5: Relative decrease in the elapsed time to optimise an $N = 40$ Lennard-Jones atomic cluster as the number of computer processors is increased. The elapsed time for a single processor is taken as unity and each point represents the relative elapsed time required for a single optimisation of this cluster.

Figures 5.6 and 5.7 show the last eight “elite” structures found by GEM* during the optimisation of an 18 atom cluster. The first structure (Figure 5.6(a)) basically consists of stacked tetrahedrons with the first basic icosahedron structure appearing in Figure 5.6(b) where the atoms not in the icosahedron are positioned at the apex of tetrahedrons based on three icosahedron atoms. Figures 5.6(c), (d) and Figure 5.7(a) show these tetrahedrons moving together on the surface of the icosahedron until, in Figure 5.7(b) atoms 4, 9, 11 and 18 form a four-sided polygon base for atom 14. These five atoms are slightly rearranged in Figure 5.7(c) and, finally the five outer

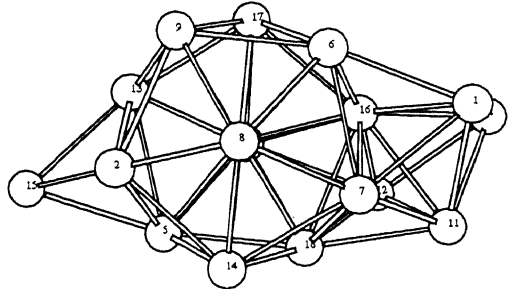
atoms (9, 11, 13, 16 and 18) form a pentagonal ring centred on, but above, atom 10 in the globally optimal structure (Figure 5.7(d)).

Figures 5.8 and 5.9 show eight of the “elite” structures found by GEM* during the optimisation of a 56 atom cluster. The globally optimal structure for this cluster is two interpenetrating icosahedrals centred on a single atom with 12 atoms in the inner shell, 42 atoms in the outer shell and the remaining atom placed at the apex of a tetrahedron based on three atoms in the outer icosahedron. The first appearance of an icosahedron during the optimisation was in the structure shown in Figure 5.8(a) where the atoms not in the icosahedron are basically attached to the icosahedral shell as a group of stacked tetrahedrons which, in subsequent structures, start to envelope the icosahedron (Figure 5.8(b), (c) and (d)) until finally, the outer icosahedral shell is basically complete (Figure 5.9(a)). The remainder of the optimisation process consists of filling in the “holes” in the outer icosahedral shell (Figure 5.9(b), (c)) until 1 atom is at the centre, 54 atoms are positioned in the icosahedral shells and the remaining atom placed at the apex of a tetrahedron based on atoms 1, 5 and 49 (Figure 5.9(d)).

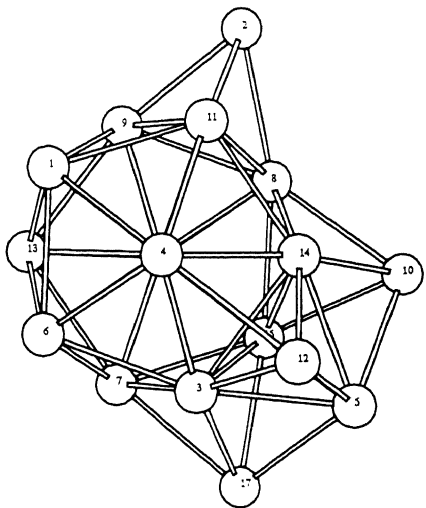
Figure 5.10(a) shows the currently accepted globally minimum energy structure for the $N = 37$ atomic cluster. Figure 5.10(b) is the structure which, until recently, was accepted as being the globally minimum structure for $N = 38$ (and is invariably the structure found by any optimisation method incorporating a build-up technique). Figures 5.10(c) and (d) show lower energy structures, first reported in [11] and also found by GEM*.



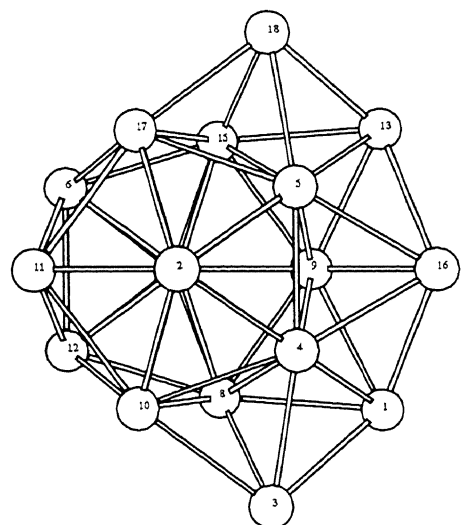
(a) $N = 18$, energy = -60.814 .



(b) $N = 18$, energy = -64.625 .

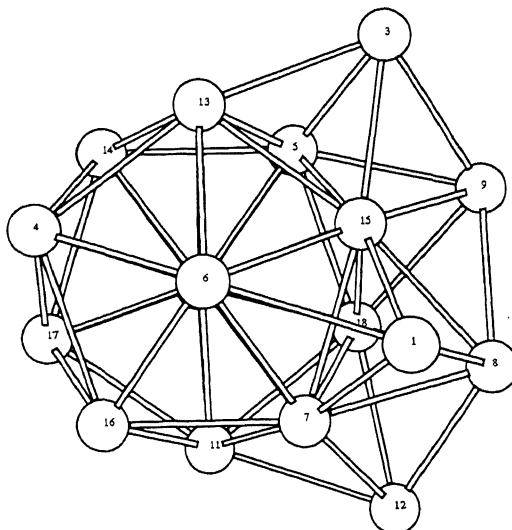


(c) $N = 18$, energy = -64.892 .

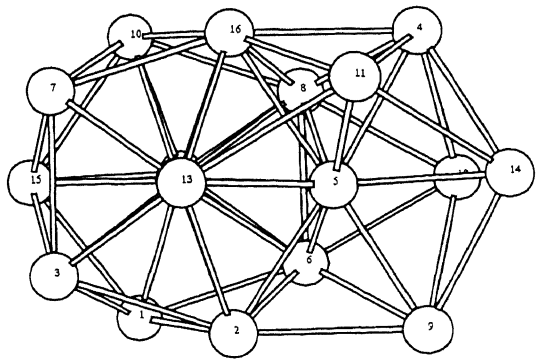


(d) $N = 18$, energy = -65.787 .

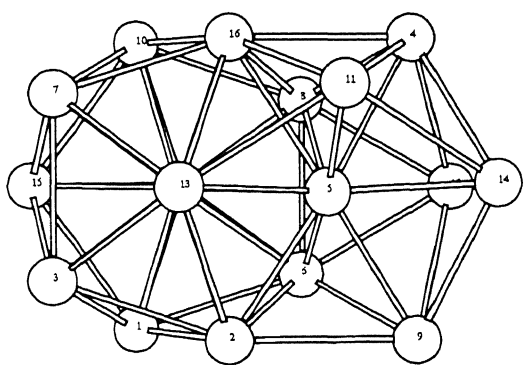
Figure 5.6: Successive elite structures found during the GEM* optimisation of an $N = 18$ atomic cluster.



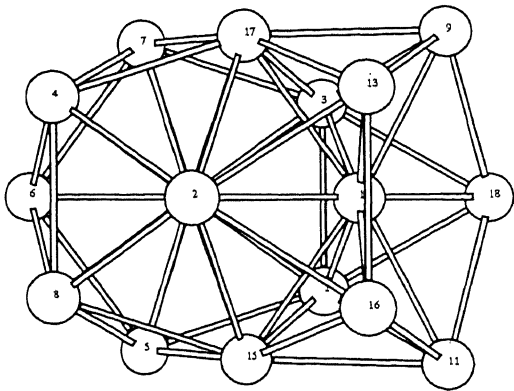
(a) $N = 18$, energy = -65.801 .



(b) $N = 18$, energy = -66.163 .

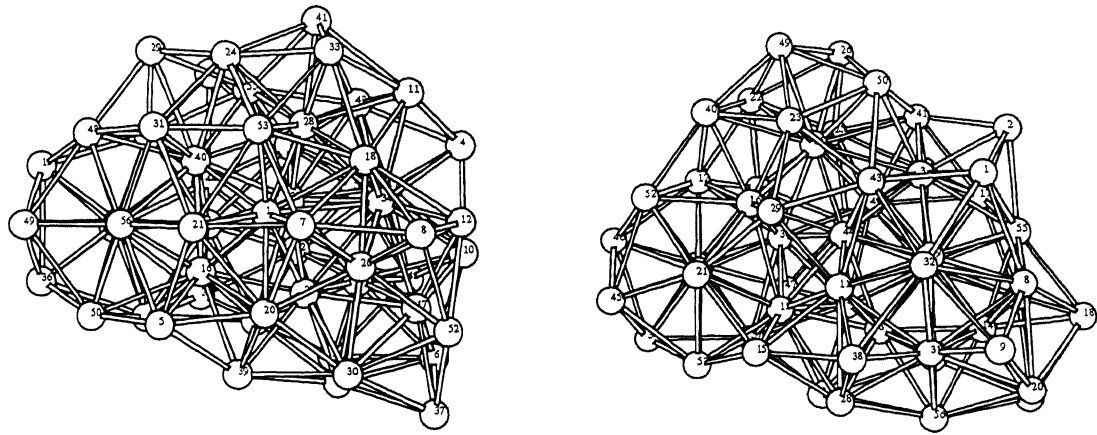


(c) $N = 18$, energy = -66.285 .



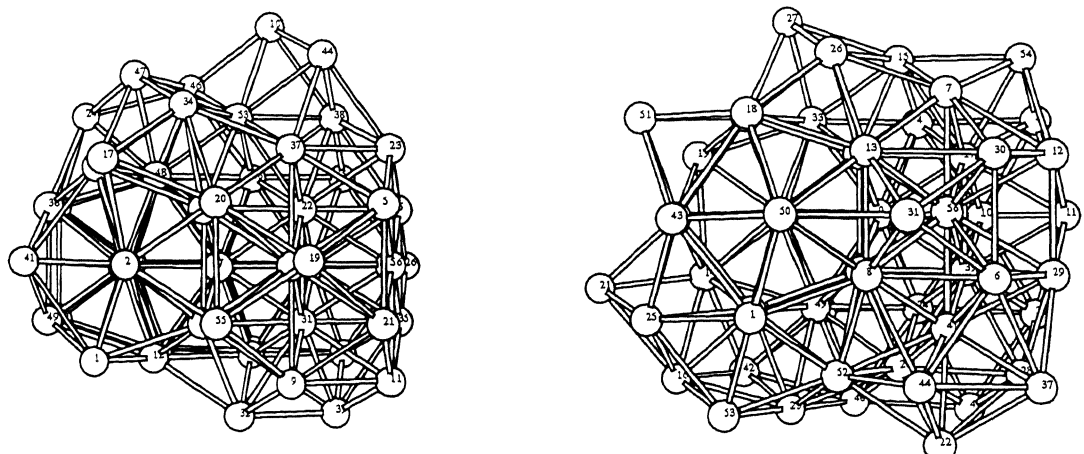
(d) $N = 18$, energy = -66.531 .

Figure 5.7: Successive elite structures found during the GEM* optimisation of an $N = 18$ atomic cluster.



(a) $N = 56$, energy = -261.990.

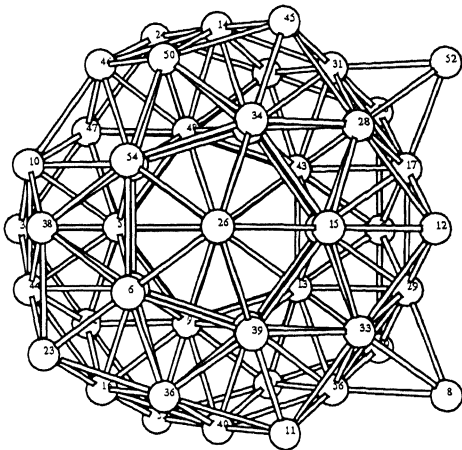
(b) $N = 56$, energy = -266.607.



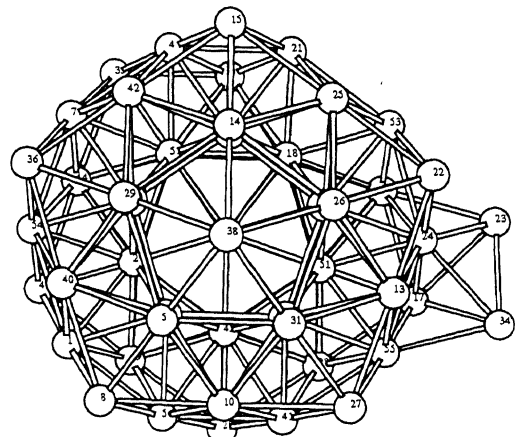
(c) $N = 56$, energy = -273.342.

(d) $N = 56$, energy = -275.215.

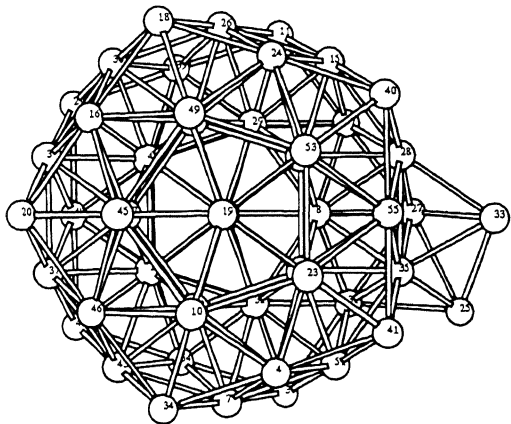
Figure 5.8: Elite structures found during the GEM* optimisation of an $N = 56$ atomic cluster.



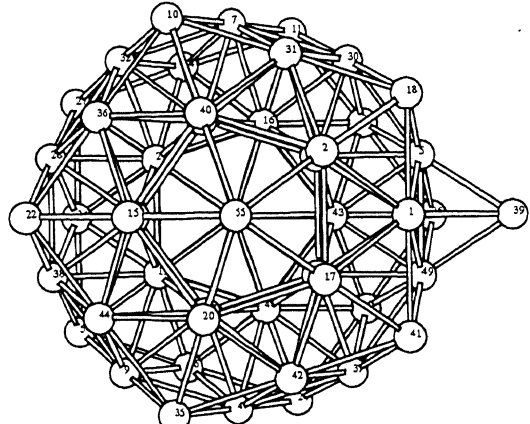
(a) $N = 56$, energy = -280.991 .



(b) $N = 56$, energy = -281.143 .

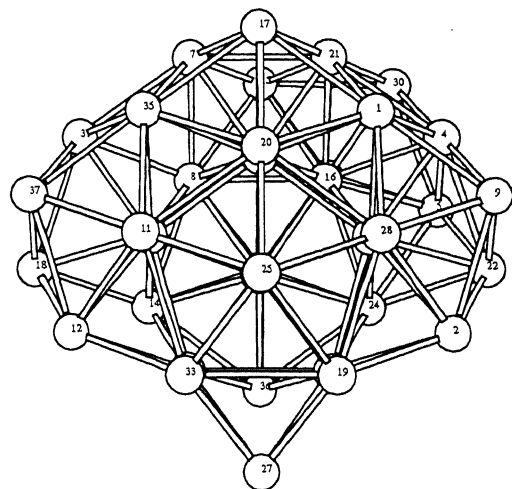


(c) $N = 56$, energy = -281.221 .

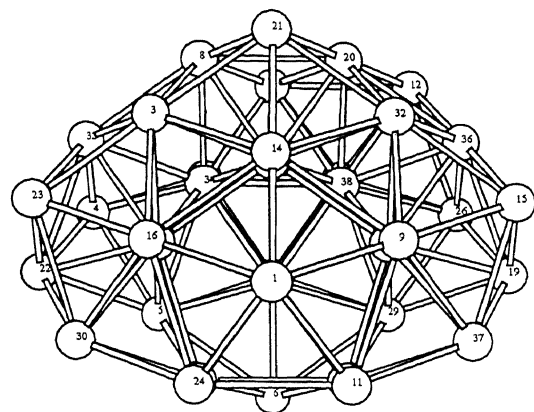


(d) $N = 56$, energy = -283.643 .

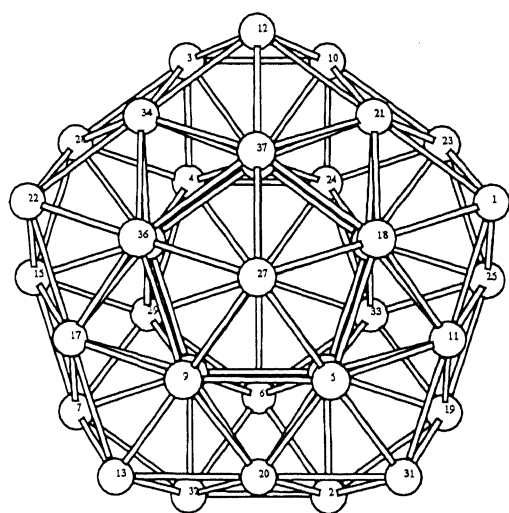
Figure 5.9: Elite structures found during the GEM* optimisation of an $N = 56$ atomic cluster.



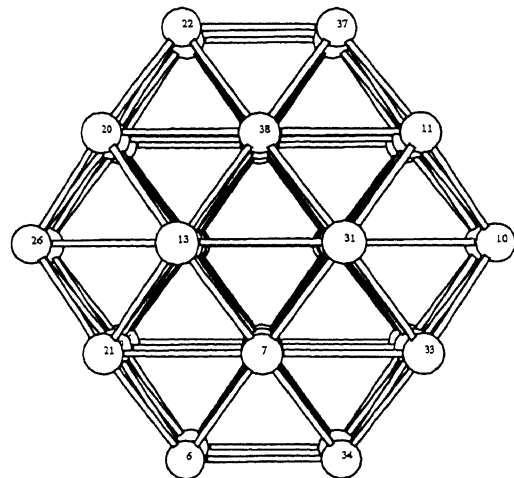
(a) $N = 37$, energy = -167.034 .



(b) $N = 38$, energy = -173.134 .



(c) $N = 38$, energy = -173.253 .



(d) $N = 38$, energy = -173.929 .

Figure 5.10: Structures found during the GEM* optimisation of $N = 37, 38$ atomic clusters.

5.4 GEM* Crossover Analysis

To evaluate the relative efficiency of phenotype as compared to genotype crossover operators, the following data was logged for χ_1 and χ_2 operators during the optimisation of an $N = 18$ atomic cluster

- the lower energy of the two parent clusters.
- the energies of both child clusters after crossover.
- the final energies after BFGS optimisation of the child clusters.

Figures 5.11 and 5.12 show the distribution of final optimised energies of child clusters, as a function of the lower energy of the two parent clusters, for χ_1 and χ_2 respectively. In both cases, data relating to clusters with positive energy has been omitted. Clearly the χ_2 crossover operator is more effective at exploring the search domain at lower energies than the χ_1 crossover. Figures 5.13 and 5.14 show the direct effect of the χ_1 and χ_2 crossover operators and also the subsequent effect of the BFGS optimisation. The trajectory highlighted in Figure 5.14 shows that in one particular case, χ_2 using a pair of parent clusters whose lower energy was approximately -38 , produced a child of approximate energy -56 , which was locally optimised to approximately -60 .

For the atomic cluster problem, one measure of the efficiency of a genetic crossover operator is the expected number of atoms which will be “close” to another atom in the child clusters created by the operator. A relatively high expected number of close atoms implies a less efficient genetic crossover operator, as these close atoms will subsequently need to be separated by the **Mutate** operator. As evidence of this measure as an arbiter of success, Figure 5.15 shows the relationship between the number of close atoms in

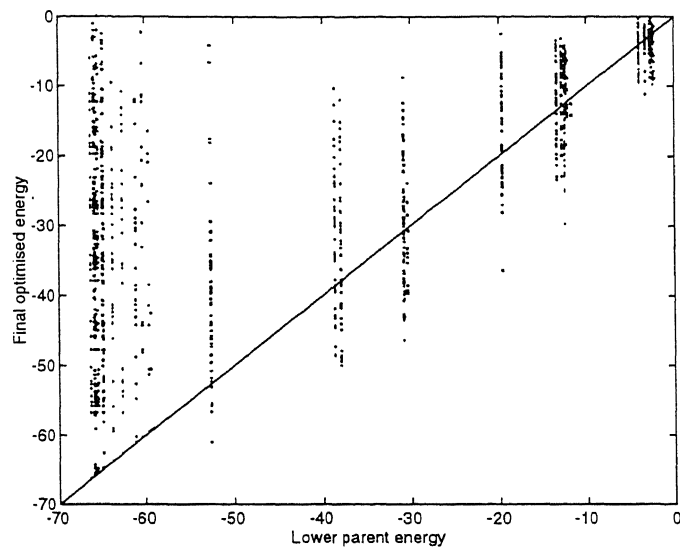


Figure 5.11: Lower parent and final optimised cluster energies for the χ_1 crossover during the optimisation of an $N = 18$ atomic cluster. All positive energy clusters have been omitted from this plot.

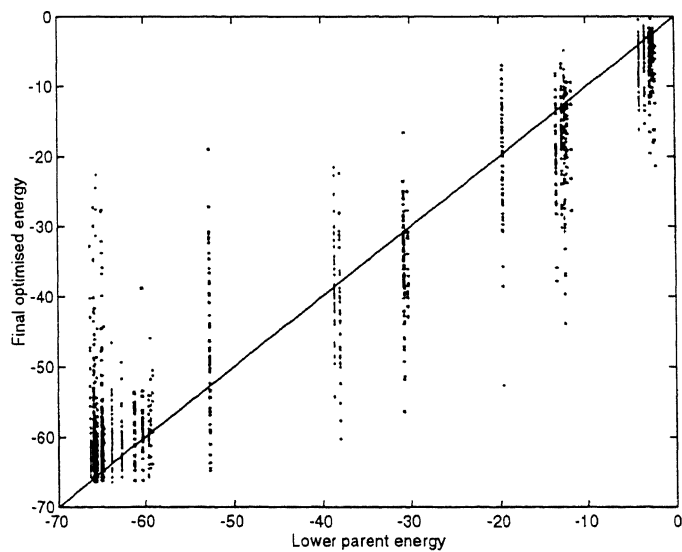


Figure 5.12: Lower parent and final optimised cluster energies for the χ_2 crossover during the optimisation of an $N = 18$ atomic cluster. All positive energy clusters have been omitted from this plot.

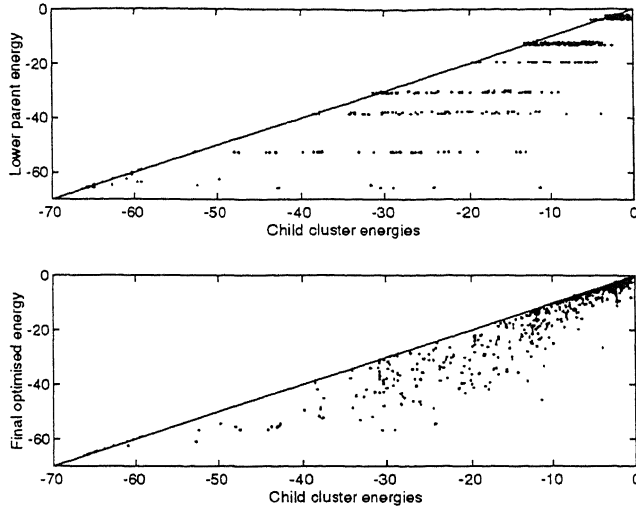


Figure 5.13: Changes in cluster energy during genetic crossover and mutation for the χ_1 crossover. Starting from the lower parent energy to each child energy and finally to the locally optimised child energies. Almost without exception, each child created by the χ_1 crossover has a higher energy than the lower parent energy.

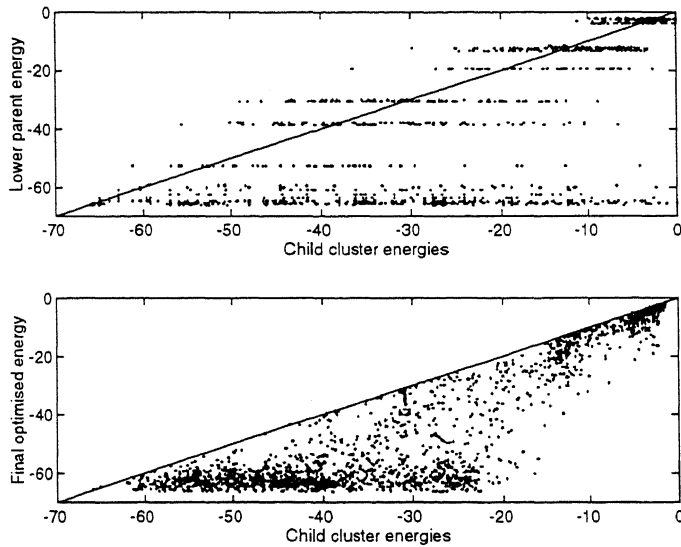


Figure 5.14: Changes in cluster energy during genetic crossover and mutation for the χ_2 crossover. Starting from the lower parent energy to each child energy and finally to the locally optimised child energies. A significant proportion of the child clusters created by the χ_2 crossover operator have an energy less than the lower parent energy. In addition, there is a dramatic increase in the sampling of low energy configurations compared to that shown in Figure 5.13.

a cluster and the final energy of the cluster after applying the BFGS local optimiser. Clearly an initially low number of close atoms tends to result in a lower final optimised energy.

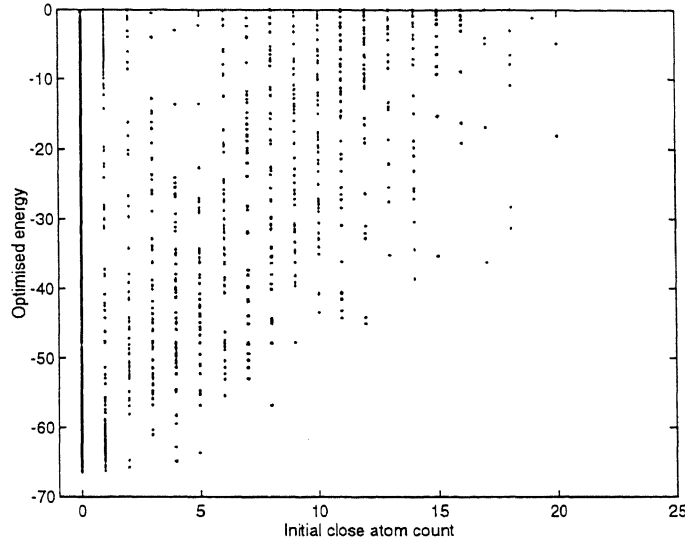


Figure 5.15: The effect that the number of close atoms in an atomic cluster has on the final energy found by the BFGS local optimiser. Generally the higher the number of close atoms, the lower the probability of the local optimiser finding a relatively lower energy.

Expressions for the expected number of close atoms after χ_1 and χ_2 crossovers are now analytically derived using the assumptions that all parent clusters contain N uniformly distributed atoms within an enclosing sphere of radius R with volume $V = 4\pi R^3/3$ and that no atom in a parent cluster is close to any other atom. In this context, atoms are defined as being close if the distance between the centres of the two atoms is less than some value r ($r = 0.8$ in this study). For the purposes of analysis of the crossover operator, it is convenient to view this in terms of the atoms already in the cluster having a “sphere of influence” of radius r while the atom being added is represented by a single point. Two atoms are defined as being close if the point representing the atom being added lies within a sphere of influence of

an existing atom.

5.4.1 χ_1 Crossover

Given two parent clusters X_1 and X_2 , let a child cluster X be created by initially randomly selecting K atoms from parent X_1 and then incrementally adding $N - K$ atoms from parent X_2 . The probability P_1 that the first atom added from X_2 lies within the sphere of influence of one of the K existing atoms in X is approximately the ratio of the volume occupied by the spheres of influence of the K atoms to the volume into which the new atom may be added, that is

$$P_1 = Kr^3/R^3$$

As no atom within a parent cluster may be close to another atom, the volume into which the second new atom may be added is $4\pi(R^3 - r^3)/3$. However, as the first atom added may have been close to one of the existing K atoms, to a first approximation the expected value of the volume which will cause an overlap is $4\pi(Kr^3 - P_1(r^3/2))/3$. Therefore the probability P_2 that the second atom added is within the sphere of influence of one of the existing K atoms is

$$P_2 = (Kr^3 - P_1(r^3/2))/(R^3 - r^3)$$

For the third atom, the volume into which it may be added is $4\pi(R^3 - 2r^3)/3$ and the expected value of the volume which will cause an overlap is $4\pi(Kr^3 - (r^3/2)(P_2 + P_1))/3$. Therefore the probability P_3 that the third atom added is within the sphere of influence of one of the existing K atoms is approximately

$$P_3 = (Kr^3 - (r^3/2)(P_1 + P_2))/(R^3 - 2r^3)$$

Continuing this process, the probability that atom i is within the sphere of influence of one of the existing K atoms is

$$P_i = (Kr^3 - (r^3/2) \sum_{j=1}^{i-1} P_j) / (R^3 - (i-1)r^3)$$

Therefore, after $N - K$ atoms have been added, the expected number of close atoms in X is

$$\begin{aligned} E[N_r] &= \sum_{i=1}^{N-K} P_i \\ &= \sum_{i=1}^{N-K} (Kr^3 - (r^3/2) \sum_{j=1}^{i-1} P_j) / (R^3 - (i-1)r^3) \end{aligned}$$

This expression for $E[N_r]$ is plotted in Figure 5.16 for $N = 40$, $K = 20$ and varying values of R . It can be seen that the χ_1 crossover operator generates a relatively high number of close atoms, particularly as R decreases (the optimal configuration for the 40 atom cluster can be enclosed by a sphere of radius slightly greater than 2 units).

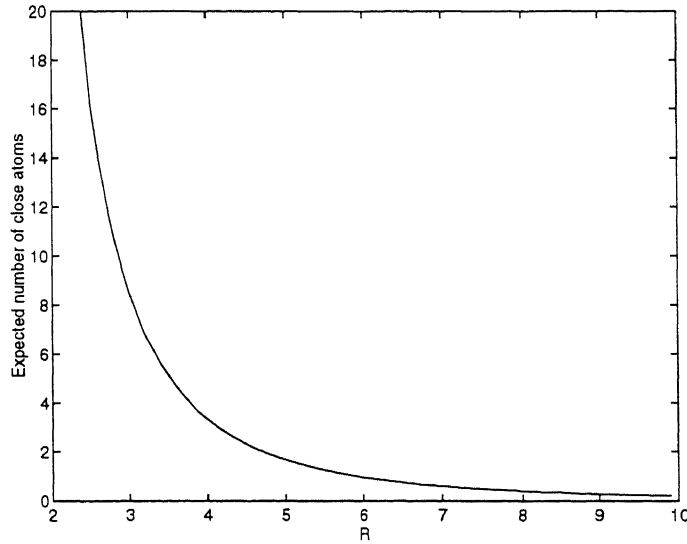


Figure 5.16: The expected number of close atoms after a χ_1 crossover as a function of the radius of the minimal sphere which encloses all atoms in the cluster ($N = 40$, $K = 20$).

5.4.2 χ_2 Crossover

Given two parent clusters X_1 and X_2 , we need to determine the expected number of close atoms in a child cluster when a volume element V_e is removed from X_1 and replaced by the corresponding volume element from X_2 . For the χ_2 crossover operator, these volume elements are restricted to hemispheres, quadrants and octants.

Given the conditions imposed above on parent clusters, only those atoms in X_1 and X_2 which are within r of a planar face of V_e will be able to be close to another atom in the child cluster X . For an atom within V_e , distance $d < r$ from a planar face and not within r of any other planar face of V_e , the volume of its sphere of influence which protrudes through this planar face is given by

$$\begin{aligned} V_p &= \int_d^r \pi(r^2 - x^2) dx \\ &= 2\pi r^3/3 - \pi d(r^2 - d^2/3) \end{aligned}$$

If we assume that atoms are uniformly distributed within a cluster, their distances from the planar faces will also be uniformly distributed. Thus, if there are N_p atoms within r of the planar face, then the expected distance from the planar face of the i th atom is

$$d_i = ir/(N_p + 1), \text{ where } 1 \leq i \leq N_p$$

Ignoring corner effects, the expected value for the total volume of all spheres of influence of atoms which protrude through this planar face of V_e is

$$V_s = \pi \sum_{i=1}^{N_p} (2r^3/3 - d_i(r^2 - d_i^2/3))$$

If the volume of a cylinder of height r and based on the planar face is denoted by V_c , then the expected number of close atoms in the child cluster is

$$E[N_c] = N(V_c/V)(V_s/V_c)$$

$$\begin{aligned}
&= NV_s/V \\
&= (3N/4R^3) \sum_{i=1}^{N_p} (2r^3/3 - d_i(r^2 - d_i^2/3))
\end{aligned}$$

The expected value of N_p is clearly dependent on the shape of V_e and, in particular, the area of the planar contact face. For a hemisphere volume element, $V_e = 2\pi R^3/3$ and there is only one planar face, of area πR^2 , that needs to be considered. The expected number of atoms within r of this planar face is

$$\begin{aligned}
E[N_p] &= (N/V) \int_0^r \pi(R^2 - x^2) dx \\
&= N\pi(R^2 r - r^3/3)/V \\
&= Nr(3R^2 - r^2)/4R^3
\end{aligned}$$

For a quadrant, $V_e = \pi R^3/3$ and there are two planar faces, each of area $\pi R^2/2$. The expected number of atoms within r of each of these planar faces is given by

$$E[N_p] = Nr(3R^2 - r^2)/8R^3$$

An octant has volume $\pi R^3/6$ and three planar faces, each of area $\pi R^2/4$. The expected number of atoms within r of each of these planar faces is given by

$$E[N_p] = Nr(3R^2 - r^2)/16R^3$$

Using these expressions for $E[N_p]$ and assuming an equal probability of applying each of the three variants of the χ_2 crossover operator, Figure 5.17 shows how $E[N_c]$ varies as a function of R ($N = 40$, $K = 20$). Clearly the number of close atoms generated is considerably less than that generated by the χ_1 crossover operator (Figure 5.16).

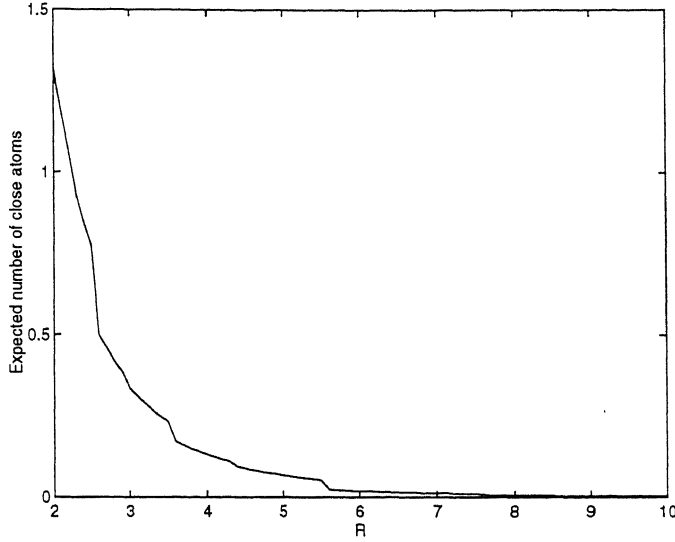


Figure 5.17: The expected number of close atoms after a χ_2 crossover as a function of the radius of the minimal sphere which encloses all atoms in the cluster ($N = 40$, $K = 20$).

5.4.3 Theoretical - Numerical Comparison

As a means of confirming the expressions obtained above for $E[N_r]$ and $E[N_p]$, optimisation of a 40 atom cluster was performed and the following data recorded

- the actual number of close atoms after χ_1 and χ_2 crossover operations.
- the value of R for each parent cluster.

Averaging the close atom counts across child clusters for each generation produced the solid lines shown in Figures 5.18 (χ_1) and 5.19 (χ_2). Using the average values obtained in a single run for R , in conjunction with the expressions obtained above for $E[N_r]$ and $E[N_c]$, produced the data points flagged by stars in these plots. The sudden increase in the average and expected number of atoms was caused by a significant reduction in R for the population between generations six and seven.

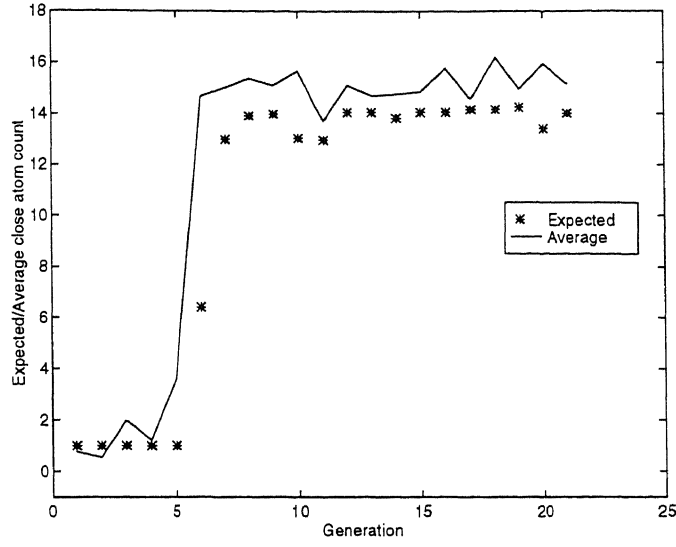


Figure 5.18: Expected and average number of close atoms for χ_1 . The expected number is calculated by determining the average radius of the clusters in the pool and using the expressions derived above for $E[N_r]$. The observed average number of close atoms is determined directly from the child clusters.

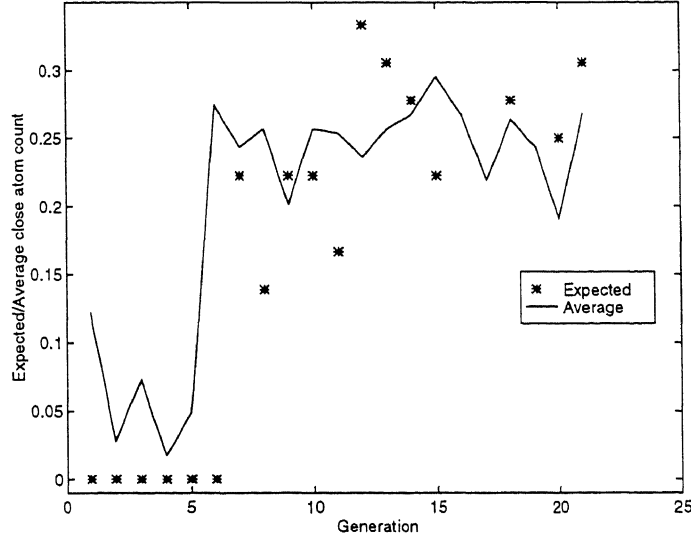


Figure 5.19: Expected and average number of close atoms for χ_2 . The expected number is calculated by determining the average radius of the clusters in the pool and using the expressions derived above for $E[N_p]$. The observed average number of close atoms is determined directly from the child clusters.

Given the stochastic nature of the process and the approximations used in the analysis, there is reasonable correlation between theory and actual results. Clearly the χ_2 geometric crossover operator is particularly effective at generating new clusters with a minimal number of close atoms. As shown by Figure 5.15, this leads to a greater probability of a lower final energy in the subsequent **Mutate** operator.

5.5 Discussion

Molecular structure problems, particularly for larger atomic clusters, are set in a large number of dimensions with complicated potential energy surfaces. GEM* was particularly successful in solving atomic cluster problems for a number of reasons. Firstly, in common with all GAs, it explores the search domain in parallel using all clusters in the current population as starting points. Secondly, and perhaps more importantly, it operates at a number of levels when generating new clusters. At the coarsest level are crossover operators such as χ_1 , χ_3 , χ_4 and the hemisphere version of χ_2 which interchange large volumes between current clusters. Fine-tuning of the cluster is provided by the quadrant and octant versions of χ_2 and the use of BFGS and APSE optimisation within the **Mutate** operation.

The major constraint on the future development of GEM* is the processor requirements of the BFGS local optimisations. Currently GEM* will, on a four processor IBM SP2 computer, optimise all atomic clusters in the range $N = 2, \dots, 41$ in two hours elapsed time. Improvements in performance will most likely come from a better balance of processor utilisation, implementation of more effective methods for early termination of the BFGS local optimisation and refinements to the crossover operators.

Chapter 6

GEM* Optimisation of Mixed Atomic Clusters

6.1 Introduction

While most studies of atomic clusters have focused on clusters containing a single type of atom, investigations have also been performed on clusters containing more than one atom type. To date, the most successful study is that of Navon et al. [35] where a lattice-based search found minimum energy structures for 7, 13 and 19 mixed atom structures. GEM* was particularly successful in optimising this type of molecular structure and found all currently accepted, and some improved, global minima for mixed argon-xenon atomic clusters containing 7, 13 and 19 atoms. In addition, minima were determined for all remaining clusters in the range $N = 2, \dots, 20$ atoms.

Section 6.2 of this chapter describes the mixed atomic cluster problem and presents a review of these previous investigations. Section 6.3 details the additional genetic operator required within GEM* to optimise these structures, while Section 6.4 and Appendix B tabulate the results obtained. A discussion of these results is presented in Section 6.5.

6.2 Mixed Atomic Clusters

As for pure atomic clusters, the total potential energy for an argon-xenon cluster is

$$V = \sum_{i=1}^{N-1} \sum_{j=i+1}^N v(r_{ij})$$

The scaled Lennard-Jones pair potential is not appropriate for argon-xenon clusters as it does not account for the differences in pairwise interaction between different atom types. Accordingly, a pair potential of the following form must be used

$$v(r) = 4\epsilon[(\sigma/r)^{12} - (\sigma/r)^6]$$

where r is the distance between atoms, with ϵ and σ being parameters whose values depend on the types of the interacting atoms. The appropriate values for ϵ and σ [35], along with the associated r_{min} and $v(r_{min})$ for argon and xenon atoms, are tabulated in Table 6.1 while the corresponding curves for $v(r)$ are shown in Figure 6.1.

| Interaction | σ (Å) | ϵ (kJ/mol) | r_{min} (Å) | $v(r_{min})$ |
|-------------|--------------|---------------------|---------------|--------------|
| Ar-Ar | 3.40 | 1.0000 | 3.82 | -1.00 |
| Ar-Xe | 3.65 | 1.4800 | 4.10 | -1.48 |
| Xe-Xe | 4.10 | 1.8525 | 4.60 | -1.85 |

Table 6.1: Lennard-Jones parameters for Ar and Xe pair potentials.

Within this study, the following notation is used to define mixed clusters of argon and xenon atoms:

| | |
|--------------------------------------|---|
| $Ar_i X e_j$ | a mixed cluster containing i argon and j xenon atoms |
| $Ar_{N-n} X e_n$ | the set of clusters $Ar_0 X e_N, \dots, Ar_N X e_0$ |
| $Ar_{N-n} X e_n _{i \leq N \leq j}$ | the set of clusters $Ar_{i-n} X e_n, \dots, Ar_{j-n} X e_n$ |

Intuitively, finding the minimum energy structure of a mixed atomic cluster would appear to be at least as difficult as finding the minimum energy structure of the corresponding pure atomic cluster. For example, compare

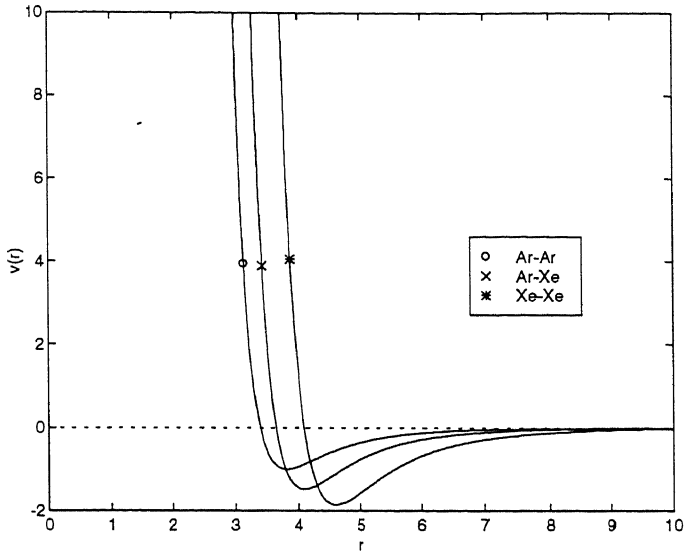


Figure 6.1: Lennard-Jones pair potentials for $Ar - Ar$, $Ar - Xe$ and $Xe - Xe$ atom pairings.

the pure Ar_5Xe_0 cluster with the mixed Ar_3Xe_2 cluster. As shown by Hoare [20], the Ar_5Xe_0 cluster has a single energy minimum corresponding to a triagonal bipyramidal structure which is slightly contracted along the symmetry axis and distended in the symmetry plane. This configuration can be constructed from the optimal Ar_4Xe_0 cluster (a tetrahedron) by adding the fifth argon atom at the apex of a tetrahedron based on a side of the optimal Ar_4Xe_0 cluster and performing local optimisation. While this operation may be performed with all three sides of the Ar_4Xe_0 tetrahedron, the resulting structures are identical under symmetry operations and all result in the same energy minima for Ar_5Xe_0 . Similarly, locally optimal Ar_3Xe_2 clusters can be constructed either by adding an argon atom to the optimal Ar_2Xe_2 cluster or by adding a xenon atom to the optimal Ar_3Xe_1 cluster. Using these operations, four triangular bipyramidal structures can be constructed as follows:

1. An argon atom positioned at the apex of a tetrahedron based on a $\{Ar, Ar, Xe\}$ face of the optimal Ar_2Xe_2 cluster.
2. An argon atom positioned at the apex of a tetrahedron based on a $\{Ar, Xe, Xe\}$ face of the optimal Ar_2Xe_2 cluster.
3. A xenon atom positioned at the apex of a tetrahedron based on a $\{Ar, Ar, Xe\}$ face of the optimal Ar_3Xe_1 cluster.
4. A xenon atom positioned at the apex of a tetrahedron based on a $\{Ar, Ar, Ar\}$ face of the optimal Ar_3Xe_1 cluster.

Under symmetry operations, structures 1 and 3 above are identical, leaving three unique structures corresponding to three distinct local minima. Extending this argument, it would be reasonable to conclude that the number of local minima for $Ar_{N-n}Xe_n$ is bounded below by the number of local minima for Ar_NXe_0 for all N .

Navon et al. [35] investigated $Ar_{7-n}Xe_n$, $Ar_{13-n}Xe_n$ and $Ar_{19-n}Xe_n$ clusters using a combination of simulated annealing and conjugate gradient descent optimisation. The approach used was, for a cluster containing N atoms, to start with the known structure of the Ar_NXe_0 cluster and randomly replace the appropriate number of Ar atoms with Xe atoms to form an initial structure, S_0 , for optimisation. Using a local optimiser, a minimum energy E_0 is located near S_0 . A new structure S_1 is then generated from S_0 by randomly interchanging the position of one Ar atom with that of one Xe atom. Using a local optimiser, a minimum energy E_1 is located near S_1 . If $E_1 < E_0$ then S_1 becomes the new starting structure. If $E_1 \geq E_0$ then S_1 is accepted with Boltzmann probability as the new starting structure. This process is repeated for a fixed number of steps. The method clearly relies on the assumption that a mixed atomic cluster has an under-

lying structure which is based on that for the corresponding pure atomic cluster. The $Ar_{7-n}Xe_n$, $Ar_{13-n}Xe_n$ and $Ar_{19-n}Xe_n$ clusters investigated by Navon et al. were chosen because their pure forms Ar_7Xe_0 , $Ar_{13}Xe_0$ and $Ar_{19}Xe_0$ respectively, are particularly stable, so this assumption was thought more likely to be valid. However, for some of the other clusters investigated in this chapter, the assumption was found to be invalid and so the optimisation method described above would be unlikely to find all minimum energy structures.

6.3 GEM* Computational Method

The only modification made to the GEM* algorithm implemented for pure atomic clusters (Section 5.2) was an additional mutation operator which interchanged randomly selected argon and xenon atoms and then performed a BFGS local optimisation. The rationale underlying this operator is that, as the three pair potentials interacting within the mixed argon-xenon cluster are similar, the basic structure of the globally optimal cluster may be relatively straight forward to determine. This structure will generally correspond to one of a number of local minima, where each of these minima relate to different relative placements of Ar and Xe atoms within the basic structure. Introducing a mutation operator which directly interchanges Ar and Xe atoms, followed by a BFGS optimisation, allows rapid sampling of these local minima.

The calculations of the analytical energy gradients V_{x_i} , V_{y_i} and V_{z_i} ($1 \leq i \leq N$) required for local optimisation of mixed atomic clusters are shown in Appendix A.2.

6.4 Results

GEM* successfully located all currently accepted global minima [35] for $Ar_{7-n}Xe_n$ and $Ar_{13-n}Xe_n$ clusters while the results for $Ar_{19-n}Xe_n$ were generally improved. In addition, minima for the remaining clusters in $Ar_{N-n}Xe_n|_{2 \leq N \leq 20}$ were determined by running GEM* for 50 generations, at which point minimum population energies had stabilised. The lowest energies E and ΔE , the change in cluster energy as Ar to Xe substitutions were performed, are presented in Appendix B. The energy E represents an upper bound on the energy of the global minima for these systems as there is no guarantee that GEM* will find the global minima. The energy values obtained and corresponding cluster structures are discussed in the following section.

The effectiveness of GEM* in optimising mixed clusters is shown by Figure 6.2 where the minimum energy in the current population of clusters, as a function of generation, is plotted for the optimisation of the $Ar_{10}Xe_{10}$ cluster. This pattern, with an initial sharp decrease in energy followed by a slow approach to the global minimum, was observed for all clusters.

6.5 Discussion

As observed in [35], in discussing the results obtained, it is important to keep in mind the relative energy minima of the three Lennard-Jones pair potentials (Table 6.1, Figure 6.1), and the interatomic distances at which they occur. The strongest attractive interaction (lowest minima) is the $Xe - Xe$ interaction, while the weakest is $Ar - Ar$. Navon et al. [35] suggested that, as a crude model, if there are more argon than xenon atoms, then the number of $Ar - Xe$ nearest neighbours should be maximised and the number of $Ar - Ar$ nearest neighbours minimised. Alternatively, if there are more

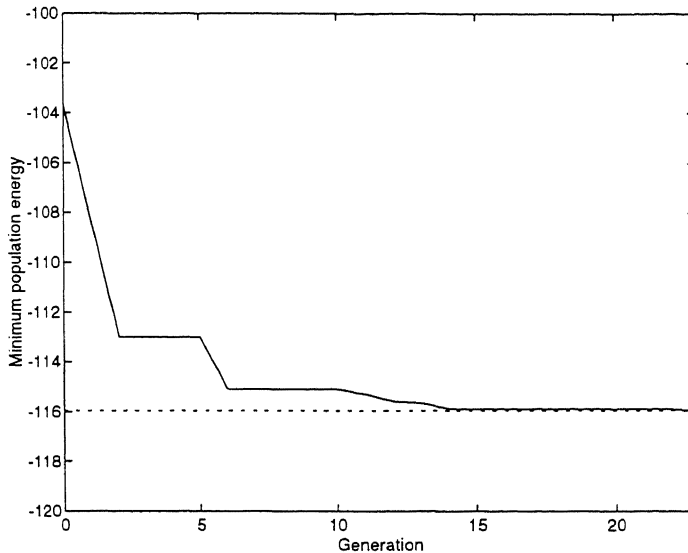


Figure 6.2: Minimum population energy at the completion of each generation while optimising $Ar_{10}Xe_{10}$ using randomly generated and locally optimised initial configurations.

xenon than argon atoms then the number of $Xe - Xe$ nearest neighbours should be maximised. Clearly, this model only takes into account the relative Lennard-Jones energy minima and not the interatomic distances at which they occur.

An alternative perspective, which does incorporate the different interatomic distances at which the energy minima occur, is to consider the number of atom pairs whose separation is within a small distance δ of the optimum (r_{min} , Table 6.1) for that atom pair. For $\delta = 0.2\text{\AA}$, N_{AA} , the count of near optimal $Ar - Ar$ pairings, N_{AX} , the count of near optimal $Ar - Xe$ pairings and N_{XX} , the count of near optimal $Xe - Xe$ pairings, are shown in Appendix B for all optimised $Ar_{N-n}Xe_n|_{2 \leq N \leq 20}$ clusters. While the value of δ is somewhat arbitrary, it is reasonable to assume that if the distance between two atoms is greater than 0.2\AA of the optimal distance for that

pair, then the optimisation process has not focused on optimising the relationship between these two atoms. If we denote the minimum value of the $Ar - Ar$ pair potential by V_{AA} , that for $Ar - Xe$ by V_{AX} and for $Xe - Xe$ by V_{XX} , then the optimisation problem is approximated by

$$\min(N_{AA}V_{AA} + N_{AX}V_{AX} + N_{XX}V_{XX}).$$

Optimisation studies of pure clusters [20] have shown that the maximum possible values of N_{AA} , N_{AX} and N_{XX} , for 2 to 13 atoms, are 1, 3, 6, 9, 12, 16, 19, 23, 27, 31, 36 and 42 respectively. Using these results, inspection of the actual counts presented in Appendix B shows that, when there is a relatively large number of argon atoms, N_{AX} is maximised. As a secondary effect, N_{AA} is minimised with respect to the number of possible pairings (which is equivalent to maximising N_{XX}). Only when there are considerably more xenon than argon atoms does the focus move to maximising N_{XX} . Intuitively, the initial maximising of N_{AX} can be understood in terms of the relative energy minima of the different pair potentials. For example, if there are only two Xe atoms, then the maximum value of N_{XX} is one. However, if the two Xe atoms are separated, then the possible values for N_{AX} have a much greater range. Even though the $Xe - Xe$ pair has a lower potential energy minimum than the $Ar - Xe$ pair, the number of possible $Ar - Xe$ pairs more than compensates. This effect is clearly seen in the optimised Ar_5Xe_2 cluster shown in Figure 6.3, where the two xenon atoms were placed at far apart apex positions, thus maximising the opportunity for $Ar - Xe$ pairings.

Analysis of the values obtained for the substitution energy, ΔE , in Appendix B, shows that, for all $Ar_{N-n}Xe_n|_{2 \leq N \leq 9}$ clusters, the ΔE values are generally higher for greater N and slowly decrease as Xe atoms are substituted for Ar atoms. However for all $Ar_{N-n}Xe_n|_{10 \leq N \leq 20}$ clusters, while

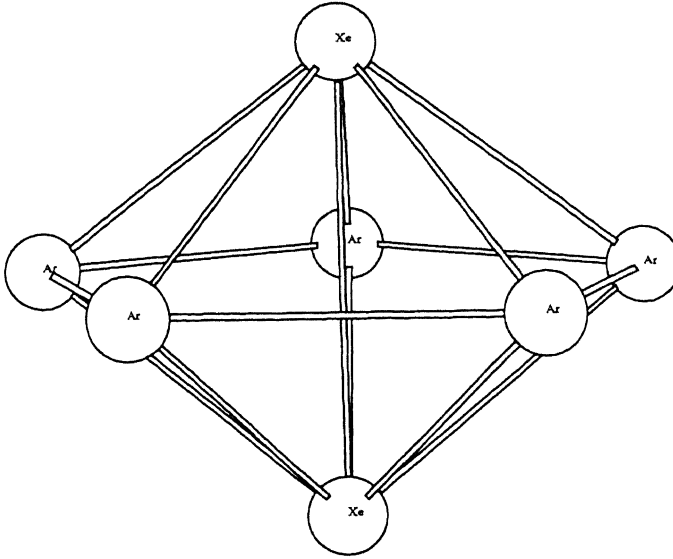


Figure 6.3: Optimised structure for Ar_5Xe_2 showing the placement of the two Xe atoms. This maximises the number of optimally paired Ar and Xe atoms.

substitution of the first seven Ar atoms follows this pattern, the ΔE are more erratic as the remaining substitutions are performed. Figure 6.4 shows the behaviour of ΔE obtained in this study, for all $Ar_{7-n}Xe_n$, $Ar_{13-n}Xe_n$ and $Ar_{19-n}Xe_n$ clusters. The substitution energies shown here follow the same pattern as found in [35].

To determine the reasons for the observed behaviour of ΔE , three clusters (for $N = 10, 12$ and 17) were investigated further.

i) $Ar_{10-n}Xe_n$

Figure 6.5 shows the variation in ΔE as xenon atoms replace argon atoms in the $Ar_{10-n}Xe_n$ clusters.

The first xenon atom is placed at the centre of the partially constructed $Ar_{10}Xe_0$ icosahedron and, up until the sixth xenon atom, substitute xenon atoms are placed in the shell of the partial icosahedron. The structure

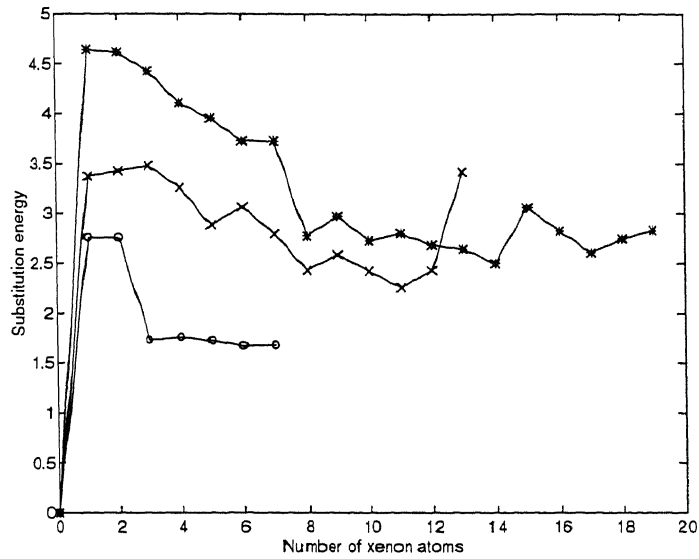


Figure 6.4: Absolute values of the substitution energies (ΔE) as Ar atoms are replaced by Xe atoms in $Ar_{7-n}Xe_n$, $Ar_{13-n}Xe_n$ and $Ar_{19-n}Xe_n$.

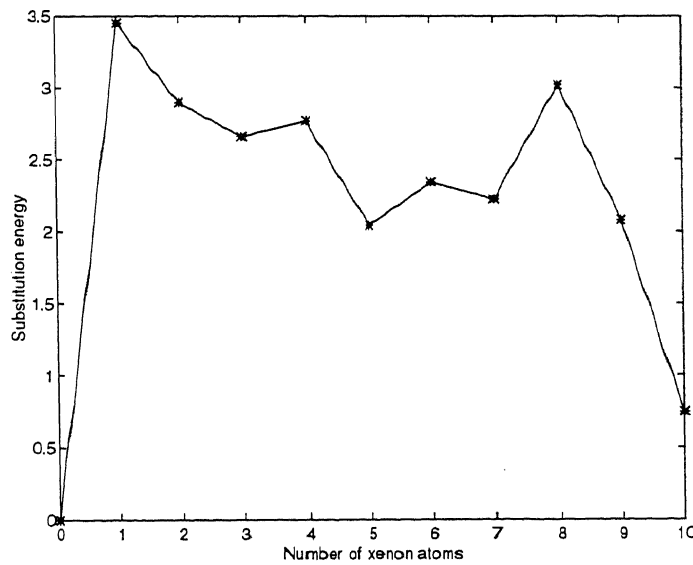


Figure 6.5: Absolute values of the substitution energies (ΔE) as Ar atoms are replaced by Xe atoms in $Ar_{10-n}Xe_n$.

changes when the sixth xenon is substituted in that the xenon atom at the centre of the icosahedron is replaced by an argon atom (Figures 6.6(a) and 6.6(b)). This corresponds to the increase in ΔE shown in Figure 6.5. As more xenon atoms are added, they are placed in the icosahedral shell which gradually envelopes the central argon atom. The subsequent increase in ΔE occurs when the eighth xenon atom is added (Figures 6.6(c) and 6.6(d)).

The rectangular base of four xenon atoms beneath the apex xenon atom in the optimised Ar_3Xe_7 cluster has sides of length 5.83Å and 4.71Å. When the eighth xenon atom is added, the remaining rectangular base of four xenon atoms is able to contract to a square of side 4.91Å which is closer to the $Xe - Xe r_{min}$ of 4.60Å. This results in a considerable increase in N_{AX} .

ii) $Ar_{12-n}Xe_n$

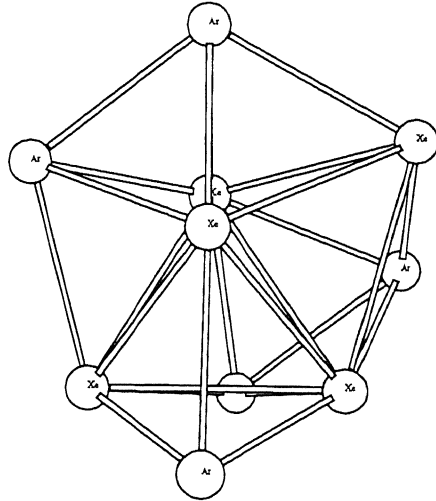
Figure 6.7 shows the variation in ΔE as xenon atoms replace argon atoms in the $Ar_{12-n}Xe_n$ clusters.

The pattern followed was that the first xenon atoms replaced argon atoms in the partial icosahedral shell. The last xenon atom replaced the argon atom at the centre of the icosahedron (Figures 6.8(a) and 6.8(b)). The subsequent relaxation and adjustment of the cluster resulted in N_{XX} increasing from 25 to 36, giving the large increase in ΔE shown in Figure 6.7.

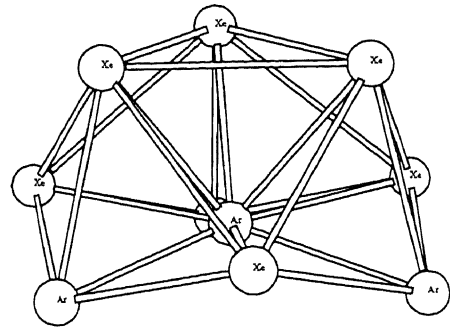
iii) $Ar_{17-n}Xe_n$

Figure 6.9 shows the variation in ΔE as xenon atoms replace argon atoms in $Ar_{17-n}Xe_n$ clusters.

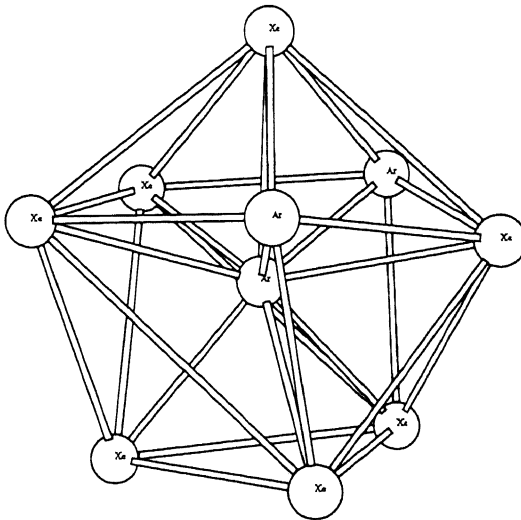
The increase in ΔE when the twelfth xenon atom is added results from a major change in structure between Ar_6Xe_{11} (Figure 6.10(a)) and Ar_5Xe_{12} (Figure 6.10(b)).



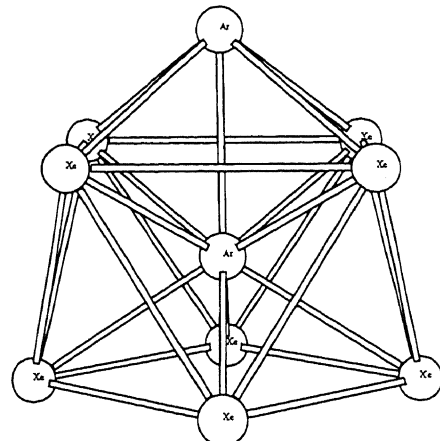
(a) Ar_5Xe_5



(b) Ar_4Xe_6



(c) Ar_3Xe_7



(d) Ar_2Xe_8

Figure 6.6: Optimised structures found by GEM* for the $Ar_5Xe_5, \dots, Ar_2Xe_8$ atomic clusters.

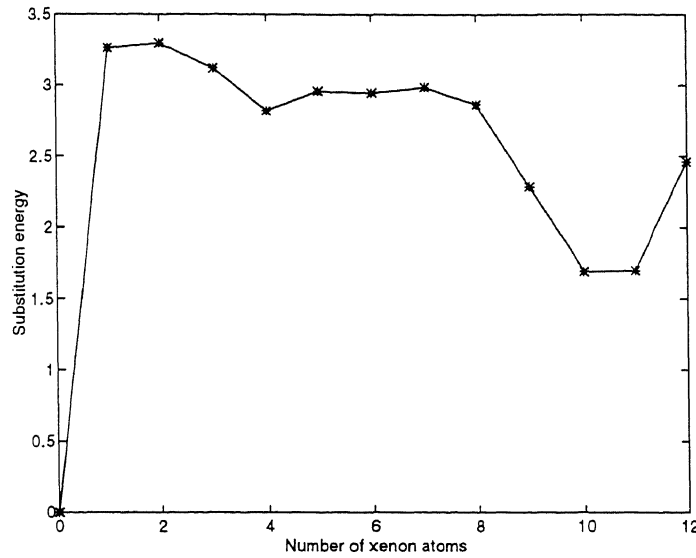


Figure 6.7: Absolute values of the substitution energies (ΔE) as Ar atoms are replaced by Xe atoms in $Ar_{12-n}Xe_n$.

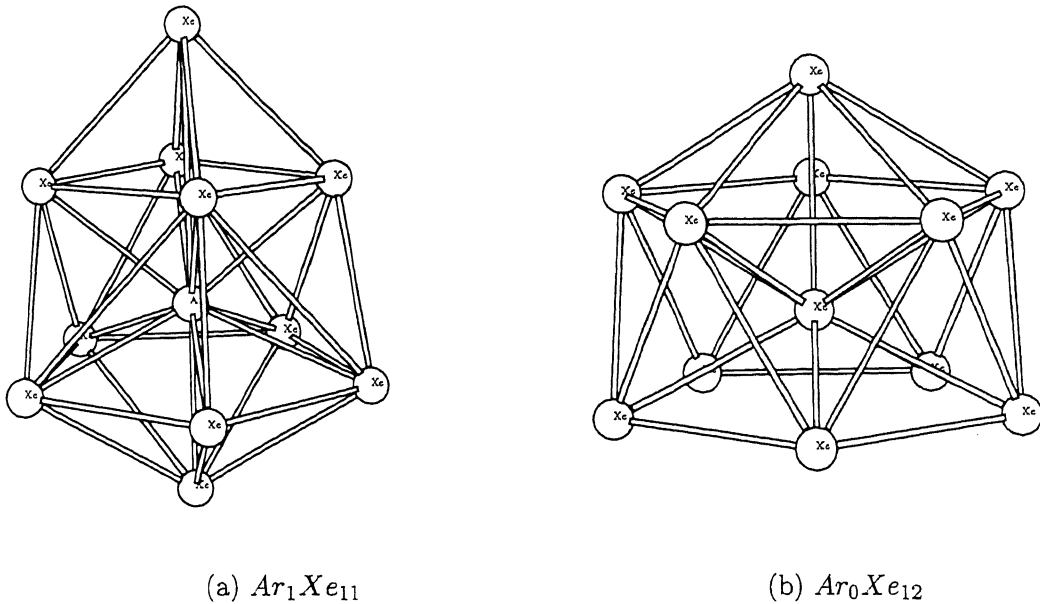


Figure 6.8: GEM* optimised structures for the Ar_1Xe_{11} and Ar_0Xe_{12} atomic clusters.

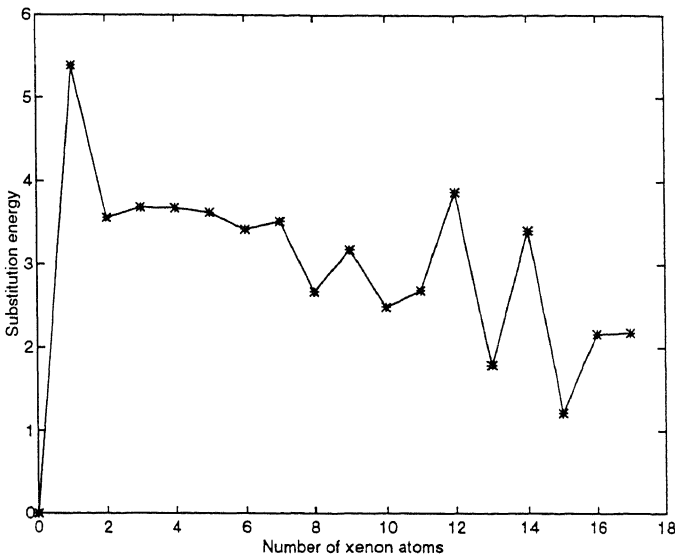


Figure 6.9: Absolute values of the substitution energies (ΔE) as Ar atoms are replaced by Xe atoms in $Ar_{17-n}Xe_n$.

At this point, the structure changes from a central xenon atom with all other argon and xenon atoms in an enclosing shell, to two interpenetrating icosahedrons centred on two argon atoms. This created a significant increase in N_{AX} . The next two major increases in ΔE occur when the fourteenth and sixteenth xenon atoms are added. As in the Ar_3Xe_7 to Ar_2Xe_8 transition, these allowed a rectangular base of xenon atoms to transform to a square whose sides were closer to r_{min} for $Xe - Xe$, so increasing N_{XX} .

An important feature of GEM* is that, as it always starts from randomly generated structures and has no bias towards any particular structure, it will perform a more complete search of the domain of possible structures. Alternative methods, which start from a particular structure, are likely to have an inherent bias towards that structure and are less able to find different structures that may have lower energy.

The energies, substitution energies, and atom pair counts have been

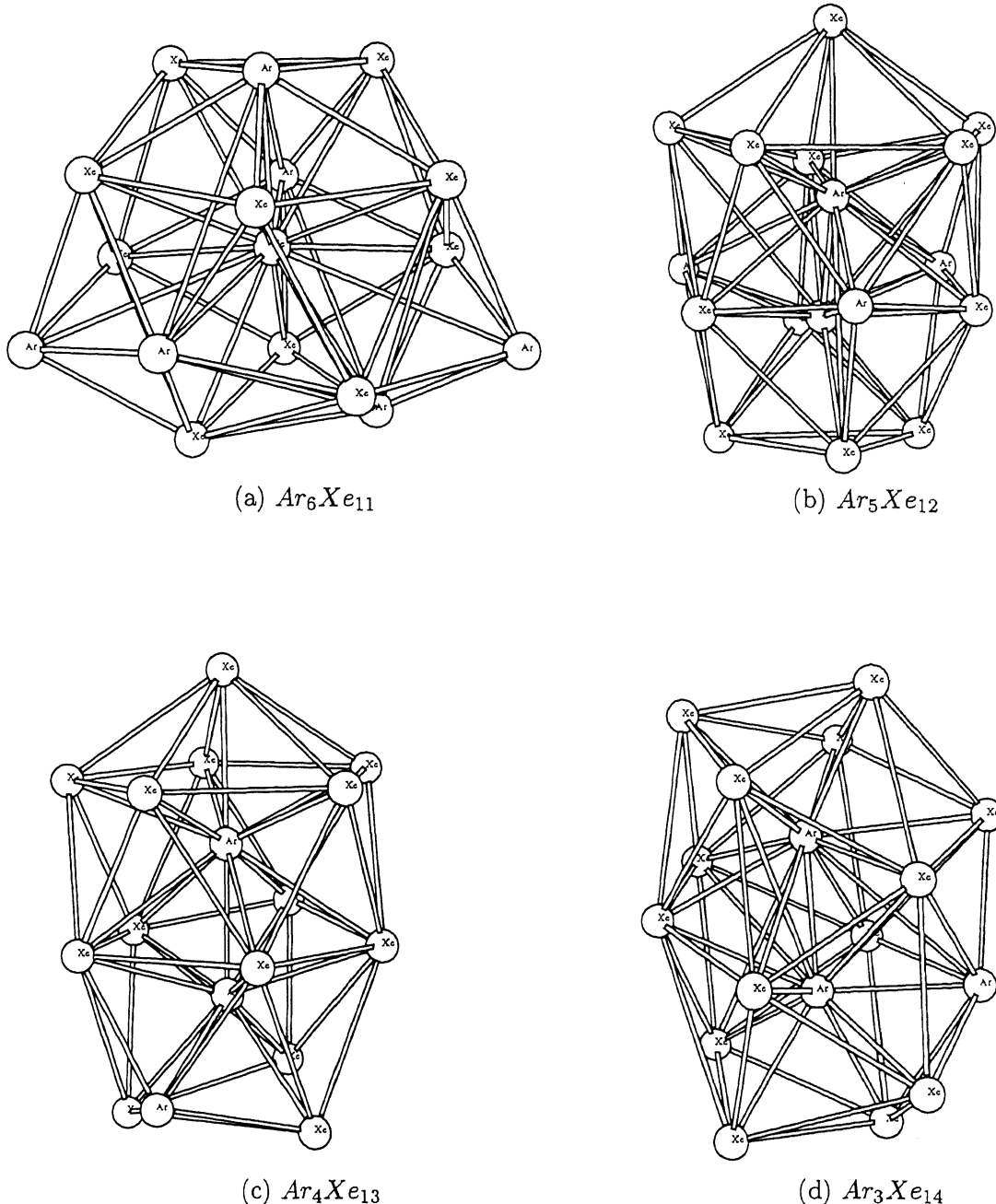


Figure 6.10: Optimised structures found by GEM* for the $Ar_6Xe_{11}, \dots, Ar_3Xe_{14}$ atomic clusters.

tabulated for all $Ar_{N-n}Xe_n|_{2 \leq N \leq 20}$ clusters. In addition, further investigation of the optimised structures for $Ar_{10-n}Xe_n$, $Ar_{12-n}Xe_n$ and $Ar_{17-n}Xe_n$ clusters was performed to determine the reasons for the observed changes in substitution energy.

Chapter 7

GEM* Optimisation of Molecular Clusters

7.1 Introduction

While considerable effort has been dedicated to the study of global optimisation methods applicable to atomic clusters, with the exception of water clusters, considerably less effort has been applied to the optimisation of molecular clusters. This chapter describes the results obtained using GEM* to optimise pure clusters of benzene and water molecules. Prior to this study, lattice-based search techniques ([55], [58]) found optimal configurations for $N = 2, 3, 4, 5, 6, 7, 9, 11, 13$ and 15 clusters of benzene molecules while a binary-coded GA [62], using random initial configurations, was successful for benzene clusters containing between 2 and 4 molecules. GEM* was particularly successful for benzene clusters and found all currently accepted global minima for clusters of 2 to 6 molecules and new minima for clusters of 8 to 12 molecules. However for water clusters, due to the computational requirements inherent in determining both the potential energy and the gradient calculations for the BFGS optimisation, GEM* was less successful and, while able to find good local minima, was unable to find globally optimal configurations. However indications are that, given more

powerful computational resources, GEM* would have greater success with this optimisation.

Section 7.2 of this chapter describes the force fields used to model interactions that exist within these two types of clusters and provides an overview of optimisation methods that have been previously applied. Section 7.3 describes the extensions made to GEM*, while the results obtained are described and discussed in Section 7.4. A summary and conclusion are presented in Section 7.5.

7.2 Molecular Clusters

Global optimisation of molecular clusters is inherently more difficult than that of atomic clusters due to the need to determine the three angular coordinates specifying the orientation of each molecule (other than the first). In addition, for a flexible molecule, there may be intramolecular interactions which determine the shape of the molecule and which require additional parameters for their specification. Also, as molecules generally consist of more than a single type of atom, the intramolecular and intermolecular force fields contain a number of terms which are likely to result in a more complex optimisation problem.

Whenever molecules are close to each other, three types of interactions occur. The long-range coulombic interaction arises from the molecular electric potential, which is usually viewed as originating from net charges on the atoms. It may be either an attractive or repulsive interaction. The intermediate-range dispersion interaction due to instantaneous dipole interactions is always attractive, while the short-range exchange repulsion interaction from electron-electron interactions increases rapidly at close range and is responsible for the “size” of the atom. This combination of short, in-

termediate and long-range interactions leads to a complicated intermolecular potential energy surface which includes many local minima.

We now describe the molecular mechanics force fields for the two types of molecular clusters investigated in this study.

7.2.1 Benzene Clusters

For this study, a rigid planar benzene (C_6H_6) molecule was assumed, with atomic coordinates shown in Table 7.1 and defined relative to a coordinate system whose origin is at the centre of mass of the benzene molecule and the xy -plane defined by the plane of the benzene molecule.

| Atom | <i>x</i> | <i>y</i> | <i>z</i> | Atom | <i>x</i> | <i>y</i> | <i>z</i> |
|-------|----------|----------|----------|--------|----------|----------|----------|
| 1 (C) | 1.3970 | 0.0000 | 0.0000 | 7 (H) | 2.4240 | 0.0000 | 0.0000 |
| 2 (C) | -1.3970 | 0.0000 | 0.0000 | 8 (H) | -2.4240 | 0.0000 | 0.0000 |
| 3 (C) | 0.6985 | 1.2098 | 0.0000 | 9 (H) | 1.2120 | 2.0992 | 0.0000 |
| 4 (C) | -0.6985 | -1.2098 | 0.0000 | 10 (H) | -1.2120 | -2.0992 | 0.0000 |
| 5 (C) | -0.6985 | 1.2098 | 0.0000 | 11 (H) | -1.2120 | 2.0992 | 0.0000 |
| 6 (C) | 0.6985 | -1.2098 | 0.0000 | 12 (H) | 1.2120 | -2.0992 | 0.0000 |

Table 7.1: Benzene molecule - Cartesian coordinates (Å).

The total potential energy for a benzene molecular cluster is

$$V = \sum_{i=1}^{N-1} \sum_{j=i+1}^N v(r_{ij})$$

with the three components of the intermolecular force field modelled by the following atom-to-atom non-bonded potential energy [58]

$$v(r_{ij}) = B \exp(-Cr_{ij}) - Ar_{ij}^{-6} + q_i q_j r_{ij}^{-1}$$

where, for atoms *i* and *j*, $V(r_{ij})$ is the potential energy of interaction and r_{ij} is the interatomic distance. The dispersion energy coefficient is *A*, while *B* and *C* are the exchange repulsion coefficients with q_i and q_j being the net

atomic charges for atoms i and j . The numeric values associated with these coefficients are dependent on the types of atoms involved in the interaction and are shown in Table 7.2 for the three possible interactions ($C-C$, $C-H$, $H-H$). Figure 7.1 shows the form of $V(r)$ for these three atom-to-atom interactions.

| | | | |
|----------|--|----------|---|
| A_{HH} | $136 \text{ kJ mol}^{-1} \text{ \AA}^6$ | A_{HC} | $573 \text{ kJ mol}^{-1} \text{ \AA}^6$ |
| A_{CC} | $2414 \text{ kJ mol}^{-1} \text{ \AA}^6$ | B_{HH} | $11677 \text{ kJ mol}^{-1}$ |
| B_{HC} | $65485 \text{ kJ mol}^{-1}$ | B_{CC} | $367250 \text{ kJ mol}^{-1}$ |
| C_{HH} | 3.74 \AA^{-1} | C_{HC} | 3.67 \AA^{-1} |
| C_{CC} | 3.60 \AA^{-1} | $q(H)$ | 0.153 e |
| $q(C)$ | -0.153 e | | |

Table 7.2: Benzene molecule - non-bonded potential parameters.

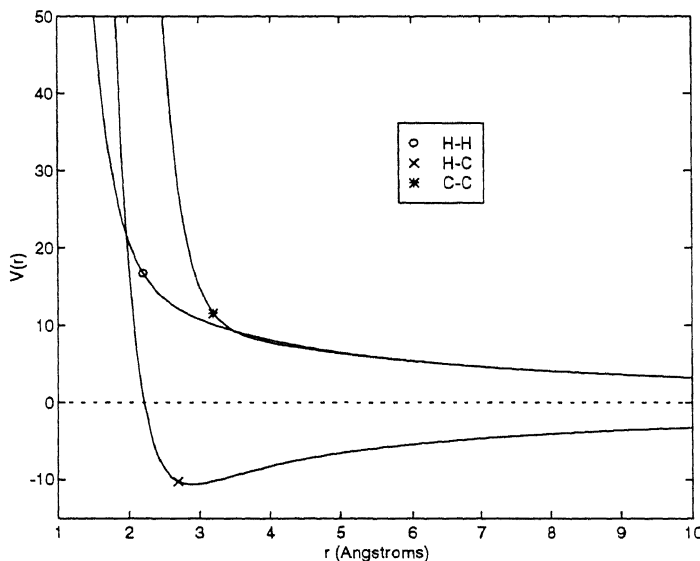


Figure 7.1: Benzene intermolecular atomic pair potentials for the $H - H$, $H - C$ and $C - C$ interactions.

In previous studies, Williams [58] investigated benzene clusters using a Newton-Raphson local optimisation method. By assuming a centre of

symmetry and with specially chosen initial configurations, local energy minima were found for benzene clusters containing 2, 3, 5, 7, 9, 11, 13 and 15 molecules. However, van der Waal [55] was subsequently able to find lower minima for benzene clusters containing between 2 and 7 molecules. This method started from configurations derived from either a 13 molecule icosahedral cluster by removal of the appropriate number of molecules or by removal of molecules from optimised clusters so obtained.

Using randomly generated initial configurations, Williams [59] with an off-ridge eigenvector minimisation with annealing technique, found energy minima for benzene clusters of 2 to 4 molecules. This technique used a combination of simulated annealing and Newton-Raphson local optimisation but, when the Hessian was no longer positive definite and the Newton-Raphson method was not guaranteed to find a minimum energy, adopted a technique of performing a linear search in the direction of the eigenvector corresponding to the largest negative eigenvalue of the Hessian. This was found to be an effective technique for quickly moving to a region where the Hessian became positive definite and the Newton-Raphson local optimiser was again reliable.

Subsequently, a binary-coded genetic algorithm implemented by Xiao and Williams [62], with randomly generated starting configurations, was able to find the currently accepted global energy minima for benzene clusters of two to four molecules.

7.2.2 Water Clusters

The force field model used for non-rigid water molecules is that described by Coker and Watts [6] and includes both intramolecular (U) and intermolecular (V) components. In the Coker and Watts model the total potential energy for an N molecule water cluster is given by (all parameter values for

this model are shown in Table 7.3)

$$E(r_1, r_2, \theta, r) = \sum_{k=1}^N U_k(r_1, r_2, \theta) + \sum_{k=1}^N \sum_{l=1}^{k-1} V_{kl}(r)$$

For intramolecular interactions, the potential U has the form

$$U(r_1, r_2, \theta) = \sum_{l=1}^3 M_l(s_l) + f_{12}s_1 s_2$$

where

$$\begin{aligned} s_1 &= r_1 \cos((\theta - \theta_0)/2) - r_0 \\ s_2 &= r_2 \cos((\theta - \theta_0)/2) - r_0 \\ s_3 &= (r_1 + r_2) \sin((\theta - \theta_0)/2)/r_0 \\ M_l(s) &= D_l(1 - \exp(-\alpha_l s))^2 \end{aligned}$$

Parameters r_1 and r_2 are the actual bond lengths between the oxygen atom and each hydrogen atom respectively, r_0 is the equilibrium length for these bonds and θ_0 is the equilibrium bond angle.

The intermolecular potential V used is the semiempirical RWK2 model of Reimers et al. [6], and includes both atom-to-atom interactions and coulombic terms acting as point charges. For two water molecules the intermolecular potential is

$$\begin{aligned} V(r) &= \sum_{HHpairs} V_{HH}(r) + \sum_{OHpairs} V_{OH}(r) + \sum_{OOpairs} V_{OO}(r) + \\ &\quad \sum_{HNpairs} V_{HN}(r) + \sum_{NNpairs} V_{NN}(r) \end{aligned}$$

where r is the distance between the respective atoms of the water molecules.

The interactions V_{HH} , V_{HO} and V_{OO} between the hydrogen and oxygen atoms of these two water molecules have the form

$$\begin{aligned} V_{HH}(r) &= A_{HH} \exp(-\alpha_{HH} r) + Q^2/r \\ V_{OH}(r) &= A_{OH} (\exp(-\alpha_{OH}(r - r_m)) - 1)^2 - A_{OH} \end{aligned}$$

$$V_{OO}(r) = A_{OO} \exp(-\alpha_{OO} r) - f(r)$$

$$\left(C_6 (g_6/r^*)^6 + C_8 (g_8/r^*)^8 + 1.5C_{10} (g_{10}/r^*)^{10} \right)$$

where

$$f(r) = 1 - 3.8845r^{2.326} \exp(-1.7921r)$$

$$g_{2n}(r) = 1 - \exp\left(-1.8817r/n - 0.2475r^2/\sqrt{n}\right)$$

In addition to these atom-to-atom terms, there are coulombic attractions between each hydrogen atom on one molecule and a negative charge located on the bisector of the *HOH* angle of the second molecule given by

$$V_{HN}(r) = -2Q^2/r$$

and a repulsive interaction between these two negative charges of

$$V_{NN}(r) = 4Q^2/r$$

The position vector of the negative charge, relative to a coordinate system centred on the oxygen atom, is given by

$$\mathbf{R}_N = d(\mathbf{R}_1 + \mathbf{R}_2)/2r_0 \cos(\theta_0/2)$$

where \mathbf{R}_1 and \mathbf{R}_2 are the position vectors for the two hydrogen atoms.

| | | | |
|---------------|---|---------------|----------------------------------|
| r_0 | 0.9572 Å | θ_0 | 104.52° |
| D_1 | 131.25025 kcal mol ⁻¹ | D_2 | 131.25025 kcal mol ⁻¹ |
| D_3 | 98.270 kcal mol ⁻¹ | α_1 | 2.14125 Å ⁻¹ |
| α_2 | 2.14125 Å ⁻¹ | α_3 | 0.70600 |
| f_{12} | -15.1533 kcal mol ⁻¹ Å ⁻² | A_{HH} | 631.92 kcal mol ⁻¹ |
| α_{HH} | 3.2806 Å ⁻¹ | Q^2 | 119.53 kcal mol ⁻¹ Å |
| A_{OH} | 2.0736 kcal mol ⁻¹ | α_{OH} | 7.3615 Å ⁻¹ |
| r_m | 1.63781 Å | r^* | 0.948347r Å |
| A_{OO} | 3.2049E6 kcal mol ⁻¹ | α_{OO} | 4.9702 Å ⁻¹ |
| C_6 | 625.45 kcal mol ⁻¹ Å | C_8 | 3390 kcal mol ⁻¹ Å |
| C_{10} | 21200 kcal mol ⁻¹ Å | d | 0.26 Å |

Table 7.3: RWK2 potential parameters.

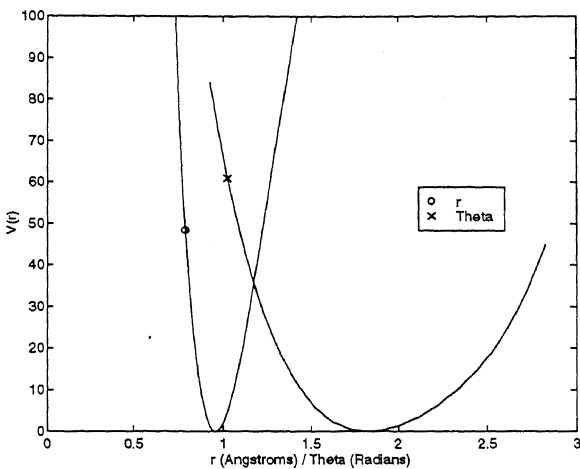


Figure 7.2: Intramolecular pair potentials for the water molecule. The r curve shows the change in potential energy as the $O - H$ bond length varies from the equilibrium value r_0 . The theta curve shows the change in potential energy as the $H - O - H$ bond angle varies from the equilibrium value θ_0 .

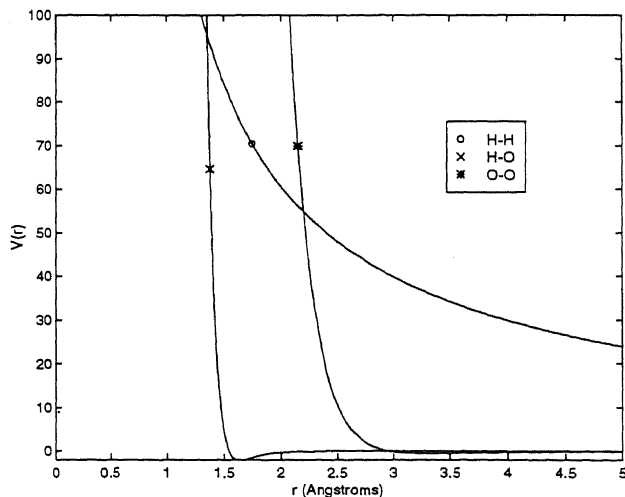


Figure 7.3: Water intermolecular atomic pair potentials for the $H - H$, $H - O$ and $O - O$ interactions.

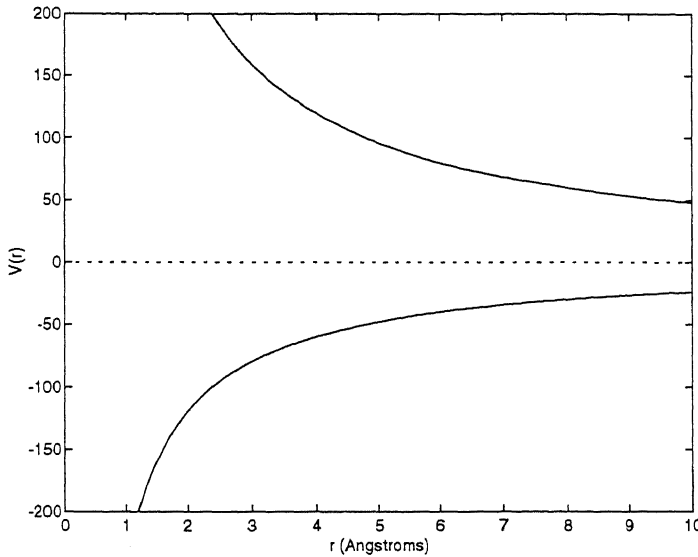


Figure 7.4: Coulombic potentials for water molecules.

Byrd et al. [5] investigated water clusters containing 2, 6, 8, 20 and 21 molecules. Using a stochastic/perturbation method with randomly generated starting configurations, they were able to find the currently accepted global minima for water clusters containing 2, 6, and 8 molecules but were initially unsuccessful for 20 and 21 molecules. By incorporating a build-up technique to generate starting configurations, they were subsequently able to improve the accepted global minima for 20 and 21 water molecules.

7.3 GEM* Computational Method

7.3.1 Genetic Encoding

For benzene clusters, molecules were treated as rigid bodies and, for other than the first molecule which defined the coordinate system, were encoded in GEM* using six real-valued parameters. With reference to an external coordinate system, three parameters specified the centre of mass of the

molecule and the three remaining parameters specified the molecular orientation using Eulerian angles. This encoding requires $6N - 6$ parameters to fully specify an N molecule benzene cluster.

Given these parameter definitions, the coordinates (x, y, z) of an atom of a benzene molecule, relative to an external coordinate system, can be calculated as [31]

$$\begin{aligned} x &= x_c + x_b(\cos(\gamma) \cos(\beta) - \cos(\alpha) \sin(\beta) \sin(\gamma)) + \\ &\quad y_b(\cos(\gamma) \sin(\beta) + \cos(\alpha) \cos(\beta) \sin(\gamma)) + z_b(\sin(\gamma) \sin(\alpha)) \\ y &= y_c + x_b(-\sin(\gamma) \cos(\beta) - \cos(\alpha) \sin(\beta) \cos(\gamma)) + \\ &\quad y_b(-\sin(\gamma) \sin(\beta) + \cos(\alpha) \cos(\beta) \cos(\gamma)) + z_b(\cos(\gamma) \sin(\alpha)) \\ z &= z_c + x_b(\sin(\alpha) \sin(\beta)) + y_b(-\sin(\alpha) \cos(\beta)) + z_b(\cos(\alpha)) \end{aligned}$$

where (x_c, y_c, z_c) are the coordinates of the centre of mass of the benzene molecule in the external coordinate system, (x_b, y_b, z_b) are the coordinates of the atom as defined in Table 7.1 and α, β and γ are the Euler angles for the molecule. The calculations of the analytical energy gradients $V_{x_i}, V_{y_i}, V_{z_i}, V_{\alpha_i}, V_{\beta_i}$ and V_{γ_i} , where $1 \leq i \leq N$, required for BFGS optimisation of benzene molecular clusters are shown in Appendix A.3.

For water clusters, each molecule was treated as a non-rigid body and encoded in GEM* using nine real-valued parameters. With reference to an external coordinate system, three parameters specified the position of the oxygen atom of each molecule and three specified the molecular orientation in terms of the Euler angles. The remaining three parameters defined the shape of the molecule by specifying each $O - H$ distance (r_1, r_2) and the HOP (θ) angle. As one molecule can be assumed to be fixed in position and orientation, $9N - 6$ parameters are required to fully specify an N molecule water cluster. Given these parameter definitions, the coordinates (x, y, z) of an atom of a water molecule, relative to an external coordinate system, can be calculated using a method analogous to that described above for the benzene molecule. The calculations of the analytical energy gradients

$U_{r_{1i}}, U_{r_{2i}}, U_{\theta_i}, V_{x_i}, V_{y_i}, V_{z_i}, V_{\alpha_i}, V_{\beta_i}$ and V_{γ_i} , where $1 \leq i \leq N$, required for local optimisation of water molecular clusters are shown in Appendix A.4.

7.3.2 Genetic Mutation

In addition to the mutation operations specified in Section 4.2, the following equally likely additional mutation operations were implemented

- randomly selected molecules were interchanged and a BFGS local minimisation performed.
- all Euler angles for a randomly chosen molecule were “stepped” through their allowed range. The minimum energy configuration found was then locally optimised.

7.4 Results

7.4.1 Benzene Clusters

The optimised structures found by GEM* for benzene clusters in the range $N = 2, \dots, 8$ are shown in Figures 7.5 and 7.6. Table 7.4 contains all previously found optimal potential energy values in addition to those obtained by GEM*. The predominant feature of these benzene cluster configurations is the tendency towards close $C \cdots H$ approaches due to the coulombic interaction between the positively charged hydrogen atoms and the negatively charged carbon atoms. This effect favours an edge-to-face structure, where the hydrogen atoms at the edge of one molecule are pointed towards the face of the other molecule. This gives rise to large dihedral angles between the molecular planes and is characteristic of the “herringbone” packing relationship found in crystalline benzene and many other crystals [58]. In more detail, the GEM* optimised structures for benzene clusters are:

- Benzene dimer (Figure 7.5(a)). A dihedral angle of 26.3° and an intermolecular centre-to-centre distance of 4.69\AA .
- Benzene trimer (Figure 7.5(b)). All dihedral angles are 61.1° and all intermolecular centre-to-centre distances are 4.98\AA .
- Benzene tetramer (Figure 7.5(c)). This is a tetrahedral configuration with dihedral angles of 77.5° (for adjacent pairs) and 55.3° (for diametrically opposing pairs). The respective intermolecular distances are 5.04\AA and 5.76\AA .
- Benzene pentamer (Figure 7.5(d)). Structurally this cluster can be viewed as two fused tetrahedra sharing a common face. Intermolecular distances within the tetrahedral cluster range from 5.0\AA to 5.7\AA and dihedral angles range from 32° to 95° .
- Benzene hexamer (Figure 7.6(a)). This structure is a flattened octahedron where the average intermolecular distance in the central square is 5.8\AA .
- Benzene septamer (Figure 7.6(b)), benzene octamer (Figure 7.6(c)) and benzene nonamer (Figure 7.6(d)). The basic structure of all these benzene clusters is a partial icosahedral shell surrounding a central molecule.

Given that, using a random initial configuration, the largest benzene cluster previously optimised was $N = 4$ by Xiao and Williams [62], GEM* performed well by successfully finding all currently accepted global minima for $N = 2, \dots, 6$ and also obtained values for $N = 7, \dots, 12$. In fact, with the exception of $N = 7$, the results obtained by GEM* either matched or improved all previously obtained results.

| N | Energy (kJ mol ⁻¹) ([55]) | Energy (kJ mol ⁻¹)(GEM*) |
|-----|---------------------------------------|--------------------------------------|
| 2 | -11.0 | -11.0 |
| 3 | -32.1 | -32.1 |
| 4 | -55.6 | -55.6 |
| 5 | -79.1 | -79.1 |
| 6 | -106.1 | -106.4 |
| 7 | -134.4 | -133.9 |
| 8 | - | -161.4 |
| 9 | -161.0 | -187.8 |
| 10 | - | -220.2 |
| 11 | -237.0 | -246.8 |
| 12 | - | -283.4 |

Table 7.4: Optimised potential energy values for benzene clusters.

7.4.2 Water Clusters

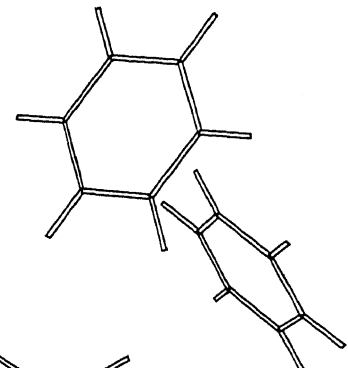
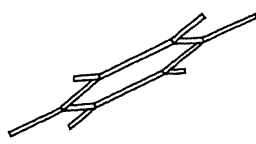
The optimised structures found by GEM* for water clusters of size $N = 2$ and $N = 6$ are shown in Figure 7.7. The minimum cluster energies found by both GEM* and Byrd et al. [5] for $N = 2, 6, 8$ and 21 are shown in Table 7.5. From Figure 7.3, a reasonable assumption is that the minimum energy for a water cluster will be obtained when the $H - O$ distance between molecules is optimal and all $H - H$ distances are maximised. As can be seen in Figure 7.7, this is the case for the GEM* optimised clusters. While GEM* was able to make some progress towards the currently accepted global minima, the computational requirements for evaluating the energy and gradient formula for water clusters are considerably greater than that for the other molecular structures investigated in this study and exceeded the capacity of the available computers.

| N | Energy (a.u.) [5] | Energy (a.u.) GEM* |
|-----|-------------------|--------------------|
| 2 | -0.0098 | -0.0094 |
| 6 | -0.0756 | -0.0742 |
| 8 | -0.1199 | -0.0997 |
| 21 | -0.3679 | -0.2856 |

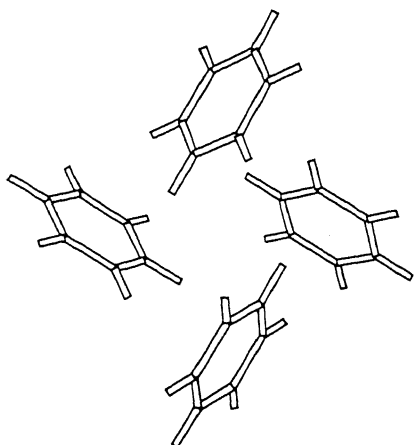
Table 7.5: Optimised potential energy values for water clusters.



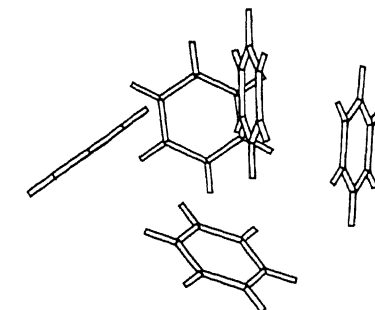
(a) Benzene dimer.



(b) Benzene trimer.

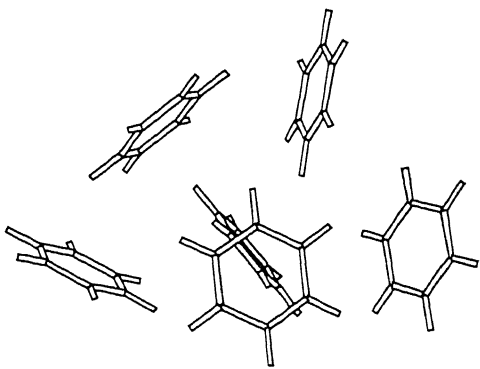


(c) Benzene tetramer.

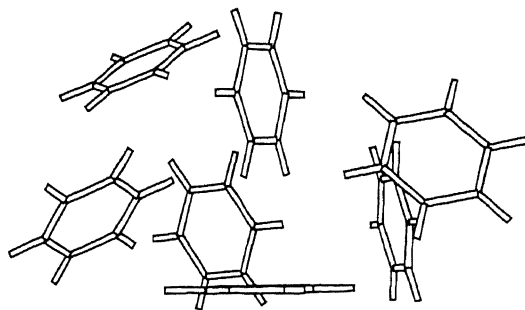


(d) Benzene pentamer.

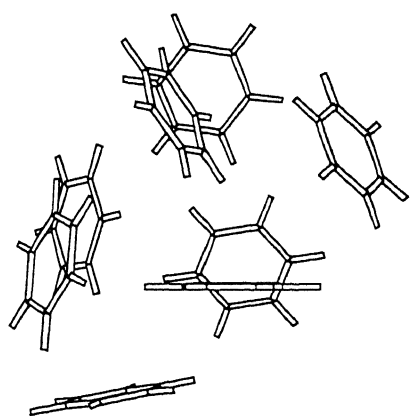
Figure 7.5: Structures found during GEM* optimisation of benzene dimer, trimer, tetramer and pentamer clusters.



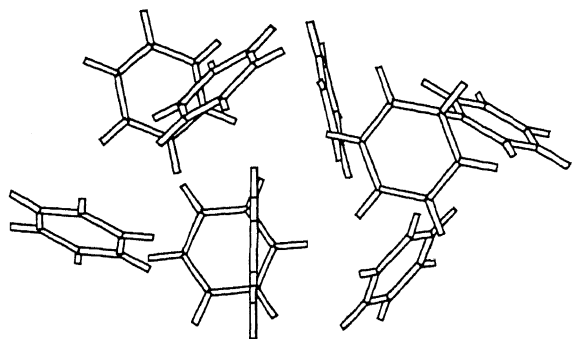
(a) Benzene hexamer.



(b) Benzene septamer.



(c) Benzene octamer.



(d) Benzene nonamer.

Figure 7.6: Structures found during GEM* optimisation of benzene hexamer, septamer, octamer and nonamer.

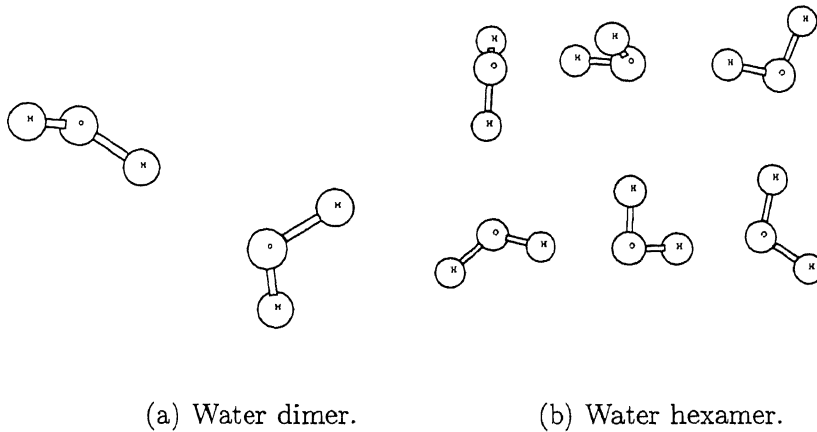


Figure 7.7: Structures found during GEM* optimisation of the water dimer and hexamer showing the dominance of the $H - O$ pair potential.

7.5 Discussion

Clearly GEM* is an improvement on previous attempts at using a genetic algorithm to optimise molecular cluster problems. In particular, for benzene clusters, GEM* found a number of new optimal configurations. However GEM* was unable to achieve the results obtained in [5] by a stochastic/perturbation method implemented specifically for the water cluster problem. It is important to note that the results in [5] were obtained on considerably more powerful computers than those currently available for this study.

Chapter 8

GEM* Optimisation of a Model Molecular Structure

8.1 Introduction

As a first step in applying GEM* to bonded molecular structures, the model molecular structure presented in [23] consisting of N atoms connected by rigid bonds of unit length and constrained to two dimensions was optimised. For this model structure, all optimal configurations are approximately located on a hexagonal grid with unit spacing [23]. Of particular interest are 19, 37 and 61 atom structures whose optimal configurations form maximally compact hexagonal structures of radii 2, 3 and 4. Prior to this study, only the 19 atom structure had been successfully optimised [34]. However GEM* successfully optimised both the 19 and 37 atom structures, all other structures in the range $N = 3, \dots, 42$ and also those for $N = 44, 45, 46, 49, 50$ and 53.

Section 8.2 of this chapter describes the model molecular structure with the modifications applied to the base GEM* software described in Section 8.3. The results obtained are presented in Section 8.4 while Section 8.5 reviews these results.

8.2 Model Molecular Structure

The model molecular problem consists of N atoms connected by rigid bonds of unit length and constrained to two dimensions. The potential energy, V , of this system is given by the pairwise addition of scaled Lennard-Jones potentials

$$V = \sum_{i < j}^N (1/r_{ij}^{12} - 2/r_{ij}^6)$$

While this model problem is a very simple representation of a molecule, it is useful for developing molecular structure optimisation methods as the dimension of the problem is easily adjusted and the global minimum energy can be easily determined for any dimension.

The globally optimal conformation for the $N = 61$ molecule is shown in Figure 8.1, while Figure 8.2 shows the variation of the optimum energy as a function of the number of atoms in the molecule. Figure 8.3 shows the energy decrements of the global minima as the number of atoms is increased. The cyclic high point in the energy decrements occurs whenever an atom is placed at a “vertex” of the hexagon and the number of neighbours at unit distance reduces from three to two.

As described in [23], the parameter space for the model has two distinguishable regions. The first region is characterised by high energy levels and corresponds to “knotted” configurations where bonds cross each other, while the second region has energies less than zero and corresponds to regions where no bonds cross. Local optimisers are unable to move between these regions because of the high energy barriers associated with attempting to directly remove a knot. Clearly, the probability of randomly generating a configuration with at least one pair of bonds crossing depends on the number of atoms in the configuration. Judson et al. [23] found that for a molecule of 19 atoms, the percentage of randomly generated configurations

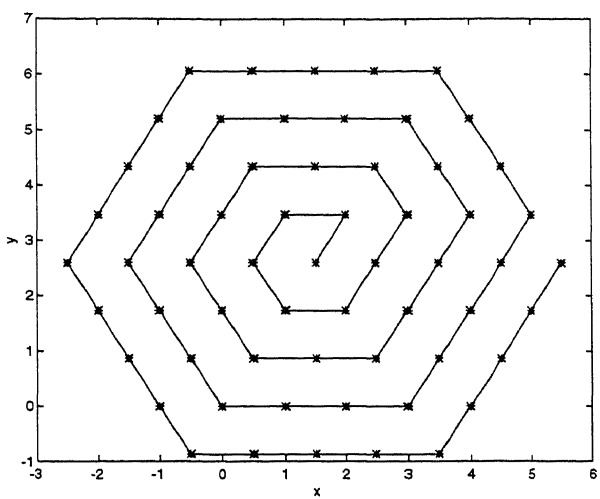


Figure 8.1: Globally optimal conformation for the $N = 61$ model molecular structure showing the dense hexagonal packing.

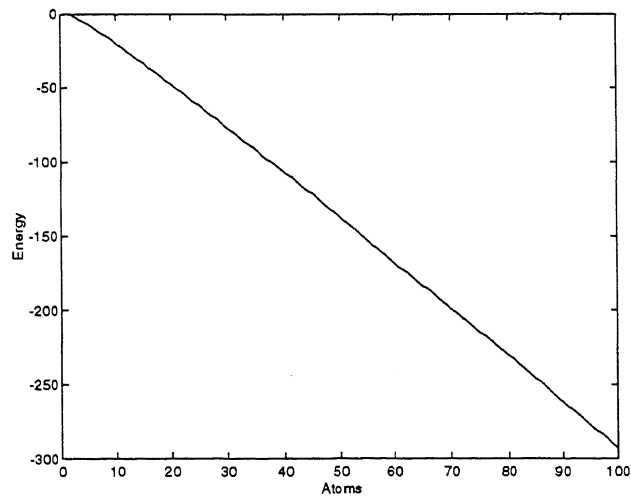


Figure 8.2: Globally optimal energies - $N = 2, \dots, 100$ model molecular structure.

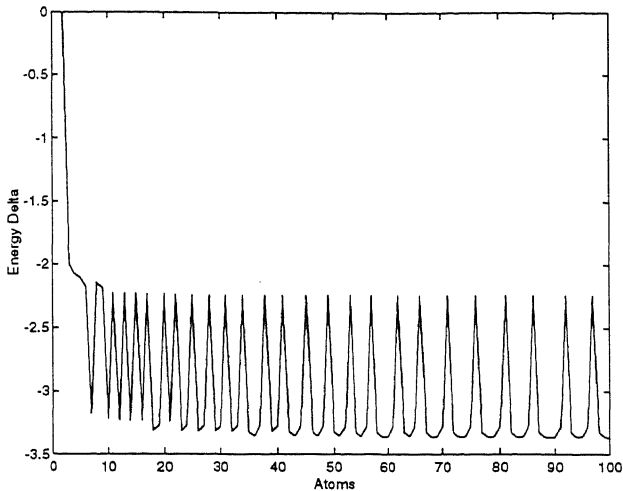


Figure 8.3: Decrements in the optimal energy for the model molecular structure, $N = 2, \dots, 100$. The cyclic high point in the energy decrements occurs whenever an atom is placed at a vertex of the hexagon and the number of neighbours at unit distance from the atom being added reduces from three to two.

which contained no knots was 0.058. The corresponding percentages for 37 and 61 atoms were 0.0012 and $\simeq 10^{-7}$ respectively. They suggested that a first measure of the robustness of an optimisation method is how often it can find any unknotted configuration having started from a random one. A second measure is how low in energy is the distribution of unknotted configurations, and a third and final measure is the nearness to the global energy minimum of the lowest energy structure found.

Given the probability of generating an initial conformation with at least one pair of intersecting bonds and the inability of local optimisers to move between the two distinct regions of the parameter space, other more flexible optimisation methods must be employed to find the global minimum. In [23], both genetic algorithms and simulated annealing techniques were used to optimise chains of 19, 37 and 61 atoms. Meza and Martinez [34] used an intelligent adaptive grid search (PDS) in conjunction with a variety of local

optimisers to also optimise these three chains. The best results obtained by each of these methods are shown in Table 8.1.

| Method | 19 atoms | 37 atoms | 61 atoms |
|----------------|----------|----------|----------|
| SA [23] | -44.2 | -94.8 | -164.4 |
| GA [23] | -44.3 | -97.3 | -166.6 |
| PDS [34] | -45.3 | -95.3 | -167.2 |
| Global Minimum | -45.3 | -98.3 | -171.5 |

Table 8.1: Comparison of previous search methods for the 19, 37, and 61 atom model molecular structures.

8.3 GEM* Computational Method

As described in the following subsections, the presence of rigid bonds had a number of implications for GEM*, particularly with regard to possible genetic encoding methods and also for the design of genetic operators.

8.3.1 Genetic Encoding

The use of Cartesian coordinates to specify atomic positions within a molecule during the optimisation process requires, if bond lengths and angles are assumed to remain constant, that a number of complex non-linear constraints be employed. However, if a set of internal coordinates such as bond angles in the two-dimensional case and dihedral (or torsional) angles in the three-dimensional situation are employed, then there is no requirement to specifically enforce these constraints. They arise naturally from the coordinate system.

With reference to Figure 8.4, the configuration of the model molecular structure can be encoded as a sequence of α angles in the range -180° to 180° . Clearly, and without loss of generality, one pair of atoms may be held in fixed positions. In the physical realisation of this model, both ends of the chain would tend to fold towards the centre of the chain. For this reason,

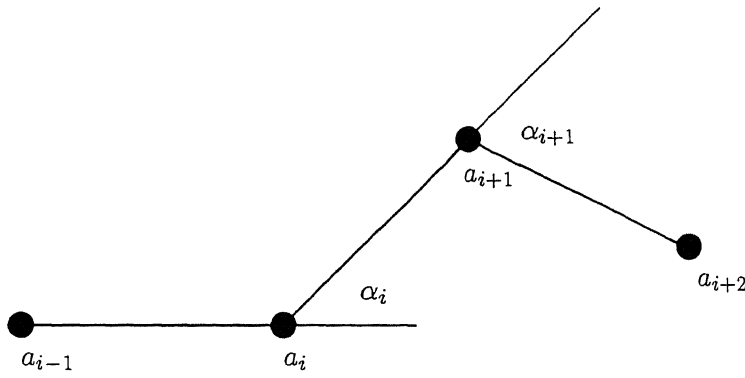


Figure 8.4: Bond angles (α) used to encode the model molecular structure.

this model was encoded in GEM*, with the two atoms nearest the centre of the chain held in fixed positions. The α angles are then divided into two sets, where each set defines the configuration of the two segments of the chain which start from each of the two fixed central atoms. Calculation of the analytical energy gradients V_{α_i} , where $1 \leq i \leq N$, required by the BFGS optimiser in this coordinate system is shown in Appendix A.5.

8.3.2 Genetic Crossover

For this structure, two specific crossover operators were implemented. The first randomly selects a crossover point and generates new solutions by interchanging corresponding segments of the parent solutions. The α angle of the crossover point in each child is then stepped through its allowed range to determine the optimal orientation of the two segments which were combined to make the child solution. The second operator performs a multi-point crossover between two parents to create each new child solution. For each α angle corresponding to the crossover points, the stepwise optimisation

process described above is performed.

8.3.3 Genetic Mutation

For this structure, in addition to the mutation operators implemented for the base GEM* algorithm (Section 4.2), two additional mutation operators were implemented. The first selected a random point and set all α angles from that point to the nearest end of the chain equal to zero. This has the effect of “straightening” the chain of atoms from an arbitrary point. A stepwise optimisation was then performed at the selected point followed by a partial local optimisation where only those α angles that were initially set to zero were allowed to vary.

The second mutation operator selected a random point and performed a stepwise optimisation on the corresponding α angle. Starting from this minimum, a full local optimisation was then performed.

8.4 Results

GEM* was particularly successful when applied to the model molecular structure and achieved the results shown in Table 8.2 in addition to finding a final energy of -166.1 for the $N = 61$ case. Of note is that GEM* found all packed hexagonal energies in the range $N = 2, \dots, 42$ and some in the range $N = 43, \dots, 55$. When GEM* was unable to find the global minimum, it was always able to find a value near the global minimum. Representative structures found by GEM* are shown in Figures 8.5 and 8.6.

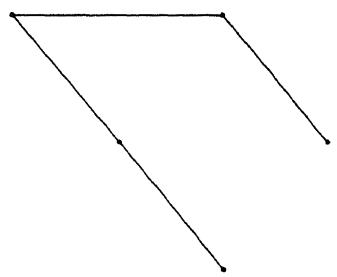
8.5 Discussion

With respect to the criteria proposed by Judson et al. [23], GEM* performed well and, with one exception ($N = 61$), improved on all previous results. The results obtained in this chapter demonstrate that it is possi-

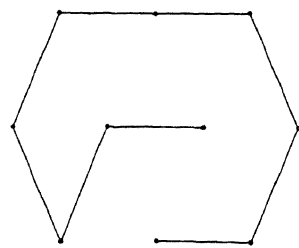
ble to extend GEM* to bonded molecular structures and that, at least for simple structures, GEM* will efficiently optimise them.

| <i>N</i> | Optimal | GEM* | Gen. | <i>N</i> | Optimal | GEM* | Gen. |
|----------|---------|-------|------|----------|---------|--------|------|
| 2 | -1.0 | -1.0 | 1 | 29 | -74.0 | -74.0 | 5 |
| 3 | -3.0 | -3.0 | 1 | 30 | -77.2 | -77.3 | 18 |
| 4 | -5.1 | -5.0 | 1 | 31 | -79.5 | -79.6 | 1 |
| 5 | -7.2 | -7.2 | 1 | 32 | -82.8 | -82.9 | 9 |
| 6 | -9.3 | -9.3 | 1 | 33 | -86.1 | -86.2 | 10 |
| 7 | -12.5 | -12.5 | 2 | 34 | -88.3 | -88.5 | 5 |
| 8 | -14.7 | -14.7 | 1 | 35 | -91.7 | -91.7 | 9 |
| 9 | -16.9 | -16.9 | 1 | 36 | -95.0 | -95.0 | 36 |
| 10 | -20.1 | -20.1 | 1 | 37 | -98.3 | -98.3 | 31 |
| 11 | -22.3 | -22.3 | 1 | 38 | -100.5 | -100.6 | 17 |
| 12 | -25.5 | -25.6 | 2 | 39 | -103.8 | -103.8 | 23 |
| 13 | -27.8 | -27.8 | 2 | 40 | -107.1 | -107.2 | 23 |
| 14 | -31.0 | -31.0 | 3 | 41 | -109.4 | -109.5 | 6 |
| 15 | -33.2 | -33.2 | 1 | 42 | -112.7 | -112.9 | 8 |
| 16 | -36.5 | -36.5 | 3 | 43 | -116.0 | -115.2 | 50 |
| 17 | -38.7 | -38.8 | 1 | 44 | -119.3 | -119.4 | 48 |
| 18 | -42.0 | -42.1 | 2 | 45 | -121.6 | -121.8 | 39 |
| 19 | -45.3 | -45.3 | 8 | 46 | -124.9 | -125.0 | 22 |
| 20 | -47.5 | -47.5 | 2 | 47 | -128.6 | -127.4 | 50 |
| 21 | -50.8 | -50.8 | 6 | 48 | -131.5 | -130.7 | 50 |
| 22 | -53.0 | -53.0 | 2 | 49 | -133.8 | -133.9 | 6 |
| 23 | -56.3 | -56.4 | 2 | 50 | -137.1 | -137.3 | 30 |
| 24 | -59.6 | -59.6 | 15 | 51 | -140.5 | -139.7 | 50 |
| 25 | -61.8 | -61.9 | 2 | 52 | -143.7 | -142.9 | 50 |
| 26 | -65.1 | -65.1 | 17 | 53 | -146.0 | -146.2 | 20 |
| 27 | -68.4 | -68.5 | 6 | 54 | -149.3 | -148.6 | 50 |
| 28 | -70.0 | -70.7 | 1 | 55 | -152.7 | -150.8 | 50 |

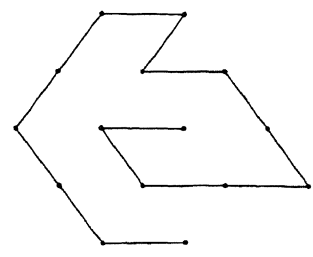
Table 8.2: Packed hexagonal energies, GEM* minima and the number of generations required to achieve these minima for the model molecular structure. GEM* optimisation was terminated when either the known global minimum was found or 50 generations had been performed.



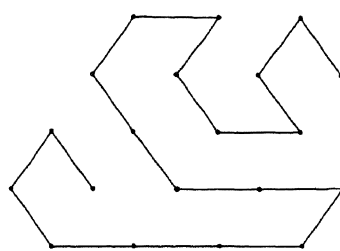
(a) $N = 5$, energy = -7.2.



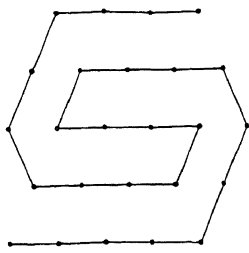
(b) $N = 10$, energy = -20.1.



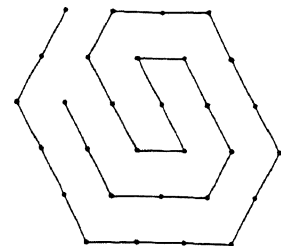
(c) $N = 15$, energy = -33.2.



(d) $N = 20$, energy = -47.5.

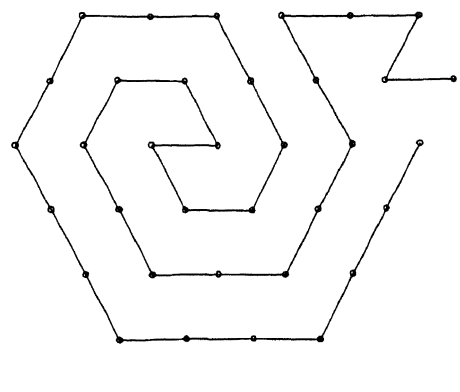


(e) $N = 25$, energy = -61.9.

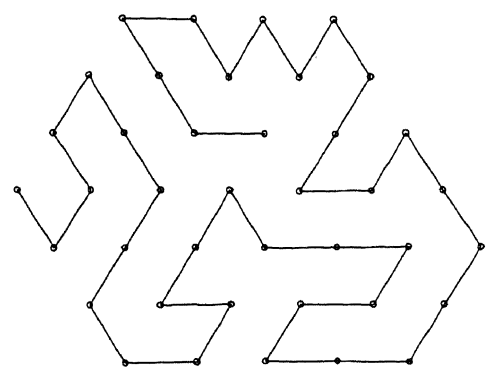


(f) $N = 30$, energy = -77.3.

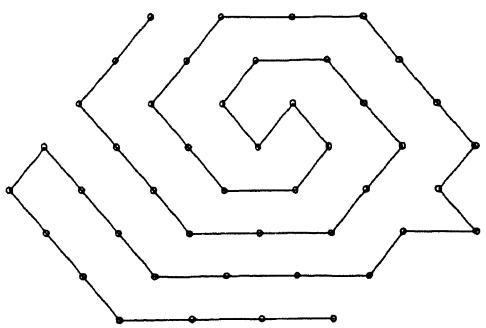
Figure 8.5: Structures found during GEM* optimisation of $N = 5, 10, 15, 20, 25$ and 30 model molecular structure.



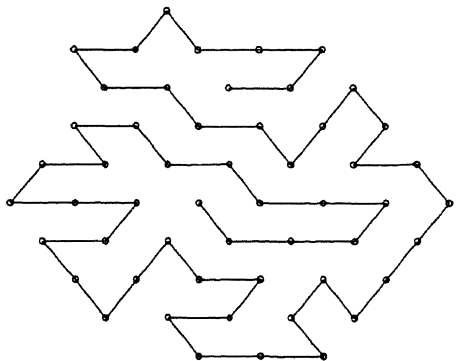
(a) $N = 35$, energy = -91.7.



(b) $N = 40$, energy = -107.2.



(c) $N = 45$, energy = -121.8.



(d) $N = 53$, energy = -146.2.

Figure 8.6: Structures found during GEM* optimisation of $N = 35, 40, 45$ and 53 model molecular structure.

Chapter 9

GEM* Optimisation of Molecules

9.1 Introduction

The application of GEM* to a number of small molecules is described in this chapter. Molecules differ from clusters in that they are created when a number of atoms are joined via electronic bonds. These bonds may involve a sharing of electrons to form a covalent bond or, alternatively, a transfer of electrons in an ionic bond. In contrast to the two-dimensional model molecular structure studied in the previous chapter, these bonds may not be treated as rigid entities within the force field models and a degree of “bond stretching” is allowed. In addition to these relatively high energy bonds, atoms within molecules interact via pairwise van der Waals potentials and possibly also through a coulombic effect.

Section 9.2 of this chapter describes the molecular mechanics force fields used to model the molecular structures optimised. The modifications needed to the base GEM* method are described in Section 9.3 while the results obtained are presented in Section 9.4. Section 9.5 reviews these results.

9.2 Molecules

Molecular mechanics force fields used to model molecules normally include bond stretching (E_s), angle bending (E_θ), torsion (E_ω) and van der Waals (E_v) interactions in their make-up [4]. The total potential energy E is given by

$$E = \sum E_s + \sum E_\theta + \sum E_\omega + \sum E_v$$

where the sums extend over all bonds, bond angles, torsion angles, and non-bonded interactions between all atoms not bound to each other or to a common atom respectively. The sum of all these terms is the steric or potential energy of the molecule. The bond stretch term, E_s , is normally approximated by a simple harmonic function

$$E_s = \sum k_s(l - l_0)^2$$

where k_s is the stretching force constant describing the deformation, l_0 is the equilibrium bond length and l the actual bond length. Historically, bond angles have been treated in the same manner as bond lengths and are usually described by a harmonic function such as

$$E_\theta = \sum k_\theta(\theta - \theta_0)^2$$

where k_θ is the bond angle constant describing the deformation, θ_0 is the equilibrium bond angle and θ the actual bond angle.

The effect of the dihedral angles is included by the use of a Fourier series

$$E_\omega = \sum V_s(1 + s \cos(n\omega))$$

where ω is the dihedral angle, V_s is the rotational barrier height, n the periodicity of rotation and $s = 1$ for staggered minima and -1 for eclipsed minima. The energy E_v from non-bonded interactions is normally regarded

to consist of both van der Waals and coulombic components. The van der Waals component can be considered as both a size parameter and representative of electron correlation (resulting from instantaneous dipole interactions) while the coulombic component provides a quantitative measurement of the influence of polarity on the energy and the structure.

Many different functional forms have been used for van der Waals interactions but the most common is the Lennard-Jones potential

$$E_{vdw} = \sum \epsilon((r_m/r)^{12} - 2(r_m/r)^6)$$

where ϵ is the well depth and r_m is the minimum energy interaction distance. The coulombic interaction is usually calculated using partial charges q on the atom centres with the energy calculated using Coulomb's law

$$E_{el} = \sum q_i q_j / D r_{ij}$$

where the dielectric constant D takes a value appropriate to a given solvent or is made proportional to the distance r_{ij} between charges.

In previous studies, Wilson et al. [60] developed an Anneal-Conformer program which was able to find global minimum energy conformations for peptides and organic molecules using both Amber and MM2 force fields. Anneal-Conformer used both SA and local minimisation techniques and was tested on molecules with up to seven dihedral angles.

Judson et al. [24] used a GA to find low-energy conformations of small to medium organic molecules (1 - 12 rotatable bonds). The GA was tested on a suite of 72 molecules and, for molecules with more than eight rotatable bonds, was more efficient than the CSEARCH algorithm in the molecular mechanics program Sybyl.

Maranas and Floudas [30] transformed the initial non-convex total potential energy function into the difference of two convex functions and applied

a primal-relaxed dual global optimisation approach to the pseudoethane molecule (1 dihedral angle) and also the 1,2,3-trichloro-1,4-bifluoro-butane molecule (3 dihedral angles). They were able to find the global minimum energy conformations in both cases.

The following sections describe the molecules whose structures were globally optimised by GEM*.

9.2.1 United Atom Butane

United atom butane [39] is created by collapsing the butane molecule (C_4H_{10}) down to four “hydrocarbon atoms” connected by flexible bonds (Figure 9.1). A potential energy function for united atom butane that has gained widespread acceptance is

$$k_s \sum_{i=1}^3 (l_i - l_0)^2 + k_\theta \sum_{i=1}^2 (\theta_i - \theta_0)^2 + V_{3/2}(1 + \cos(3\phi)) + \epsilon_{14}((\sigma_{14}/r_{14})^{12} - 2(\sigma_{14}/r_{14})^6)$$

where r_{14} is the distance between the first and fourth molecules (and is therefore completely dependent on the variables $l_1, l_2, l_3, \theta_1, \theta_2$ and ϕ), $k_s = 310.0$ kcal/ \AA^2 , $k_\theta = 40.0$ kcal/rad 2 , $V_{3/2} = 1.3$ kcal, $\epsilon_{14} = 0.06$ kcal, $\sigma_{14} = 3.6$ \AA , $l_0 = 1.536$ \AA , and $\theta_0 = 70.5^\circ$.

The optimal configuration for united atom butane [39] has (with reference to Figure 9.1) $l_1 = l_2 = l_3 = 1.526$ \AA , $\theta_1 = \theta_2 = 70.5^\circ$ and $\phi = 180^\circ$.

9.2.2 Pseudoethane

Pseudoethane is a one-dimensional conformation problem of the fully substituted ethane molecule (Figure 9.2). All three hydrogen atoms of both carbon atoms are replaced with one carbon, one oxygen and one nitrogen atom. While such a molecule does not exist, it is still a useful model for testing methods that predict molecular conformations based on the energies of non-bonded atom interactions.

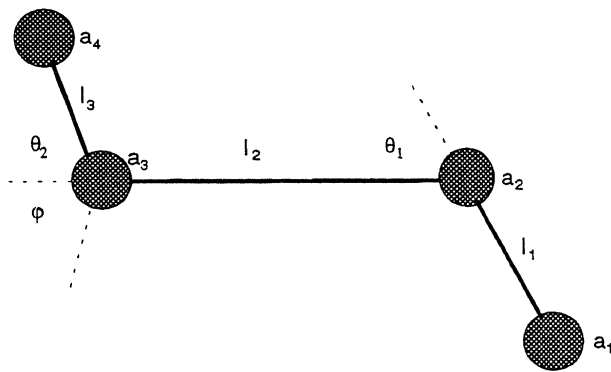


Figure 9.1: Structure of the united atom butane molecule.

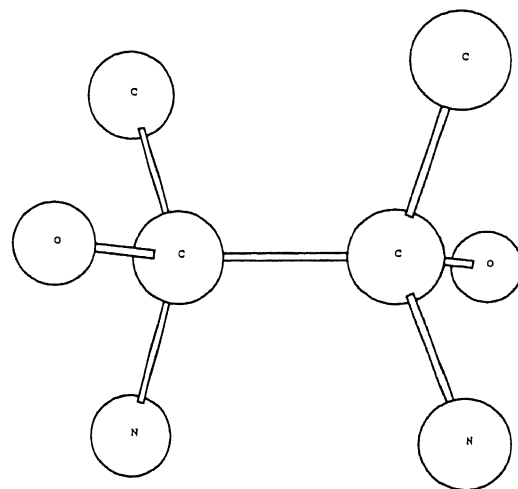


Figure 9.2: Structure of the pseudoethane molecule.

For the pseudoethane molecule all covalent bond lengths are assumed to be 1.54\AA and all covalent bond angles 109.5° . Only one parameter is required to define the structure of pseudoethane, θ the torsion angle about the $C - C$ bond. The non-bonded atom interactions are given by the following Lennard-Jones potential function

$$v(r_{ij}) = B_{ij}/r_{ij}^{12} - A_{ij}/r_{ij}^6$$

where the values of the interaction parameters A_{ij} and B_{ij} are given in Table 9.1. This problem has been reported [30] to have the three local minima shown in Table 9.2.

| Atom-Atom | $B (10^{-4}\text{kcal \AA}^{12}/\text{mol})$ | $A (\text{kcal \AA}^6/\text{mol})$ |
|-----------|--|------------------------------------|
| $C - C$ | 28.58 | 372.5 |
| $N - N$ | 17.82 | 344.7 |
| $O - O$ | 14.49 | 367.2 |
| $C - N$ | 16.82 | 348.7 |
| $C - O$ | 20.52 | 367.2 |
| $N - O$ | 15.75 | 349.5 |

Table 9.1: Lennard-Jones parameters - pseudoethane.

| θ | $V_{\min}(\text{kcal/mol})$ |
|----------------|-----------------------------|
| 61.42° | -0.79733156 |
| 296.12° | -1.03989551 |
| 183.45° | -1.07111459 |

Table 9.2: Local minima for the pseudoethane molecule.

9.2.3 Acetyl Chloride

The potential energy for acetyl chloride (C_2H_3OCl , Figure 9.3) is modelled using a sum of cosine type terms, associated with torsions, and a modified Buckingham pair potential, summed over all non-bonded atom pairs, and augmented with a coulombic term [12]

$$V = \sum_i (A_i 10^4 \exp(-B_i r_i) - C_i/r_i^6 + D_i/r_i^3) + E \cos(F\theta)/2$$

where $E = -1.11$, $F = 3.0$ and the remaining parameters are as shown in Table 9.3. The global minimum potential energy for acetyl chloride is -2.2551 kJ/mol [12].

| Atom-Atom | A (kJ/mol) | B (\AA^{-1}) | C (kJ $\text{\AA}^6/\text{mol}$) | D (kJ $\text{\AA}^3/\text{mol}$) |
|-----------|------------|-------------------------|-----------------------------------|-----------------------------------|
| $H - O$ | 3.46 | 4.57 | 122.0 | 0.0 |
| $H - Cl$ | 3.90 | 4.15 | 321.0 | 0.0 |

Table 9.3: Van der Waals parameters for acetyl chloride.

The Cartesian coordinates used for the atomic positions of the initial configuration are shown in Table 9.4 and give an initial potential energy of -0.9898 kJ/mol [12].

| $x (\text{\AA})$ | $y (\text{\AA})$ | $z (\text{\AA})$ |
|------------------|------------------|------------------|
| 0.0000 | 0.0000 | -1.5058 |
| 0.0000 | -1.0379 | -1.8908 |
| 0.8989 | 0.5189 | -1.8908 |
| -0.8989 | 0.5189 | -1.8908 |
| 0.0000 | 0.0000 | 0.0000 |
| -0.8155 | -0.4709 | 0.7213 |
| 1.4404 | 0.8316 | 0.6798 |

Table 9.4: Cartesian coordinates used for the initial configuration of the acetyl chloride molecule.

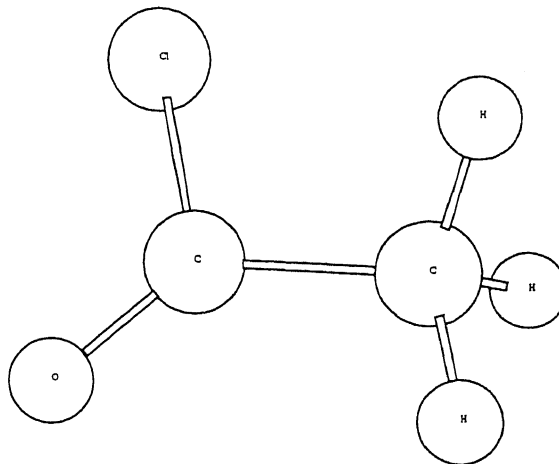


Figure 9.3: Structure of the acetyl chloride molecule.

9.3 GEM* Computational Method

9.3.1 Genetic Encoding

As shown in [50], the Cartesian coordinates of atom j' , connected to atom j are given by

$$\begin{bmatrix} x_{j'} \\ y_{j'} \\ z_{j'} \\ 1 \end{bmatrix} = \begin{bmatrix} -\cos \alpha_j & -\sin \alpha_j & 0 & -R_j \cos \alpha_j \\ \sin \alpha_j \cos \beta_j & -\cos \alpha_j \cos \beta_j & -\sin \beta_j & R_j \sin \alpha_j \cos \beta_j \\ \sin \alpha_j \sin \beta_j & -\cos \alpha_j \sin \beta_j & \cos \beta_j & R_j \sin \alpha_j \sin \beta_j \\ 0 & 0 & 0 & 1 \end{bmatrix} \begin{bmatrix} x_j \\ y_j \\ z_j \\ 1 \end{bmatrix}$$

where R_j is the bond length between atoms j and j' , α_j is the bond angle $jj'j''$ and β_j is the dihedral angle $jj'j''j'''$ where atom j'' is connected to atom j' and atom j''' is connected to atom j'' . To calculate the distance between any atom pair, it is first necessary to establish a connecting path, formed by a sequence of bonds, which links these atoms. Then repeatedly apply the transformation shown above to calculate the Cartesian coordinates of each atom in the connecting path.

Initial molecular definitions are loaded into GEM* using MOPAC [53] internal format molecular definition files which may be generated from a number of other molecular definition formats using the Babel [56] software.

Local optimisation for molecules was performed using a Powell's Direction Set optimiser.

9.3.2 Genetic Mutation

For molecules, one additional mutation operator was added to those specified for the base GEM* algorithm (Section 4.2). This operator performed a stepwise optimisation on the dihedral angle. Starting from the lowest minimum found, a full local optimisation was then performed.

9.4 Results

9.4.1 United Atom Butane

The optimal configuration for united atom butane described in Section 9.2.1 was found by GEM* consistently within the first generation.

9.4.2 Pseudoethane

As described above, the pseudoethane molecule has only one degree of freedom and the potential energy has only three minima. As such, it constitutes a trivial optimisation problem but is useful for verifying the genetic encoding method used in GEM* for three-dimensional molecules. GEM* was able to consistently find the global minimum within a single generation.

9.4.3 Acetyl Chloride

While the acetyl chloride molecule is structurally similar to the pseudoethane molecule, its potential energy function is very different as it includes coulombic and torsion terms in addition to the van der Waals term. This gives rise to a rather more complex PES than that of pseudoethane and presents a more difficult optimisation problem. However GEM* was able to consistently find the global minimum within a single generation.

9.5 Discussion

While all molecules successfully optimised by GEM* were relatively simple in structure, they did require that all features necessary for optimisation of larger molecules be implemented. These features included the interface to the MOPAC internal format molecular definition files and the software necessary to handle bonded molecular structures. In addition, genetic operators were developed to implement crossover and mutation techniques suitable for bonded molecular structures.

Chapter 10

Conclusion

10.1 Thesis Summary

This thesis addressed the problem of determining globally minimum potential energy configurations for a number of different types of molecular structures. For each of these molecular structures, molecular force field models were used to calculate potential energies. The more important outcomes of this study were

- the development of optimisation algorithms able to efficiently optimise non-bonded molecular structures such as pure and mixed atomic clusters and molecular clusters.
- the extension of these algorithms to handle simple bonded molecular structures.
- implementation, on a number of non-parallel and parallel computing platforms, of these algorithms in the GEM* computer software using the C++ programming language.
- reproducing results obtained previously by other methods for both pure and mixed atomic clusters, molecular clusters, a two-dimensional model molecule and simple molecules. In particular, GEM* is one

of a small number of optimisation methods able to find all currently accepted globally minimum structures for pure scaled Lennard-Jones atomic clusters in the range $N = 2, \dots, 80$.

- the identification of new lower energy molecular structures for both pure and mixed atomic clusters, molecular clusters and a two-dimensional model molecule.

The following subsections present a summary of the development of the optimisation algorithms implemented in GEM* and also describe their application to a number of molecular structure problems.

10.1.1 APSE

Initially APSE, an adaptive stochastic global optimiser was developed as a global optimisation method, using APS as a base algorithm. The major extension introduced in APSE was a mechanism which adaptively focused on those subsets of the search domain which have a greater probability of producing an improving objective function value. Subsequently, a proof of convergence was developed for APSE and validation testing performed using several standard test functions. Results from these tests demonstrated that, on average, and using appropriate values for the λ and β parameters, APSE required considerably fewer function evaluations than APS to solve these problems and there was also less variability between trials. Testing was also performed to determine the effect of problem dimension (d) and showed that, for the test problem at least, APSE was basically $O(d^2)$ while APS was $O(d^6)$.

In conjunction with local optimisation and a build-up approach, APSE was able to globally optimise scaled Lennard-Jones atomic clusters in the range $N = 2, \dots, 20$. With the addition of local optimisation and a PES

smoothing technique, this was extended to all scaled Lennard-Jones atomic clusters in the range $N = 2, \dots, 30$.

10.1.2 GEM*

The major global optimisation method developed within this study, GEM*, uses both local and APSE optimisations within a genetic algorithm based environment. In the context of optimising molecular structures, important components and features of GEM* are

- Within the GEM* environment, APSE was used in two distinct modes. Firstly, it was used to perform a global search of the entire problem domain and secondly, it could be configured to perform a global optimisation within a search domain restricted to be structurally “close” to a nominated configuration. In this restricted mode, APSE provided the ability for the search to move from one catchment basin on the PES to a neighbouring catchment basin so allowing an “intense” search around an existing configuration.
- Deterministic local optimisations were performed on configurations during each genetic generation using either Powell’s Direction Set method or a BFGS local optimiser. Within GEM*, local optimisations were performed by either allowing all parameters to vary, or by restricting the optimisation so that only a subset of parameters varied (within appropriate constraints). This partial local optimisation was performed on slightly perturbed random subsets of the parameters and also selectively applied to portions of the structure which had a relatively high contribution to the potential energy of the molecular structure.

- Stepwise optimisations were performed within GEM* by selecting a parameter of the solution and “stepping” this parameter through its allowed range. At each step, the energy of the resulting structure was calculated and the lowest energy structure became the starting point for a full local optimisation. This allowed optimisation operations such as, for cluster problems, physically separating the two parent hemispheres used to construct a new child configuration and, by slowly moving them towards each other, obtaining a new low energy configuration as a starting point for both global and local optimisations. For bonded structures, the bond or torsion angle at a crossover point was the parameter that was “stepped” through its allowed range.
- GEM* implemented these optimisation methods within a parallel real-coded genetic algorithm environment. Parallel computation occurred both through the implicit parallelism inherent within a genetic algorithm and also, at a higher level, using an arbitrary number of processors sharing a common pool of configurations.
- To maximise the efficiency of the optimisation process, molecular structures were encoded using the minimum representation possible with implicit implementation of constraints.
- Phenotype genetic operators, tailored to the molecular structure being optimised, were developed. While some random crossover operators were used, most were designed to specifically produce “good” solutions for input to subsequent mutation operations. A theoretical comparison, confirmed by experimental evidence, demonstrated the effectiveness of these phenotype operators as compared to the standard single point genetic crossover.

- GEM* always started from randomly generated structures and, as it has no bias towards any particular structure, was not inhibited from searching the complete domain of possible structures. Alternative methods, which start from a particular structure and use a build-up approach, have an inherent bias towards that structure and are less able to find alternative, lower energy structures.
- GEM* was successful in solving molecular structure problems for a number of reasons. Firstly, in common with all genetic algorithms, it explores the search domain in parallel using all clusters in the current population as starting points. Secondly, and perhaps more importantly, it operates at a number of levels when generating new structures. At the coarsest level are crossover operators such as χ_1 , χ_3 , χ_4 and the hemisphere version of χ_2 which interchange large volumes between current clusters. Fine-tuning is provided by the quadrant and octant versions of χ_2 and the use of BFGS and APSE optimisations within the **Mutate** operation.

In the operational context, GEM* has a number of features which are important when performing computationally demanding global optimisation problems. These include

- The ability to restart at the last completed genetic generation of a previous optimisation run. This allows recovery from system and software problems with minimal loss of computational processing.
- Dynamic reconfiguration so that the use of the multi-processing environment is maximised. As the multi-processing computer used during this study was a shared resource, the number of available processors varied continuously. Using the restart facility, GEM* was able to dis-

continue an optimisation run at any point and restart using additional processors as they became available.

- Automatic creation, at the completion of each generation, of data files containing the atomic coordinates for all configurations in the genetic pool. These files were used to produce structural diagrams giving a visual record of algorithm performance.

10.1.3 Pure Atomic Clusters

GEM* was able to find all currently accepted global minima for atomic clusters, modelled using a scaled Lennard-Jones pair potential, in the range $N = 2, \dots, 80$. In addition, GEM* found new global energy minima for the $N = 77$ and $N = 78$ clusters. Importantly, all these minima where found using randomly generated starting structures.

In addition, a theoretical analysis was presented which quantified the effectiveness, when applied to atomic clusters, of phenotype genetic operators. The theoretical predictions of this analysis were subsequently confirmed by experimental evidence.

10.1.4 Mixed Atomic Clusters

With the addition of one genetic mutation operator to those used for pure atomic clusters, GEM* was able to determine the energies, substitution energies, and atom counts for all $Ar_{N-n}Xe_n|_{2 \leq N \leq 20}$ clusters. In addition, further investigation of the optimised structures for $Ar_{10-n}Xe_n$, $Ar_{12-n}Xe_n$ and $Ar_{17-n}Xe_n$ clusters was performed to determine the reasons for the observed changes in substitution energy. These were found to be caused by discontinuities in the sequence of structures corresponding to the global minima as xenon atoms were substituted for argon atoms. The previous attempt at determining this substitution sequence used, as an initial con-

figuration, the global minimum for the corresponding pure atomic cluster in conjunction with local optimisation. This technique was unable to find these new global minima due to the resulting inherent bias towards this initial configuration.

10.1.5 Benzene Clusters

Prior to this study, there had been only two other attempts to find global optimisers for benzene clusters using randomly generated initial configurations. These involved a multi-start method and a standard (binary-coded) genetic algorithm and both successfully globally optimised clusters in the range $N = 2, \dots, 4$. GEM* obtained the currently accepted global minima for clusters in the range $N = 2, \dots, 6$ and in addition, new minima were determined for clusters in the range $N = 8, \dots, 12$.

10.1.6 Water Clusters

The force field model used for water clusters demands significantly more intensive computation than that required for the other molecular structures investigated in this study. While GEM* did not find the currently accepted global minima, it did approach them. This gives reason to believe that, given appropriate computational resources, GEM* would be successful for this problem. It is appropriate to note that, for this study, the maximum configuration possible is a 12 processor IBM SP2 which was only available in a dedicated mode for relatively short periods of time. Other investigators of the water cluster problem have access to parallel computers of up to 128 processors for much greater time periods, greatly increasing the chances of success.

10.1.7 Model Molecular Structure

A two-dimensional model molecular structure was utilised to develop genetic operators applicable to a molecular structure containing tightly constrained bonds and bond angles. GEM* was more successful than all optimisation methods previously applied to this model and determined the global minima for all chains in the range $N = 3, \dots, 42$ from random initial configurations.

10.1.8 Molecules

GEM* was also able to determine globally minimum energy structures for united atom butane, pseudoethane and acetyl chloride molecules. While these are small molecules, they did demonstrate the ability of GEM* to optimise bonded three-dimensional structures using potential energy functions which included terms other than a van der Waals function.

10.2 Further Work

By far the most computationally intensive activity performed by GEM* is the local optimisations. To extend GEM* to more complicated molecular structures, this computational overhead could be reduced by

- smoothing of the PES to remove a proportion of the local minima.

This technique was demonstrated with APSE where the maximum size pure Lennard-Jones atomic cluster able to be optimised was increased from $N = 20$ to $N = 30$ by incorporation of a relatively simple pair potential smoothing technique.

- development of a reliable detection mechanism within local optimisations so that local optimisation may be terminated early when further optimisation is unlikely to produce a solution that will be included in the solution pool at the next generation. This detection mechanism

could be based on the rate of decrease of the potential energy in conjunction with how close the potential energy is to the highest potential energy in the solution pool. This measure could be adaptive in the sense that the termination criteria may change as generations increase.

- development of structural parameters which identify portions of a structure requiring further optimisation. For example, use of atomic binding energies or counts of structural elements that are “near” their optimal position, could be used to restrict local optimisations or APSE to portions of a structure. Another use of these structural parameters could be to identify structures from which it is impossible to build an optimal solution. For example, in the two-dimensional model molecular structure, local optimisation of a “knotted” solution will never produce a global optimum. In two dimensions, detection of knots is a relatively simple procedure. The corresponding three-dimensional problem is much more difficult but probably not intractable.

Development of innovative genetic operators that are applicable to bonded molecular structures is also of major importance. The phenotype crossover operators that function well with clusters do not translate simply to more important molecular architectures such as molecules and proteins. While a genetic algorithm will recognise good building blocks within a solution, when optimising complex objects such as large molecular structures, this happens over a relatively long time frame. Intelligent genetic operators should be sought which are able to adaptively recognise these good building blocks and accelerate their utilisation.

Bibliography

- [1] Emile Aarts, Ja Korst, *Simulated Annealing and Boltzmann Machines*, John Wiley and Sons (1990).
- [2] P.W. Atkins, *Molecular Quantum Mechanics*, Oxford University Press (1983).
- [3] K.K. Benke, D.R. Skinner, A Direct Search Algorithm for Global Optimisation of Multivariate Functions, *Australian Computer Journal*, 23 73-85 (1991).
- [4] Ulrich Burkert, Norman Allinger, *Molecular Mechanics*, American Chemical Society Monograph, 177 (1982).
- [5] Richard H. Byrd, Thomas Derby, Elizabeth Eskow, Klaas P.B. Oldenkamp, Robert B. Schnabel, A New Stochastic/Perturbation Method for Large-Scale Global Optimization and its Application to Water Cluster Problems, *Dept. of Computer Science, University of Colorado at Boulder, CU-CS-652-93* (1993).
- [6] D.E. Coker, R.O. Watts, Structure and Vibrational Spectroscopy of the Water Dimer using Quantum Simulation, *Journal of Physical Chemistry*, 91 2513-2518 (1987).
- [7] Thomas Coleman, David Shalloway, Zhijun Wu, Isotropic Effective Energy Simulated Annealing Searches for Low Energy Molecular Clus.

ter States, *Cornell Theory Center Technical Report - CTC92TR113* (1992).

- [8] Thomas Coleman, David Shalloway, Zhijun Wu, A Parallel Build-up Algorithm for Global Energy Minimizations of Molecules using Effective Energy Simulated Annealing, *Cornell Theory Center Technical Report - CTC93TR130* (1993).
- [9] Thomas F. Coleman, Zhijun Wu, Parallel Continuation-Based Global Optimization for Molecular Conformation and Protein Folding, *Cornell Theory Center Technical Report - CTC94TR175* (1994).
- [10] D.M. Deaven, K.M. Ho, Molecular Geometry Optimization with a Genetic Algorithm, *Physical Review Letters*, 75 288-291 (1995).
- [11] D.M. Deaven, N. Tit, J.R. Morris, K. Ho, Structural Optimization of Lennard-Jones Clusters by a Genetic Algorithm, *Preprint* (1996).
- [12] R. Fausto, J.J.C. Teixeira-Dias, NBI: A Fortran Program for Molecular Mechanics Calculations on a Microcomputer, *Computers and Chemistry*, 15 175-177 (1991).
- [13] D. Goldberg, *Genetic Algorithms in Search, Optimization and Machine Learning*, Addison-Wesley Publishing Company Inc., Reading, Mass. (1989).
- [14] Scott M. Le Grand, Kenneth M. Merz Jr., The Application of the Genetic Algorithm to the Minimization of Potential Energy Functions, *Journal of Global Optimization*, 3 49-66 (1993).
- [15] S.K. Gregurick, M.H. Alexander, B. Hardtke, Global Geometry Optimisation of $(Ar)_n$ and $B(Ar)_n$ Clusters using a Modified Genetic Algorithm, *Journal of Chemical Physics*, 104 2684-2691 (1996).

- [16] Bernd Hartke, Global Geometry Optimization of Clusters using Genetic Algorithms, *Journal of Physical Chemistry*, 97 9973-9976 (1993).
- [17] Bruce A. Hendrikson, The Molecular Problem: Determining Conformation from Pairwise Distances, *Cornell Theory Center Technical Report - CTC90TR28* (1990).
- [18] M.R. Hoare, P. Pal, Physical Cluster Mechanics: Statics and Energy Surfaces for Monatomic Systems, *Advances in Physics*, 20 161-196 (1971).
- [19] M.R. Hoare, J.A. McInnes, Statistical Mechanics and Morphology of Very Small Atomic Clusters, *Faraday Discussions of the Chemistry Society*, 61 12-24 (1976).
- [20] M.R. Hoare, Structure and Dynamics of Simple Microclusters, *Advances in Chemical Physics*, 40 49-135 (1979).
- [21] M.R. Hoare, J.A. McInnes, Morphology and Statistical Statics of Simple Microclusters, *Advances in Physics*, 32 791-821 (1983).
- [22] J.H. Holland, *Adaptation in Natural and Artificial Systems*, The University of Michigan Press, Ann Arbor (1975).
- [23] R.S. Judson, M.E. Colvin, J.C. Meza, A. Huffer, D. Gutierrez, Do Intelligent Search Techniques Outperform Random Search for Large Molecules, *International Journal of Quantum Chemistry*, 44 277-290 (1992).
- [24] R.S. Judson, E.P. Jaeger, A.M. Treasurywala, M.L. Peterson, Conformational Searching Methods for Small Molecules II. Genetic Algorithm Approach, *Journal of Computational Chemistry*, 14 1407-1414 (1993).

- [25] S. Kirkpatrick, C.D. Gelatt Jr., M.P. Vecchi, Optimization by Simulated Annealing, *Science*, 220 671-680 (1983).
- [26] S. Kirkpatrick, Optimization by Simulated Annealing: Quantitative Studies, *Journal of Statistical Physics*, 34 975-986 (1984).
- [27] J. Kostrowicki, L. Piela, B.J. Cherayil, H.A. Scheraga, Performance of the Diffusion Equation Method in Searches for Optimum Structures of Clusters of Lennard-Jones Atoms, *Journal of Physical Chemistry*, 95 4113-4119 (1991).
- [28] Aiping Liao, A New Parallel Algorithm for Global Optimization with Application to the Molecular Cluster Problem, *Cornell Theory Center Technical Report - CTC94TR190* (1994).
- [29] C.D. Maranas, A.C. Floudas, A Global Optimization Approach for Lennard-Jones Microclusters, *Journal of Chemical Physics*, 97 7667-7678 (1992).
- [30] C.D. Maranas, A.C. Floudas, Global Minimum Potential Energy Conformations of Small Molecules, *Journal of Global Optimization*, 4 135-170 (1994).
- [31] H. Margenau, G.M. Murphy, *The Mathematics of Physics and Chemistry*, D. Van Nostrand Company Ltd. (1964).
- [32] Jordi Mestres, Gustavo E. Scuseria, Genetic Algorithms: A Robust Scheme for Geometry Optimizations and Global Minimum Structure Problems, *Journal of Computational Chemistry*, 16 729-742 (1995).
- [33] N. Metropolis, A.W. Rosenbluth, M.N. Rosenbluth, A.H. Teller, E. Teller, Equation of State Calculations by Fast Computing Machines, *Journal of Chemical Physics*, 21 1087-1092 (1952).

- [34] J.C. Meza, M.L. Martinez, Direct Search Methods for the Molecular Conformation Problem, *Journal of Computational Chemistry*, 15 627-632 (1994).
- [35] I.M. Navon, F.B. Brown, D.H. Robertson, A Combined Simulated Annealing and Quasi-Newton Like Conjugate-Gradient Method for Determining the Structure of Mixed Argon-Xenon Clusters, *Computers and Chemistry*, 14 305-311 (1990).
- [36] A. Neumaier, The Mathematics of Protein Folding: A Feasibility Study of Mathematical Prediction of Protein Structure, *Preprint* (1994).
- [37] J.A. Northby, Structure and Binding of Lennard-Jones Clusters: $13 \leq N \leq 147$, *Journal of Chemical Physics*, 87 6166-6177 (1987).
- [38] P.M. Pardalos, D. Shalloway, G. Xue, *Global Minimization of Non-convex Energy Functions: Molecular Conformation and Protein Folding*, DIMACS Series in Discrete Mathematics and Computer Science, 23, American Mathematical Society (1996).
- [39] A.T. Phillips, J.B. Rosen, A Quadratic Assignment Formulation of the Molecular Conformation Problem, *Journal of Global Optimization*, 4 229-241 (1994).
- [40] L. Piela, J. Kostrowicki, H.A. Scheraga, The Multiple-Minima Problem in the Conformational Analysis of Molecules. Deformation of the Potential Energy Hypersurface by the Diffusion Equation Method, *Journal of Physical Chemistry*, 93 3339-3346 (1989).
- [41] Donald A. Pierre, *Optimization Theory with Applications*, Dover Publications (1986).

- [42] William H. Press, Saul A. Teukolsky, William T. Vetterling, Brian P. Flannery, *Numerical Recipes in C*, Cambridge University Press (1992).
- [43] F.M. Richards, The Protein Folding Problem, *Scientific American*, January, 54-63 (1991).
- [44] A.H.G. Rinnooy Kan, G.T. Timmer, Stochastic Global Optimization Methods Part 1: Clustering Methods, *Mathematical Programming*, 39 27-56 (1987).
- [45] A.H.G. Rinnooy Kan, G.T. Timmer, Stochastic Global Optimization Methods Part II: Multi Level Methods, *Mathematical Programming*, 39 57-78 (1987).
- [46] Gunter Rudolph, Convergence Analysis of Canonical Genetic Algorithms, *IEEE Transactions on Neural Networks*, 5 96-101 (1994).
- [47] C.S. Shao, R.H. Byrd, E. Eskow, R.B. Schnabel, Global Optimization for Molecular Clusters using a New Smoothing Approach, *Preprint* (1996).
- [48] N.J.A. Sloane, R.H. Hardin, T.D.S. Duff, J.H. Conway, Minimal-Energy Clusters of Hard Spheres, *Discrete Computational Geometry*, 14 237-259 (1995).
- [49] Francisco J. Solis, Roger J-B. Wets, Minimisation by Random Search Techniques, *Mathematics of Operations Research*, 6 (1981).
- [50] H. Bradford Thompson, Calculation of Cartesian Coordinates and their Derivatives from Internal Molecular Coordinates, *Journal of Chemical Physics*, 47 3407-3410 (1967).

- [51] A. Torn, A. Zilinskas, Global Optimization, *Lecture Notes in Computer Science*, 350 Springer-Verlag (1987).
- [52] Chiachin Tsoo, Charles L. Brooks III, Cluster Structure Determination using Gaussian Density Distribution Global Minimization Methods, *Journal of Chemical Physics*, 101 6405-6411 (1994).
- [53] United States Air Force Academy, MOPAC version 6.0, Quantum Chemistry Program Exchange, Indiana University, Bloomington, Indiana (1990).
- [54] B.W. van de Waal, Calculated Ground-State Structures of 13-molecule Clusters of Carbon Dioxide, Methane, Benzene, Cyclohexane and Napthalene, *Journal of Chemical Physics*, 79 3948-3961 (1983).
- [55] B.W. van de Waal, Computed Structures of Small Benzene Clusters, *Chemical Physics Letters*, 123 69-72 (1986).
- [56] Pat Walters, Matt Stahl, Babel Version 1.06, Dolata Research Group, Department of Chemistry, University of Arizona, Tucson, AZ 85721, babel@mercury.aichem.arizona.edu (1994).
- [57] L.T. Wille, Minimum Energy Configurations of Atomic Clusters: New Results Obtained by Simulated Annealing, *Chemical Physics Letters*, 133 405-410 (1987).
- [58] Donald E. Williams, Calculated Energy and Conformation of Clusters of Benzene Molecules and their Relationship to Crystalline Benzene, *Acta. Cryst.*, 36 715-723 (1980).
- [59] Donald E. Williams, OREMWA Prediction of the Structure of Benzene Clusters: Transition from Subsidiary to Global Energy Minima, *Chemical Physics Letters*, 192 538-543 (1992).

- [60] Stephen R. Wilson, Weili Cui, Jules W. Moskowitz, Kevin E. Schmidt, Applications of Simulated Annealing to the Conformational Analysis of Flexible Molecules, *Journal of Computational Chemistry*, 12 342-349 (1991).
- [61] Zhijun Wu, The Effective Energy Transformation Scheme as a General Continuation Approach to Global Optimization with Application to Molecular Conformation, *Cornell Theory Center Technical Report - CTC93TR143* (1993).
- [62] Yongliang Xiao, Donald E. Williams, Genetic Algorithms: A New Approach to the Prediction of the Structure of Molecular Clusters, *Chemical Physics Letters*, 215 17-24 (1993).
- [63] *XMol 1.3.1, X-based molecule viewer and format converter*, Minnesota Supercomputer Center Inc. (1993).
- [64] Guoliang Xue, Improvement on the Northby Algorithm for Molecular Conformation: Better Solutions, *Journal of Global Optimization*, 4 425-440 (1994).
- [65] Guoliang Xue, Molecular Conformation on the CM-5 by Parallel Two-Level Simulated Annealing, *Journal of Global Optimization*, 4 187-208 (1994).
- [66] Zelda B. Zabinsky, Douglas L. Graesser, Mark E. Tuttle, Gun-In Kim, Global Optimization of Composite Laminates using Improving Hit and Run, *Recent Advances in Global Optimization*, Editors: Floudas and Pardalos, Princeton University Press (1992).

APPENDICES

Appendix A

Analytical Energy Gradients

A.1 Pure Atomic Clusters

To implement the BFGS local optimiser, we require V_x , V_y and V_z for each atom in the cluster. The total potential energy for the cluster is given by

$$V = \sum_{i=1}^{N-1} \sum_{j=i+1}^N v_{ij}$$

For atoms i and j we have

$$\begin{aligned} v_{ij} &= 1/r_{ij}^{12} - 2/r_{ij}^6 \\ r_{ij}^2 &= x_{ij}^2 + y_{ij}^2 + z_{ij}^2 \end{aligned}$$

For atom j

$$\begin{aligned} V_{x_j} &= V_{x_{1j}} + \dots + V_{x_{(j-1)j}} + V_{x_{(j+1)j}} + \dots + V_{x_{Nj}} \\ &= \sum_{i=1, i \neq j}^N v_{ij} x_{ij} \\ &= \sum_{i=1, i \neq j}^N v_{ij} r_{ij} r_{ij} x_{ij} \\ &= \sum_{i=1, i \neq j}^N (12x_{ij})/r_{ij}^2 (1/r_{ij}^6 - 1/r_{ij}^{12}) \end{aligned}$$

V_{y_j} and V_{z_j} may be calculated in a similar manner.

A.2 Mixed Atomic Clusters

For mixed atomic clusters, the expression derived above for V_{x_j} becomes

$$V_{x_j} = \sum_{i=1, i \neq j}^N (12x_{ij}\epsilon)/r_{ij}^2)(\sigma/r_{ij}^6 - \sigma/r_{ij}^{12})$$

where the values used for ϵ and σ are dependent on the types of atoms involved in the interaction. Similar expressions may be derived for V_{y_j} and V_{z_j} .

A.3 Benzene Clusters

To implement the BFGS local optimiser, we require E_x , E_y , E_z , E_α , E_β and E_γ for each molecule in the cluster. These gradients, for the i th molecule, are the sum of the independent gradients resulting from all pairwise atomic interactions with all other molecules in the cluster. The potential energy associated with the i th molecule is

$$E_i = \sum_{j=1, j \neq i}^N V_{ij}$$

where

$$V_{ij} = B \exp(-Cr_{ij}) - Ar_{ij}^{-6} + q_i q_j r_{ij}^{-1}$$

The expression E_x for the i th molecule is

$$\begin{aligned} E_{i_x} &= \sum_{j=1, j \neq i}^N V_{ij_x} \\ &= \sum_{j=1, j \neq i}^N V_{ij} r_{ij_x} r_{ij_x} \end{aligned}$$

Similar expressions may be derived for E_y , E_z , E_α , E_β and E_γ .

To evaluate r_{ij_x} , we consider two atoms, one in molecule W and the other in molecule W' . With a coordinate system centred at the centre of

mass of W' , with all H' and C' atoms lying in the xy -plane and the y axis bisecting two C' atoms then, relative to this coordinate system, the atomic positions (x'_i, y'_i, z'_i) for W' are those shown in Table 7.2.

If we represent the position of the centre of mass of the W molecule, relative to this coordinate system by (x_0, y_0, z_0) , and the Eulerian angles for W , relative to those of W' , as α, β, γ , then the atomic coordinates for atom i of W are

$$\begin{aligned} x_i &= x_0 + x'_i(\cos(\alpha) \cos(\gamma) - \sin(\alpha) \cos(\beta) \sin(\gamma)) + \\ &\quad y'_i(-\cos(\alpha) \sin(\gamma) - \sin(\alpha) \cos(\beta) \cos(\gamma)) \\ y_i &= y_0 + x'_i(\sin(\alpha) \cos(\gamma) + \cos(\alpha) \cos(\beta) \sin(\gamma)) + \\ &\quad y'_i(\cos(\alpha) \cos(\beta) \cos(\gamma) - \sin(\alpha) \sin(\gamma)) \\ z_i &= z_0 + x'_i \sin(\beta) \sin(\gamma) + y'_i \sin(\beta) \cos(\gamma) \end{aligned}$$

Let (x, y, z) be the differences in the Cartesian coordinates of the atom pair that we are considering. Then r , the distance between the two atoms, is given by $r^2 = x^2 + y^2 + z^2$ and

$$\begin{aligned} r_x &= x/r \\ r_y &= y/r \\ r_z &= z/r \\ r_\alpha &= (xx_\alpha + yy_\alpha + zz_\alpha)/r \\ r_\beta &= (xx_\beta + yy_\beta + zz_\beta)/r \\ r_\gamma &= (xx_\gamma + yy_\gamma + zz_\gamma)/r \end{aligned}$$

where

$$x_\alpha = x'(-\sin(\alpha) \cos(\gamma) - \cos(\alpha) \cos(\beta) \sin(\gamma)) +$$

$$\begin{aligned}
& y'(\sin(\alpha)\sin(\gamma) - \cos(\alpha)\cos(\beta)\cos(\gamma)) \\
x_\beta &= x'(-\sin(\alpha)\sin(\beta)\sin(\gamma)) + \\
& y'(\sin(\alpha)\sin(\beta)\cos(\gamma)) \\
x_\gamma &= x'(-\cos(\alpha)\sin(\gamma) - \sin(\alpha)\cos(\beta)\cos(\gamma)) + \\
& y'(-\cos(\alpha)\cos(\gamma) + \sin(\alpha)\cos(\beta)\sin(\gamma)) \\
y_\alpha &= x'(\cos(\alpha)\cos(\gamma) - \sin(\alpha)\cos(\beta)\sin(\gamma)) + \\
& y'(-\sin(\alpha)\cos(\beta)\cos(\gamma) - \cos(\alpha)\sin(\gamma)) \\
y_\beta &= x'(-\cos(\alpha)\sin(\beta)\sin(\gamma)) + \\
& y'(-\cos(\alpha)\sin(\beta)\cos(\gamma)) \\
y_\gamma &= x'(-\sin(\alpha)\sin(\gamma) + \cos(\alpha)\cos(\beta)\cos(\gamma)) + \\
& y'(-\cos(\alpha)\cos(\beta)\sin(\gamma) - \sin(\alpha)\cos(\gamma)) \\
z_\alpha &= 0 \\
z_\beta &= x'\cos(\beta)\sin(\gamma) + y'\cos(\beta)\cos(\gamma) \\
z_\gamma &= x'\sin(\beta)\cos(\gamma) - y'\sin(\beta)\sin(\gamma)
\end{aligned}$$

The first derivative of the intermolecular potential energy ($V(r)$) is

$$V_r = -CB \exp(-Cr) + 6Ar^{-7} - q_i q_j r^{-2}$$

where the values used for A , B and C depend on the types of atoms involved in the pairwise interaction. The six partial derivatives for the atom pair may now be calculated as

$$\begin{aligned}
E_x &= V_r r_x \\
E_y &= V_r r_y \\
E_z &= V_r r_z \\
E_\alpha &= V_r r_\alpha
\end{aligned}$$

$$E_\beta = V_r r_\beta$$

$$E_\gamma = V_r r_\gamma$$

A.4 Water Clusters

The position, orientation and shape of each water molecule is completely determined by (x, y, z) , the position of the oxygen atom, (α, β, γ) , the Eulerian angles and (a, b, θ) , the bond lengths and angle. To implement the BFGS local optimiser, we require E_x , E_y , E_z , E_α , E_β , E_γ , E_a , E_b and E_θ for each molecule in the cluster. Note that only the last three have a contribution from the intramolecular energy U of a molecule. These gradients, for the i th molecule, are the sum of the independent gradients resulting from all pairwise atomic interactions with all other molecules in the cluster. The potential energy associated with the i th molecule is

$$E_i = U_i + \sum_{j=1, j \neq i}^N V_{ij}$$

The expression E_x for the i th molecule is

$$\begin{aligned} E_x &= U_x + V_x \\ &= V_r r_x \end{aligned}$$

Similar expressions may be derived for E_y , E_z , E_α , E_β and E_γ . However, for E_a , E_b and E_θ , the effect of the intramolecular energy must also be included

$$\begin{aligned} E_a &= U_a + V_a \\ &= U_a + V_r r_a \end{aligned}$$

Similar expressions may be derived for E_b and E_θ . The first derivatives of the intermolecular potential energy ($V(r)$) are

$$V_r = V_{HH_r} + V_{OH_r} + V_{OO_r} + V_{HN_r} + V_{NN_r}$$

where

$$\begin{aligned} V_{HH_r} &= -\alpha_{HH} A_{HH} \exp(-\alpha_{HH} r) - Q^2/r^2 \\ V_{OH_r} &= A_{OH} \exp(-2\alpha_{OH}(r - r_m)) - 2A_{OH} \exp(-\alpha_{OH}(r - r_m)) \\ V_{OO_r} &= -\alpha_{OO} A_{OO} \exp(-\alpha_{OO} r) - \\ &\quad f_r C_6 (g_6/r^*)^6 + (6f C_6 (g_6/r^*)^6)/r^* - (6f C_6 g_6^5 g_{6_r})/(r^*)^6 - \\ &\quad f_r C_8 (g_8/r^*)^8 + (8f C_8 (g_8/r^*)^8)/r^* - (8f C_8 g_8^7 g_{8_r})/(r^*)^8 - \\ &\quad 1.5(f_r C_{10} (g_{10}/r^*)^{10} + (10f C_{10} (g_{10}/r^*)^{10})/r^* - (10f C_{10} g_{10}^9 g_{10_r})/(r^*)^{10}) \\ V_{HN_r} &= 2Q^2/r^2 \\ V_{NN_r} &= -4Q^2/r^2 \\ f_r &= -2.326 \times 3.8845 r^{1.326} \exp(-1.7921 r) + 3.8845 \times 1.7921 r^{2.326} \exp(-1.7921 r) \\ g_{2n_r} &= (1.8817/n + 2.0.2475r/\sqrt{n}) \exp(-1.8817r/n - 0.2475r^2/\sqrt{n}) \end{aligned}$$

First derivatives of the intramolecular potential energy ($U(a, b, \theta)$) are

$$\begin{aligned} U_a &= M_{1,s_1} s_{1a} + M_{2,s_2} s_{2a} + M_{3,s_3} s_{3a} + f_{12} s_2 s_{1a} + f_{12} s_1 s_{2a} \\ U_b &= M_{1,s_1} s_{1b} + M_{2,s_2} s_{2b} + M_{3,s_3} s_{3b} + f_{12} s_2 s_{1b} + f_{12} s_1 s_{2b} \\ U_\theta &= M_{1,s_1} s_{1\theta} + M_{2,s_2} s_{2\theta} + M_{3,s_3} s_{3\theta} + f_{12} s_2 s_{1\theta} + f_{12} s_1 s_{2\theta} \end{aligned}$$

where

$$M_{1,s_1} = 2\alpha_1 D_1 \exp(-\alpha_1 s_1)(1 - \exp(-\alpha_1 s_1))$$

$$\begin{aligned}
M_{2s_2} &= 2\alpha_2 D_2 \exp(-\alpha_2 s_2)(1 - \exp(-\alpha_2 s_2)) \\
M_{3s_3} &= 2\alpha_3 D_3 \exp(-\alpha_3 s_3)(1 - \exp(-\alpha_3 s_3)) \\
s_{1a} &= \cos((\theta - \theta_0)/2) \\
s_{2a} &= 0 \\
s_{3a} &= \sin((\theta - \theta_0)/2)/r_0 \\
s_{1b} &= 0 \\
s_{2b} &= \cos((\theta - \theta_0)/2) \\
s_{3b} &= \sin((\theta - \theta_0)/2)/r_0 \\
s_{1\theta} &= -(a/2) \sin((\theta - \theta_0)/2) \\
s_{2\theta} &= -(a/2) \sin((\theta - \theta_0)/2) \\
s_{3\theta} &= (a + b) \cos((\theta - \theta_0)/2)/r_0
\end{aligned}$$

The partial derivatives r_x , r_y , r_z , r_α , r_β , r_γ , r_a , r_b and r_θ are calculated as follows:

Let (x, y, z) be the differences in the Cartesian coordinates of the atom pair that we are considering. Then r , the distance between the two atoms is given by $r^2 = x^2 + y^2 + z^2$ and

$$\begin{aligned}
r_x &= x/r \\
r_y &= y/r \\
r_z &= z/r \\
r_\alpha &= (xx_\alpha + yy_\alpha + zz_\alpha)/r \\
r_\beta &= (xx_\beta + yy_\beta + zz_\beta)/r \\
r_\gamma &= (xx_\gamma + yy_\gamma + zz_\gamma)/r \\
r_a &= (xx_a + yy_a + zz_a)/r
\end{aligned}$$

$$r_b = (xx_b + yy_b + zz_b)/r$$

$$r_\theta = (xx_\theta + yy_\theta + zz_\theta)/r$$

The expressions required to complete the evaluation of these gradients may be evaluated as follows:

Given two molecules, W' and W , with the O' atom of W' at $(0, 0, 0)$, H'_1 and H'_2 in the xy -plane with the y axis bisecting the $H'_1O'H'_2$ angle. If the bond lengths of W' are a' and b' respectively, and the bond angle θ' , then the atomic coordinates for W' are

$$\begin{aligned}x'_O &= 0 \\y'_O &= 0 \\z'_O &= 0 \\x'_{H_1} &= -a' \sin(\theta'/2) \\y'_{H_1} &= b' \cos(\theta'/2) \\z'_{H_1} &= 0 \\x'_{H_2} &= a' \sin(\theta'/2) \\y'_{H_2} &= b' \cos(\theta'/2) \\z'_{H_2} &= 0 \\x'_N &= K(b' - a') \sin(\theta'/2) \\y'_N &= K((a' + b')/2) \cos(\theta'/2) \\z'_N &= 0\end{aligned}$$

where $K = d/2r_0 \cos(\theta_0/2)$.

If we represent the position of the O atom of the W molecule, relative to the coordinate axis defined by W' , as (x_0, y_0, z_0) , the Eulerian angles for

W , relative to those of W' , as α, β, γ , the bond lengths as a, b and the bond angle as θ then the atomic coordinates for W are

$$x_O = x_0$$

$$y_O = y_0$$

$$z_O = z_0$$

$$\begin{aligned} x_{H_1} &= x_0 - a \sin(\theta/2)(\cos(\alpha) \cos(\gamma) - \sin(\alpha) \cos(\beta) \sin(\gamma)) + \\ &\quad a \cos(\theta/2)(-\cos(\alpha) \sin(\gamma) - \sin(\alpha) \cos(\beta) \cos(\gamma)) \end{aligned}$$

$$\begin{aligned} y_{H_1} &= y_0 - a \sin(\theta/2)(\sin(\alpha) \cos(\gamma) + \cos(\alpha) \cos(\beta) \sin(\gamma)) + \\ &\quad a \cos(\theta/2)(\cos(\alpha) \cos(\beta) \cos(\gamma) - \sin(\alpha) \sin(\gamma)) \end{aligned}$$

$$z_{H_1} = z_0 - a \sin(\theta/2) \sin(\beta) \sin(\gamma) + a \cos(\theta/2) \sin(\beta) \cos(\gamma)$$

$$\begin{aligned} x_{H_2} &= x_0 + b \sin(\theta/2)(\cos(\alpha) \cos(\gamma) - \sin(\alpha) \cos(\beta) \sin(\gamma)) + \\ &\quad b \cos(\theta/2)(-\cos(\alpha) \sin(\gamma) - \sin(\alpha) \cos(\beta) \cos(\gamma)) \end{aligned}$$

$$\begin{aligned} y_{H_2} &= y_0 + b \sin(\theta/2)(\sin(\alpha) \cos(\gamma) + \cos(\alpha) \cos(\beta) \sin(\gamma)) + \\ &\quad b \cos(\theta/2)(\cos(\alpha) \cos(\beta) \cos(\gamma) - \sin(\alpha) \sin(\gamma)) \end{aligned}$$

$$z_{H_2} = z_0 + b \sin(\theta/2) \sin(\beta) \sin(\gamma) + b \cos(\theta/2) \sin(\beta) \cos(\gamma)$$

$$\begin{aligned} x_N &= x_0 + K(b - a) \sin(\theta/2)(\cos(\alpha) \cos(\gamma) - \sin(\alpha) \cos(\beta) \sin(\gamma)) + \\ &\quad K((a + b)/2) \cos(\theta/2)(-\cos(\alpha) \sin(\gamma) - \sin(\alpha) \cos(\beta) \cos(\gamma)) \end{aligned}$$

$$\begin{aligned} y_N &= y_0 + K(b - a) \sin(\theta/2)(\sin(\alpha) \cos(\gamma) + \cos(\alpha) \cos(\beta) \sin(\gamma)) + \\ &\quad K((a + b)/2) \cos(\theta/2)(\cos(\alpha) \cos(\beta) \cos(\gamma) - \sin(\alpha) \sin(\gamma)) \end{aligned}$$

$$z_N = z_0 + K(b - a) \sin(\theta/2) \sin(\beta) \sin(\gamma) + K((a + b)/2) \cos(\theta/2) \sin(\beta) \cos(\gamma)$$

The differences (x, y, z) and their first derivatives clearly depend on which atoms are involved in the pairwise interaction. For the first hydrogen atom,

the required derivatives are:

$$x_\alpha = -a \sin(\theta/2)(-\sin(\alpha) \cos(\gamma) - \cos(\alpha) \cos(\beta) \sin(\gamma)) +$$

$$a \cos(\theta/2)(\sin(\alpha) \sin(\gamma) - \cos(\alpha) \cos(\beta) \cos(\gamma))$$

$$x_\beta = -a \sin(\theta/2) \sin(\alpha) \sin(\beta) \sin(\gamma) +$$

$$a \cos(\theta/2) \sin(\alpha) \sin(\beta) \cos(\gamma)$$

$$x_\gamma = -a \sin(\theta/2)(-\cos(\alpha) \sin(\gamma) - \sin(\alpha) \cos(\beta) \cos(\gamma)) +$$

$$a \cos(\theta/2)(-\cos(\alpha) \cos(\gamma) + \sin(\alpha) \cos(\beta) \sin(\gamma))$$

$$x_a = -\sin(\theta/2)(\cos(\alpha) \cos(\gamma) - \sin(\alpha) \cos(\beta) \sin(\gamma)) +$$

$$\cos(\theta/2)(-\cos(\alpha) \sin(\gamma) - \sin(\alpha) \cos(\beta) \cos(\gamma))$$

$$x_b = 0$$

$$x_\theta = -(a/2) \cos(\theta/2)(\cos(\alpha) \cos(\gamma) - \sin(\alpha) \cos(\beta) \sin(\gamma)) -$$

$$(a/2) \sin(\theta/2)(-\cos(\alpha) \sin(\gamma) - \sin(\alpha) \cos(\beta) \cos(\gamma))$$

$$y_\alpha = -a \sin(\theta/2)(\cos(\alpha) \cos(\gamma) - \sin(\alpha) \cos(\beta) \sin(\gamma)) +$$

$$a \cos(\theta/2)(-\sin(\alpha) \cos(\beta) \cos(\gamma) - \cos(\alpha) \sin(\gamma))$$

$$y_\beta = -a \sin(\theta/2)(-\cos(\alpha) \sin(\beta) \sin(\gamma)) +$$

$$a \cos(\theta/2)(-\cos(\alpha) \sin(\beta) \cos(\gamma))$$

$$y_\gamma = -a \sin(\theta/2)(-\sin(\alpha) \sin(\gamma) + \cos(\alpha) \cos(\beta) \cos(\gamma)) +$$

$$a \cos(\theta/2)(-\cos(\alpha) \cos(\gamma) + \sin(\alpha) \cos(\beta) \sin(\gamma))$$

$$y_a = -\sin(\theta/2)(\sin(\alpha) \cos(\gamma)) + \cos(\alpha) \cos(\beta) \sin(\gamma) +$$

$$\cos(\theta/2)(\cos(\alpha) \cos(\beta) \cos(\gamma) - \sin(\alpha) \sin(\gamma))$$

$$y_b = 0$$

$$y_\theta = -(a/2) \cos(\theta/2)(\sin(\alpha) \cos(\gamma) + \cos(\alpha) \cos(\beta) \sin(\gamma)) -$$

$$(a/2) \sin(\theta/2)(\cos(\alpha) \cos(\beta) \cos(\gamma) - \sin(\alpha) \sin(\gamma))$$

$$z_\alpha = 0$$

$$\begin{aligned}
z_\beta &= -a \sin(\theta/2) \cos(\beta) \sin(\gamma) + a \cos(\theta/2) \cos(\beta) \cos(\gamma) \\
z_\gamma &= -a \sin(\theta/2) \sin(\beta) \cos(\gamma) - a \cos(\theta/2) \sin(\beta) \sin(\gamma) \\
z_a &= -\sin(\theta/2) \sin(\beta) \sin(\gamma) + \cos(\theta/2) \sin(\beta) \cos(\gamma) \\
z_b &= 0 \\
z_\theta &= -(a/2) \cos(\theta/2) \sin(\beta) \sin(\gamma) - (a/2) \sin(\theta/2) \sin(\beta) \cos(\gamma)
\end{aligned}$$

For the second hydrogen atom, the required derivatives are:

$$\begin{aligned}
x_\alpha &= b \sin(\theta/2) (-\sin(\alpha) \cos(\gamma) - \cos(\alpha) \cos(\beta) \sin(\gamma)) + \\
&\quad b \cos(\theta/2) (\sin(\alpha) \sin(\gamma) - \cos(\alpha) \cos(\beta) \cos(\gamma)) \\
x_\beta &= b \sin(\theta/2) \sin(\alpha) \sin(\beta) \sin(\gamma) + \\
&\quad b \cos(\theta/2) \sin(\alpha) \sin(\beta) \cos(\gamma) \\
x_\gamma &= b \sin(\theta/2) (-\cos(\alpha) \sin(\gamma) - \sin(\alpha) \cos(\beta) \cos(\gamma)) + \\
&\quad b \cos(\theta/2) (-\cos(\alpha) \cos(\gamma) + \sin(\alpha) \cos(\beta) \sin(\gamma)) \\
x_a &= 0 \\
x_b &= \sin(\theta/2) (\cos(\alpha) \cos(\gamma) - \sin(\alpha) \cos(\beta) \sin(\gamma)) + \\
&\quad \cos(\theta/2) (-\cos(\alpha) \sin(\gamma) - \sin(\alpha) \cos(\beta) \cos(\gamma)) \\
x_\theta &= (b/2) \cos(\theta/2) (\cos(\alpha) \cos(\gamma) - \sin(\alpha) \cos(\beta) \sin(\gamma)) - \\
&\quad (b/2) \sin(\theta/2) (-\cos(\alpha) \sin(\gamma) - \sin(\alpha) \cos(\beta) \cos(\gamma)) \\
y_\alpha &= b \sin(\theta/2) (\cos(\alpha) \cos(\gamma) - \sin(\alpha) \cos(\beta) \sin(\gamma)) + \\
&\quad b \cos(\theta/2) (-\sin(\alpha) \cos(\beta) \cos(\gamma) - \cos(\alpha) \sin(\gamma)) \\
y_\beta &= b \sin(\theta/2) (-\cos(\alpha) \sin(\beta) \sin(\gamma)) + \\
&\quad b \cos(\theta/2) (-\cos(\alpha) \sin(\beta) \cos(\gamma)) \\
y_\gamma &= b \sin(\theta/2) (-\sin(\alpha) \sin(\gamma)) + \cos(\alpha) \cos(\beta) \cos(\gamma) + \\
&\quad b \cos(\theta/2) (-\cos(\alpha) \cos(\beta) \sin(\gamma) - \sin(\alpha) \cos(\gamma))
\end{aligned}$$

$$y_a = 0$$

$$\begin{aligned} y_b &= \sin(\theta/2)(\sin(\alpha) \cos(\gamma)) + \cos(\alpha) \cos(\beta) \sin(\gamma) + \\ &\quad \cos(\theta/2)(\cos(\alpha) \cos(\beta) \cos(\gamma) - \sin(\alpha) \sin(\gamma)) \end{aligned}$$

$$\begin{aligned} y_\theta &= (b/2) \cos(\theta/2)(\sin(\alpha) \cos(\gamma) + \cos(\alpha) \cos(\beta) \sin(\gamma)) - \\ &\quad (b/2) \sin(\theta/2)(\cos(\alpha) \cos(\beta) \cos(\gamma) - \sin(\alpha) \sin(\gamma)) \end{aligned}$$

$$z_\alpha = 0$$

$$z_\beta = b \sin(\theta/2) \cos(\beta) \sin(\gamma) + b \cos(\theta/2) \cos(\beta) \cos(\gamma)$$

$$z_\gamma = b \sin(\theta/2) \sin(\beta) \cos(\gamma) - b \cos(\theta/2) \sin(\beta) \sin(\gamma)$$

$$z_a = 0$$

$$z_b = \sin(\theta/2) \sin(\beta) \sin(\gamma) + \cos(\theta/2) \sin(\beta) \cos(\gamma)$$

$$z_\theta = (b/2) \cos(\theta/2) \sin(\beta) \sin(\gamma) - (b/2) \sin(\theta/2) \sin(\beta) \cos(\gamma)$$

For the oxygen atom all corresponding derivatives are equal to zero, while for the coulombic charge, the required derivatives are:

$$\begin{aligned} x_\alpha &= K(b-a) \sin(\theta/2)(-\sin(\alpha) \cos(\gamma) - \cos(\alpha) \cos(\beta) \sin(\gamma)) + \\ &\quad K((a+b)/2) \cos(\theta/2)(\sin(\alpha) \sin(\gamma) - \cos(\alpha) \cos(\beta) \cos(\gamma)) \end{aligned}$$

$$x_\beta = K(b-a) \sin(\theta/2)(\sin(\alpha) \sin(\beta) \sin(\gamma)) +$$

$$K((a+b)/2) \cos(\theta/2)(\sin(\alpha) \sin(\beta) \cos(\gamma))$$

$$\begin{aligned} x_\gamma &= K(b-a) \sin(\theta/2)(-\cos(\alpha) \sin(\gamma) - \sin(\alpha) \cos(\beta) \cos(\gamma)) + \\ &\quad K((a+b)/2) \cos(\theta/2)(-\cos(\alpha) \cos(\gamma) + \sin(\alpha) \cos(\beta) \sin(\gamma)) \end{aligned}$$

$$\begin{aligned} x_a &= -K \sin(\theta/2)(\cos(\alpha) \cos(\gamma) - \sin(\alpha) \cos(\beta) \sin(\gamma)) + \\ &\quad (K/2) \cos(\theta/2)(-\cos(\alpha) \sin(\gamma) - \sin(\alpha) \cos(\beta) \cos(\gamma)) \end{aligned}$$

$$\begin{aligned} x_b &= Kb \sin(\theta/2)(\cos(\alpha) \cos(\gamma) - \sin(\alpha) \cos(\beta) \sin(\gamma)) + \\ &\quad (K/2) \cos(\theta/2)(-\cos(\alpha) \sin(\gamma) - \sin(\alpha) \cos(\beta) \cos(\gamma)) \end{aligned}$$

$$\begin{aligned}
x_\theta &= K((b-a)/2) \cos(\theta/2)(\cos(\alpha)\cos(\gamma) - \sin(\alpha)\cos(\beta)\sin(\gamma)) - \\
&\quad K((a+b)/4) \sin(\theta/2)(-\cos(\alpha)\sin(\gamma) - \sin(\alpha)\cos(\beta)\cos(\gamma)) \\
y_\alpha &= K(b-a) \sin(\theta/2)(\sin(\alpha)\cos(\gamma) + \cos(\alpha)\cos(\beta)\sin(\gamma)) + \\
&\quad K((a+b)/2) \cos(\theta/2)(-\sin(\alpha)\cos(\beta)\cos(\gamma) - \cos(\alpha)\sin(\gamma)) \\
y_\beta &= K(b-a) \sin(\theta/2)(-\cos(\alpha)\sin(\beta)\sin(\gamma)) + \\
&\quad K((a+b)/2) \cos(\theta/2)(-\cos(\alpha)\sin(\beta)\cos(\gamma) - \sin(\alpha)\sin(\gamma)) \\
y_\gamma &= K(b-a) \sin(\theta/2)(-\sin(\alpha)\sin(\gamma) + \cos(\alpha)\cos(\beta)\cos(\gamma)) + \\
&\quad K((a+b)/2) \cos(\theta/2)(-\cos(\alpha)\cos(\beta)\sin(\gamma) - \sin(\alpha)\cos(\gamma)) \\
y_a &= -K \sin(\theta/2)(\sin(\alpha)\cos(\gamma) + \cos(\alpha)\cos(\beta)\sin(\gamma)) + \\
&\quad (K/2) \cos(\theta/2)(\cos(\alpha)\cos(\beta)\cos(\gamma) - \sin(\alpha)\sin(\gamma)) \\
y_b &= K \sin(\theta/2)(\sin(\alpha)\cos(\gamma) + \cos(\alpha)\cos(\beta)\sin(\gamma)) + \\
&\quad (K/2) \cos(\theta/2)(\cos(\alpha)\cos(\beta)\cos(\gamma) - \sin(\alpha)\sin(\gamma)) \\
y_\theta &= (K(b-a)/2) \cos(\theta/2)(\sin(\alpha)\cos(\gamma) + \cos(\alpha)\cos(\beta)\sin(\gamma)) - \\
&\quad K((a+b)/4) \sin(\theta/2)(\cos(\alpha)\cos(\beta)\cos(\gamma) - \sin(\alpha)\sin(\gamma)) \\
z_\alpha &= 0 \\
z_\beta &= K(b-a) \sin(\theta/2) \cos(\beta)\sin(\gamma) + K((a+b)/2) \cos(\theta/2) \cos(\beta)\cos(\gamma) \\
z_\gamma &= K(b-a) \sin(\theta/2) \sin(\beta)\cos(\gamma) - K((a+b)/2) \cos(\theta/2) \sin(\beta)\sin(\gamma) \\
z_a &= -K \sin(\theta/2) \sin(\beta)\sin(\gamma) + (K/2) \cos(\theta/2) \sin(\beta)\cos(\gamma) \\
z_b &= K \sin(\theta/2) \sin(\beta)\sin(\gamma) + (K/2) \cos(\theta/2) \sin(\beta)\cos(\gamma) \\
z_\theta &= (K(b-a)/2) \cos(\theta/2) \sin(\beta)\sin(\gamma) - K((a+b)/4) \sin(\theta/2) \sin(\beta)\cos(\gamma)
\end{aligned}$$

A.5 Model Molecular Structure

To implement the BFGS local optimiser (for an N atom model) we require $V_{\alpha_1}, \dots, V_{\alpha_{N-2}}$, where α_i is as defined in Figure 8.4. The total potential

energy of the system is given by

$$V = \sum_{i < j}^N (1/r_{ij}^{12} - 2/r_{ij}^6)$$

where

$$r_{ij}^2 = x_{ij}^2 + y_{ij}^2$$

Let

$$\Psi_k = \sum_{i=1}^k \alpha_i$$

and $(x_0, y_0) = (0, 0)$ and $\Psi_0 = 0$. Then

$$\begin{aligned} x_i &= \sum_{k=0}^{i-1} \cos(\Psi_k) \\ y_i &= \sum_{k=0}^{i-1} \sin(\Psi_k) \end{aligned}$$

Now

$$V_{\alpha_m} = -12 \sum_{i < j} (1/r_{ij}^{13} - 1/r_{ij}^7) r_{ij\alpha_m}$$

and

$$(r_{ij})_{\alpha_m} = ((x_i - x_j)(x_i - x_j)_{\alpha_m} + (y_i - y_j)(y_i - y_j)_{\alpha_m})/r_{ij}$$

Assuming that $j > i$ we have

$$\begin{aligned} (x_i - x_j)_{\alpha_m} &= - \sum_{k=i}^{j-1} (\cos(\Psi_k))_{\alpha_m} = \sum_{k=\max(i,m)}^{j-1} \sin(\Psi_k) \\ (y_i - y_j)_{\alpha_m} &= - \sum_{k=i}^{j-1} (\sin(\Psi_k))_{\alpha_m} = - \sum_{k=\max(i,m)}^{j-1} \cos(\Psi_k) \end{aligned}$$

Therefore

$$(r_{ij})_{\alpha_m} = ((x_i - x_j) \left(\sum_{k=\max(i,m)}^{j-1} \sin(\Psi_k) \right) + (y_i - y_j) \left(- \sum_{k=\max(i,m)}^{j-1} \cos(\Psi_k) \right)) / r_{ij}$$

which is zero when $m \leq i$. Assuming that $m > i$, we have

$$- \sum_{k=m}^{j-1} \cos(\Psi_k) = x_m - x_j$$

$$\sum_{k=m}^{j-1} \sin(\Psi_k) = -(y_m - y_j)$$

and

$$(r_{ij})_{\alpha_m} = (x_i - x_j)(y_j - y_m) + (y_i - y_j)(x_m - x_j)$$

Combining terms we have

$$V_{\alpha_m} = -12 \sum_{i=0}^{m-1} \sum_{j=m+1}^n (1/r_{ij}^{14} - 1/r_{ij}^8)((x_i - x_j)(y_j - y_m) + (y_i - y_j)(x_m - x_j))$$

Appendix B

Argon-Xenon Clusters

The following tables contain

- the optimised energies for all $Ar_{N-n}Xe_n | 2 \leq N \leq 20$ atomic clusters.
- the substitution energy, ΔE , as Xe atoms are substituted for Ar atoms in each cluster. ΔE is tabulated as an absolute value.
- the counts of $Ar - Ar$, $Ar - Xe$ and $Xe - Xe$ atom pairings where the distance between the atoms is within 0.2\AA of r_{min} for the respective atom types.

| <u><i>n</i></u> | <u>E</u> | <u>ΔE</u> | <u>N_{AA}</u> | <u>N_{AX}</u> | <u>N_{XX}</u> |
|---|----------|------------------------------|----------------------------|----------------------------|----------------------------|
| <i>Ar</i> _{2-<i>n</i>} <i>Xe</i> _{<i>n</i>} | | | | | |
| 0 | -1.0000 | | 1 | 0 | 0 |
| 1 | -1.4800 | 0.4800 | 0 | 1 | 0 |
| 2 | -1.8525 | 0.3725 | 0 | 0 | 1 |
| <i>Ar</i> _{3-<i>n</i>} <i>Xe</i> _{<i>n</i>} | | | | | |
| 0 | -3.0000 | | 3 | 0 | 0 |
| 1 | -3.9600 | 0.9600 | 1 | 2 | 0 |
| 2 | -4.8125 | 0.8525 | 0 | 2 | 1 |
| 3 | -5.5575 | 0.7450 | 0 | 0 | 3 |
| <i>Ar</i> _{4-<i>n</i>} <i>Xe</i> _{<i>n</i>} | | | | | |
| 0 | -6.0000 | | 6 | 0 | 0 |
| 1 | -7.4400 | 1.4400 | 3 | 3 | 0 |
| 2 | -8.7725 | 1.3325 | 1 | 4 | 1 |
| 3 | -9.9975 | 1.2250 | 0 | 3 | 3 |
| 4 | -11.1150 | 1.1175 | 0 | 0 | 6 |
| <i>Ar</i> _{5-<i>n</i>} <i>Xe</i> _{<i>n</i>} | | | | | |
| 0 | -9.1039 | | 9 | 0 | 0 |
| 1 | -11.0176 | 1.9137 | 5 | 4 | 0 |
| 2 | -12.8290 | 1.8114 | 2 | 6 | 1 |
| 3 | -14.5408 | 1.7118 | 0 | 6 | 3 |
| 4 | -15.6858 | 1.1450 | 0 | 3 | 6 |
| 5 | -16.8649 | 1.1791 | 0 | 0 | 9 |
| <i>Ar</i> _{6-<i>n</i>} <i>Xe</i> _{<i>n</i>} | | | | | |
| 0 | -12.7121 | | 12 | 0 | 0 |
| 1 | -14.7512 | 2.0391 | 8 | 4 | 0 |
| 2 | -16.9602 | 2.2090 | 3 | 8 | 1 |
| 3 | -18.7090 | 1.7488 | 1 | 8 | 3 |
| 4 | -20.5018 | 1.7928 | 0 | 8 | 4 |
| 5 | -21.9889 | 1.4871 | 0 | 4 | 8 |
| 6 | -23.5491 | 1.5602 | 0 | 0 | 12 |

| <i>n</i> | E | ΔE | N_{AA} | N_{AX} | N_{XX} |
|----------------|----------|------------|----------|----------|----------|
| $Ar_{7-n}Xe_n$ | | | | | |
| 0 | -16.5054 | | 15 | 0 | 0 |
| 1 | -19.2622 | 2.7568 | 10 | 6 | 0 |
| 2 | -22.0179 | 2.7557 | 5 | 9 | 1 |
| 3 | -23.7468 | 1.7289 | 3 | 10 | 2 |
| 4 | -25.5027 | 1.7559 | 1 | 10 | 4 |
| 5 | -27.2248 | 1.7221 | 0 | 8 | 7 |
| 6 | -28.8997 | 1.6749 | 0 | 4 | 12 |
| 7 | -30.5762 | 1.6765 | 0 | 0 | 15 |
| $Ar_{8-n}Xe_n$ | | | | | |
| 0 | -19.8215 | | 19 | 0 | 0 |
| 1 | -23.0058 | 3.1843 | 12 | 7 | 0 |
| 2 | -25.8141 | 2.8083 | 7 | 11 | 1 |
| 3 | -28.0031 | 2.1890 | 4 | 12 | 2 |
| 4 | -30.1491 | 2.1460 | 2 | 11 | 5 |
| 5 | -31.9569 | 1.8078 | 0 | 11 | 7 |
| 6 | -33.6846 | 1.7277 | 0 | 7 | 12 |
| 7 | -35.3818 | 1.6972 | 0 | 3 | 16 |
| 8 | -36.7193 | 1.3375 | 0 | 0 | 19 |
| $Ar_{9-n}Xe_n$ | | | | | |
| 0 | -24.1134 | | 23 | 0 | 0 |
| 1 | -27.5466 | 3.4332 | 15 | 8 | 0 |
| 2 | -30.3876 | 2.8410 | 10 | 12 | 1 |
| 3 | -32.9050 | 2.5174 | 6 | 14 | 3 |
| 4 | -35.1329 | 2.2279 | 4 | 13 | 6 |
| 5 | -37.3987 | 2.2658 | 2 | 12 | 9 |
| 6 | -39.1971 | 1.7984 | 1 | 10 | 12 |
| 7 | -41.0267 | 1.8296 | 0 | 8 | 15 |
| 8 | -42.8423 | 1.8156 | 0 | 4 | 19 |
| 9 | -44.6700 | 1.8277 | 0 | 0 | 23 |

| <i>n</i> | E | ΔE | N_{AA} | N_{AX} | N_{XX} |
|-----------------|----------|------------|----------|----------|----------|
| $Ar_{10-n}Xe_n$ | | | | | |
| 0 | -28.4225 | | 27 | 0 | 0 |
| 1 | -31.8734 | 3.4509 | 12 | 9 | 0 |
| 2 | -34.7706 | 2.8972 | 7 | 13 | 1 |
| 3 | -37.4314 | 2.6608 | 5 | 15 | 3 |
| 4 | -40.2013 | 2.7699 | 4 | 16 | 6 |
| 5 | -42.2426 | 2.0413 | 2 | 15 | 9 |
| 6 | -44.5857 | 2.3431 | 3 | 15 | 9 |
| 7 | -46.8097 | 2.2240 | 2 | 8 | 11 |
| 8 | -49.8288 | 3.0191 | 1 | 12 | 12 |
| 9 | -51.9091 | 2.0803 | 0 | 9 | 18 |
| 10 | -52.6528 | 0.7437 | 0 | 0 | 27 |
| $Ar_{11-n}Xe_n$ | | | | | |
| 0 | -32.7660 | | 31 | 0 | 0 |
| 1 | -36.1896 | 3.4236 | 19 | 10 | 0 |
| 2 | -39.1815 | 2.9919 | 14 | 14 | 1 |
| 3 | -42.1373 | 2.9558 | 10 | 17 | 3 |
| 4 | -45.1324 | 2.9951 | 4 | 18 | 6 |
| 5 | -47.6269 | 2.4945 | 0 | 18 | 9 |
| 6 | -50.5539 | 2.9270 | 6 | 18 | 8 |
| 7 | -53.3974 | 2.8435 | 4 | 16 | 10 |
| 8 | -56.9554 | 3.5580 | 0 | 16 | 8 |
| 9 | -58.6126 | 1.6572 | 0 | 12 | 16 |
| 10 | -60.2662 | 1.6536 | 0 | 9 | 20 |
| 11 | -60.6990 | 0.4328 | 0 | 0 | 31 |
| $Ar_{12-n}Xe_n$ | | | | | |
| 0 | -37.9676 | | 36 | 0 | 0 |
| 1 | -41.2283 | 3.2607 | 30 | 6 | 0 |
| 2 | -44.5236 | 3.2953 | 24 | 12 | 0 |
| 3 | -47.6411 | 3.1175 | 19 | 16 | 1 |
| 4 | -50.4576 | 2.8165 | 15 | 19 | 2 |
| 5 | -53.4130 | 2.9554 | 11 | 22 | 3 |
| 6 | -56.3567 | 2.9437 | 8 | 18 | 7 |
| 7 | -59.3386 | 2.9819 | 5 | 20 | 10 |
| 8 | -62.1998 | 2.8612 | 3 | 18 | 12 |
| 9 | -64.4855 | 2.2857 | 1 | 16 | 17 |
| 10 | -66.1764 | 1.6909 | 0 | 13 | 21 |
| 11 | -67.8740 | 1.6976 | 0 | 9 | 25 |
| 12 | -70.3350 | 2.4610 | 0 | 0 | 36 |

| <i>n</i> | E | ΔE | N_{AA} | N_{AX} | N_{XX} |
|-----------------|----------|------------|----------|----------|----------|
| $Ar_{13-n}Xe_n$ | | | | | |
| 0 | -44.3268 | | 39 | 0 | 0 |
| 1 | -47.6968 | 3.3700 | 36 | 6 | 0 |
| 2 | -51.1213 | 3.4245 | 19 | 16 | 1 |
| 3 | -54.5957 | 3.4744 | 24 | 18 | 0 |
| 4 | -57.8543 | 3.2586 | 19 | 22 | 1 |
| 5 | -60.7363 | 2.8820 | 17 | 20 | 5 |
| 6 | -63.7979 | 3.0616 | 12 | 24 | 6 |
| 7 | -66.5918 | 2.7939 | 10 | 22 | 10 |
| 8 | -69.0209 | 2.4291 | 3 | 23 | 13 |
| 9 | -71.6010 | 2.5801 | 5 | 20 | 17 |
| 10 | -74.0185 | 2.4175 | 2 | 20 | 20 |
| 11 | -76.2746 | 2.2561 | 1 | 11 | 25 |
| 12 | -78.7008 | 2.4262 | 0 | 1 | 36 |
| 13 | -82.1154 | 3.4146 | 0 | 0 | 39 |
| $Ar_{14-n}Xe_n$ | | | | | |
| 0 | -47.8452 | | 45 | 0 | 0 |
| 1 | -51.6528 | 3.8076 | 38 | 7 | 0 |
| 2 | -55.2653 | 3.6125 | 32 | 12 | 1 |
| 3 | -58.8911 | 3.6258 | 27 | 15 | 3 |
| 4 | -62.3267 | 3.4356 | 21 | 21 | 3 |
| 5 | -65.5107 | 3.1840 | 16 | 25 | 4 |
| 6 | -68.6972 | 3.1865 | 12 | 27 | 6 |
| 7 | -71.5258 | 2.8286 | 10 | 25 | 10 |
| 8 | -73.9865 | 2.4607 | 7 | 25 | 13 |
| 9 | -76.5749 | 2.5884 | 5 | 23 | 17 |
| 10 | -79.0019 | 2.4270 | 3 | 19 | 21 |
| 11 | -81.2590 | 2.2571 | 1 | 14 | 25 |
| 12 | -83.7123 | 2.4533 | 0 | 7 | 36 |
| 13 | -87.1603 | 3.4480 | 0 | 3 | 42 |
| 14 | -88.6800 | 1.5197 | 0 | 0 | 45 |

| <i>n</i> | E | ΔE | N_{AA} | N_{AX} | N_{XX} |
|-----------------|-----------|------------|----------|----------|----------|
| $Ar_{15-n}Xe_n$ | | | | | |
| 0 | -52.3227 | | 49 | 0 | 0 |
| 1 | -56.3670 | 4.0443 | 30 | 14 | 0 |
| 2 | -60.1992 | 3.8322 | 33 | 14 | 1 |
| 3 | -63.9532 | 3.7540 | 28 | 17 | 3 |
| 4 | -67.6800 | 3.7268 | 24 | 20 | 4 |
| 5 | -71.1313 | 3.4513 | 17 | 26 | 4 |
| 6 | -74.3084 | 3.1771 | 11 | 30 | 5 |
| 7 | -77.1841 | 2.8757 | 11 | 28 | 10 |
| 8 | -79.6808 | 2.4967 | 0 | 32 | 12 |
| 9 | -82.2536 | 2.5728 | 5 | 26 | 17 |
| 10 | -84.7267 | 2.4731 | 4 | 23 | 21 |
| 11 | -86.9356 | 2.2089 | 1 | 17 | 25 |
| 12 | -89.5321 | 2.5965 | 1 | 10 | 35 |
| 13 | -92.9570 | 3.4249 | 1 | 6 | 41 |
| 14 | -94.9799 | 2.0229 | 0 | 4 | 44 |
| 15 | -97.0191 | 2.0392 | 0 | 0 | 48 |
| $Ar_{16-n}Xe_n$ | | | | | |
| 0 | -56.8158 | | 53 | 0 | 0 |
| 1 | -61.8505 | 5.0347 | 33 | 14 | 0 |
| 2 | -65.1729 | 3.3224 | 29 | 18 | 0 |
| 3 | -68.8390 | 3.6661 | 27 | 19 | 3 |
| 4 | -72.5794 | 3.7404 | 25 | 22 | 3 |
| 5 | -76.1583 | 3.5789 | 19 | 28 | 3 |
| 6 | -79.6076 | 3.4493 | 13 | 31 | 7 |
| 7 | -82.6623 | 3.0547 | 10 | 31 | 10 |
| 8 | -85.1669 | 2.3458 | 8 | 29 | 14 |
| 9 | -87.7763 | 2.7682 | 4 | 30 | 16 |
| 10 | -90.2711 | 2.4948 | 2 | 26 | 19 |
| 11 | -92.8687 | 2.5976 | 1 | 23 | 24 |
| 12 | -95.5958 | 2.7271 | 1 | 24 | 16 |
| 13 | -98.5781 | 2.9823 | 0 | 9 | 40 |
| 14 | -101.0880 | 2.5101 | 0 | 8 | 43 |
| 15 | -103.2260 | 2.1382 | 0 | 4 | 47 |
| 16 | -105.3870 | 2.1609 | 0 | 0 | 51 |

| <i>n</i> | E | ΔE | N_{AA} | N_{AX} | N_{XX} |
|-----------------|-----------|------------|----------|----------|----------|
| $Ar_{17-n}Xe_n$ | | | | | |
| 0 | -61.3180 | | 57 | 0 | 0 |
| 1 | -66.7034 | 5.3854 | 36 | 14 | 0 |
| 2 | -70.2609 | 3.5575 | 31 | 19 | 1 |
| 3 | -73.9456 | 3.6847 | 26 | 22 | 3 |
| 4 | -77.6197 | 3.6741 | 28 | 25 | 3 |
| 5 | -81.2377 | 3.6180 | 22 | 31 | 3 |
| 6 | -84.6540 | 3.4163 | 17 | 30 | 7 |
| 7 | -88.1712 | 3.5172 | 10 | 34 | 10 |
| 8 | -90.8381 | 2.6669 | 8 | 33 | 11 |
| 9 | -94.0120 | 3.1739 | 5 | 32 | 16 |
| 10 | -96.4962 | 2.4842 | 3 | 29 | 20 |
| 11 | -99.1802 | 2.6840 | 2 | 26 | 23 |
| 12 | -103.0480 | 3.8679 | 3 | 30 | 22 |
| 13 | -104.8350 | 1.7873 | 2 | 22 | 27 |
| 14 | -108.2390 | 3.4039 | 1 | 21 | 32 |
| 15 | -109.4510 | 1.2115 | 0 | 8 | 45 |
| 16 | -111.6100 | 2.1595 | 0 | 4 | 49 |
| 17 | -113.7890 | 2.1788 | 0 | 0 | 54 |
| $Ar_{18-n}Xe_n$ | | | | | |
| 0 | -66.5310 | | 61 | 0 | 0 |
| 1 | -71.6344 | 5.1034 | 42 | 14 | 0 |
| 2 | -75.4300 | 3.7956 | 43 | 16 | 0 |
| 3 | -79.6966 | 4.2666 | 38 | 22 | 1 |
| 4 | -83.7028 | 4.0062 | 32 | 26 | 3 |
| 5 | -87.5703 | 3.8675 | 26 | 30 | 5 |
| 6 | -91.2575 | 3.6872 | 20 | 36 | 5 |
| 7 | -94.1626 | 2.0879 | 17 | 37 | 7 |
| 8 | -97.2132 | 3.8678 | 14 | 38 | 9 |
| 9 | -99.9746 | 2.7614 | 11 | 38 | 12 |
| 10 | -102.9080 | 2.9334 | 9 | 34 | 16 |
| 11 | -105.6790 | 2.7706 | 7 | 31 | 20 |
| 12 | -108.2810 | 2.6019 | 0 | 26 | 31 |
| 13 | -111.0780 | 2.7979 | 2 | 29 | 27 |
| 14 | -113.5770 | 2.4987 | 1 | 25 | 32 |
| 15 | -116.1860 | 2.6091 | 2 | 12 | 43 |
| 16 | -118.2490 | 2.0625 | 1 | 12 | 47 |
| 17 | -120.4410 | 2.1925 | 0 | 3 | 53 |
| 18 | -123.4810 | 3.0398 | 0 | 0 | 56 |